GLUCOSE BIOSENSOR APPLICATION OF ELECTROSPUN POLYVINYL ALCOHOL (PVA) FIBERS

A Thesis Submitted to
the Graduate School of Engineering and Sciences of
İzmir Institute of Technology
In Partial Fulfillment of the Requirements for the Degree of

MASTER OF SCIENCE

in Biotechnology

by
Emine BERBER

September, 2016
İZMİR

We approve the thesis of **Emine BERBER**

Examining Committee Members:

Prof. Dr. Mustafa M. DEMİR
Department of Materials Science and Engineering, İzmir Institute of Technology

Assoc. Prof. Volkan ÇEÇEN
Department of Mechanical Engineering, Dokuz Eylül University

Assist. Prof. Nur Başak SÜRMELİ
Department of Bioengineering, İzmir Institute of Technology

21 September 2016

Prof. Dr. Mustafa M. DEMİR
Supervisor, Department of
Materials Science and Engineering
İzmir Institute of Technology

Assist. Prof. Ümit Hakan YILDIZ
Co-Supervisor, Department of Chemistry
İzmir Institute of Technology

Assoc. Prof. Engin ÖZÇİVİCİ
Head of the Department of
Biotechnology and Bioengineering

Prof. Dr. Bilge KARAÇALI
Dean of the Graduate School of
Engineering and Sciences

ACKNOWLEDGEMENTS

I would like to express my special gratitude to my adviser Prof. Dr. Mustafa M. DEMİR for his scientific guidance, endless support, and trust throughout my thesis study. In all the stage of this study, he patiently led me and encouraged me to overcome the problems. I tried to gain his scientific aspect, productivity and working discipline during my master study and I belive that, scientific abilities he saved me, will bright my way throughout my academic studies in the future. To have a chance to work with him was a unique privilege for me.

Special thank to my co-adviser Asst. Prof. Ümit Hakan YILDIZ, for his academic guidance and support throught my thesis study.

I also thank to Alina SEKRETARYOVA and Onur PARLAK from Stanford University for their great deal of effort for the some part of my study. They have been always kind and helpful.

I thank to all my lab mates and friends for their friendship and support throughout my master stage.

And the warmest thanks to Ayşegül GÜMÜŞ and Özlem KAP. They were always on my side in the ups and downs that involved all the parts of master stage.

Finally, but in the first place of my life, I thank to my parents Av. Hasan BERBER and Yıldız BERBER for their endless support, trust and love. And my twin sister Hatice BERBER, my brother Şerif BERBER… I owe my deepest thanks to them.

ABSTRACT

GLUCOSE BIOSENSOR APPLICATION OF ELECTROSPUN POLYVINYL ALCOHOL (PVA) FIBERS

Electrospinning is a simple and versatile technique for the fabrication of polymeric nanofibrous membranes with high surface to volume ratio. Besides the large surface area of the fibrous membranes, their dimensional stability and flexibility allows the immobilization of biomolecules on to the nanofiber surfaces. Therefore, electrospun nanofibers have been extensively used in enzyme electrodes. This thesis examines the glucose biosensor application of electrospun polyvinyl alcohol (PVA) nanofibers – carbon nanotube (CNT) nanocomposite membranes. By manipulating the structural design and the composition of the nanocomposite membranes, glucose sensing efficiency of the five different enzyme electrodes **a)** *Glucose oxidase (GOx) immobilized PVA electrospun electrode,* **b)** *Glucose oxidase (GOx) immobilized PVA electrospun electrode containing multi-walled carbon nanotube (MWCNT),* **c)** *Glucose oxidase (GOx) immobilized PVA electrospun electrode containing Poly(diallyldimethylammonium chloride) (PDDA) functionalized multi-walled carbon nanotube (MWCNT)* **d)** *Glucose oxidase (GOx) immobilized PVA electrospun electrode containing Poly(diallyldimethylammonium chloride) (PDDA) functionalized single-walled carbon nanotube (SWCNT),* **e)** *Interfacially cross-linked PVA electrospun electrode containing Poly(diallyldimethylammonium chloride) (PDDA) functionalized multi-walled carbon nanotube (MWCNT)* were comperatively studied. PVA electrospun nanofibers were fabricated by using electrospinning technique. Morphology and average diameter of the fibers were characterized by using Scanning Electron Microscopy (SEM). Average diameter for the neat PVA electrospun fibers were 115 nm. Carbon nanotubes were oxidatively functionalized by acid treatment and addition of functional groups after acid treatment was proved by using Raman Spectroscopy. Glucose sensing activities of the electrodes were amperometrically measured at an applied voltage -0.5 V (vs. Ag/AgCl) in 0.1M phosphate buffer solution (PBS pH 7). Glucose detection sensitivies of the electrodes were calculated as 19.6, 27.7, 67.5, 44.4, 4.0 $\mu A\ mM^{-1}cm^{-2}$ respectively.

ÖZET

POLİVİNİL ALKOL (PVA) ELEKTROEĞİRME LİFLERİN GLUKOZ BİYOSENSÖRÜ UYGULAMASI

Elektroeğirme, çap ölçüleri nanometreden mikrometreye kadar değişebilen polimerik lif üretiminde kullanılan basit ve çok yönlü bir yöntemdir. Son derece küçük çap ölçüleri nedeniyle, yüksek yüzey/hacim oranına sahip olan elektroeğirme nanolifler, aynı zamanda yapısal olarak sağlam ve esnek yapılardır. Bu özelliklerine bağlı olarak, elektroeğirme nanolifler, biyomolekül tespiti için uygun malzemelerdir ve enzim tabanlı biyosensör uygulamalarında sıklıkla kullanılmaktadırlar. Bu tez çalışması, polivinil alkol (PVA) elektroeğirme lif – karbon nanotüp (CNT) nanokompozit malzemelerin glukoz biyosensor uygulamasını içermektedir. Çalışmada, içerik ve yapı olarak farklı beş sensör elektrodu, glukoz algılama aktivitelerine göre karşılaştırmalı olarak çalışıldı. Elektrotlar **a)** *Glukoz Oksidaz (GOx) içeren PVA elektroeğirme elektrot*, **b)** *Glukoz Oksidaz (GOx)- Çok katmanlı karbon nanotüp (MWCNT) içeren PVA elektroeğirme elektrot,* **c)** *Glukoz Oksidaz (GOx) ve poli dialil dimetil amonyum klorür (PDDA) ile modifiye edilmiş çok katmanlı karbon nanotüp (MWCNT) içeren PVA elektroeğirme elektrot,* **d)** *Glukoz Oksidaz (GOx)- poli dialil dimetil amonyum klorür (PDDA) ile modifiye edilmiş tek Katmanlı karbon nanotüp (SWCNT) içeren PVA elektroeğirme elektrot,* **e)** *Arayüzey çapraz bağlanmış ve Glukoz Oksidaz (GOx)- poli dialil dimetil amonyum klorür (PDDA) ile modifiye edilmiş çok Katmanlı karbon nanotüp (MWCNT) içeren PVA elektroeğirme elektrot* olarak adlandırıldı. PVA nanolifler, elektroeğirme yöntemi kullanılarak üretildi. Nanoliflerin morfoloji ve ortalama çap uzunlukları, Taramalı Elektron Mikroskopu (SEM) kullanılarak gözlemlendi ve nanoliflerin ortalama çap uzunluğu 115 nm olarak belirlendi. Karbon nanotüp oksidatif yüzey modifikasyonunun sağlanması amacıyla, karbon nanotüpler asit ile muamele edildi ve öngörülen karbon nanotüp yüzey modifikasyonu, Raman Spektroskopisi kullanılarak gözlemlendi. Elektrotların glukoz algılama aktiviteleri amperometrik olarak -0.5 V potansiyel fark uygulanarak, 0.1 M fosfat tampon çözeltisi (PBS, pH 0.7) içerisinde gerçekleştirildi. Üretilen **a-b-c-d-e** sensor elektrotlarının glukoz algılama hassasiyetleri ise sırasıyla 19.6, 27.7, 67.5, 44.4, 4.0 $\mu A\ mM^{-1}\ cm^{-2}$ olarak tespit edildi.

"Her ölüm dünyada bir çatlak açar – bir boşluk bırakıp öyle gider her kişi : öteki kişiler de, şimdi, o çatlağı kapatmakla, o boşluğu doldurmakla görevlendirilmiş hissederler kendilerini. Oysa, önemli olan, çatlağı açıkça görebilmek, boşluğu olduğu gibi yüklenebilmekti. Çünkü, ölüm, onmaz; yaşam, onarılmazdır." O. Aruoba

Bu dünyada bizimle kalan, tüm çatlak ve boşlukların anısına…

Dedicated to my father…

TABLE OF CONTENTS

LIST OF FIGURES

Figure **Page**

LIST OF TABLES

Table **Page**

LIST OF ABBREVIATIONS

ABTS	2,2'-Azino-di-[3-ethylbenzthiazolin-sulfonate]
APTES	(3-Aminopropyl) triethoxysilane
CA	chronoamperometry
CNT	carbon nanotube
CV	cyclic voltammetry
EIS	electrochemical impedance spectroscopy
FAD	flavin adenine dinucleotide
FT-IR	fourier transformed infrared spectroscopy
GA	glutaraldehyde
GCE	glassy carbon electrode
GDH	glucose dehydrogenase
GOx	glucose oxidase
HF	hydroxyl fullerene
HIV	Human Immunodeficiency Virus
HK	hexokinase
HRP	horseradish peroxidase
IDF	International Diabetes Federation
ITO	indium tin oxide
MWCNT	multi-walled carbon nanotube
NSPANI	nanostructured polyaniline
PGE	pencil graphite electrode
PBS	phosphated buffered saline
PDDA	poly(diallyldimethylammonium chloride)
PVA	polyvinyl alcohol
PVAc	polyvinyl acetate
RBM	radial breathing mode
SECM	scanning electrochemical microscopy
SEM	scanning electron microscopy
SWCNT	single-walled carbon nanotube
UME	ultra-micro electrode
WHO	World Health Organization

CHAPTER 1

INTRODUCTION

Nanoscience and nanotechnology are based on the fabrication of materials below the sub-microscopic level by the manipulation of individual atoms and molecules. Nanotechnology contains biological, physical and chemical knowledge in range of 0.1-100 nm (López-Lorente and Valcárcel 2014). Through the nanotechnology, nanostructures can be integrated into bulk systems. Definitions of nanotechnology frequently refer to the term of *dimension.* According to the definition of National Nanotechnology Initiative (NNI), "It is the understanding and control of matter at dimensions between approximately 1 and 100 nanometers, where unique phenomena enable novel applications" (Adams and Barbante 2013).

Nanoscale world is different from the macroscale world. Materials represent bulk phase at the micron and above size levels and they correspond to the law of classical science. On the other hand, at nano dimension, materials gain unique properties that is not present in their corresponding bulk forms (Hochella Jr 2002).

Throughout the history, nano-scaled materials were used for different applications by the earliest civilizations. The Mayans used magnesium aluminum silicate clay called *palygorskite* which include nano-scaled channels. The Mesopotamian civilizations made metal nanoparticle embedded colored glasses for decorative usage. Also, thousand years ago the Chinese used gold nanoparticles in their ceramic porcelain to incorporate red color into the patterns (Pokropivny and Skorokhod 2008) .

At the end of the 19^{th} century, discovery of the radioactivity was the first conscious approach to the atomic nature of the matter. From the beginning of the 20^{th} century, it is realized that the nano-metric size is not beyond the human perception and range of action. Nanos are now guests of our everyday life. Three-dimensional morphology (shape, size and surface topography), surrounding media and arrangement in space are defining parameters for the physicochemical properties of the nanomaterials. Appropriate correlation between these parameters is the primary requirement to discover novel properties and applications of nanomaterials (Adams and Barbante 2013).

Nanofibers are fiber formed structures with diameters around 100 nm. Because of their high surface area to volume ratio, they have significantly enhanced physical and mechanical properties (Rando, Kohring, and Giffhorn 1997). Nanofibers have variety of application area ranging from consumer products to medical and industrial to drug delivery systems, capacitors, fuel cells, high-tech applications for aerospace, energy storage, transistors, and information technology (Bhardwaj and Kundu 2010). There are various ways for fabrication of nanofibers such as drawing, template synthesis, phase separation and self assembly. Among them, electrospinning appears the most significant one because it provides high-strength, low-cost and high-value added nanofiber fabrication facilities. Electrospinning is a technique which utilizes electrical forces to produce polymer fibers with diameters ranging from 2 nm to several micrometers using polymer solutions (Reneker and Yarin 2008). Electrospun polymer fibers have large surface area per unit mass because of their small diameters and in this manner they have high potential for many applications such as drug delivery, catalysis, sensors, functional textiles, tissue engineering, ion exchange membranes, bioengineering etc. (Agarwal, Wendorff, and Greiner 2010) This technique was firstly observed by Rayleigh in 1897 and studied in depth by Zeleny (1914) as on electro spraying and patented by Formhals (Formhals, A., Process and apparatus for preparing artificial threads. U.S. Patent No. 1, 975, 504, 1934.). Studies of Taylor in 1969 on electrically driven jets have built background for electrospinning process. Formhals published a series of patents, describing an experimental setup for the production of polymer filaments using an electrostatic force (Huang and Chang 2003). The first patent (US Patent Number: 2116942) was subjected to the textile yarns fabrication. In the process a voltage of 57 kV was used for electrospinning of cellulose acetate in acetone and monomethyl ether of ethylene glycol as solvents. This process is patented by Antonin Formhals in 1934 (Boland et al. 2004). In the past 60 years approximately 50 patents have been filed for electrospinning of polymer melts and solutions (Li and Xia 2004). Since the 1980's electrospinning has gained more attention especially because of the surging interests to the submicron or nanometer scaled ultrafine fibers and fibrous structures (Huang and Chang 2003). In the present day, 200 universities and research institutes are studying on electrospinning process (Bhardwaj and Kundu 2010).

1.1. Overview of Electrospinning

A typical electrospinning setup contains three main components as high voltage power supply, a spinneret and grounded metal collector. Under an electric field, charged polymer solution feeding through the spinneret forms a conical drop in the equilibrium point between the surface tension of the polymer and the electric field. When the electric field reached to a defined value to overcome the surface tension of the droplet, a jet formed polymer is ejected from the droplet to the metal collector. During the jet formation, solvent evaporates gradually and non-woven fibers are formed on the collector. Figure 1.1 shows a typical electrospinning set-up. Fiber morphology and diameter can be controlled by adjusting the processing parameters as solution properties, applied voltage, spinneret- collector distance, temperature and humidity (Liang, Hsiao, and Chu 2007). Electrospun polymer fibers have a large variety of application area for the polymer based composite material production.

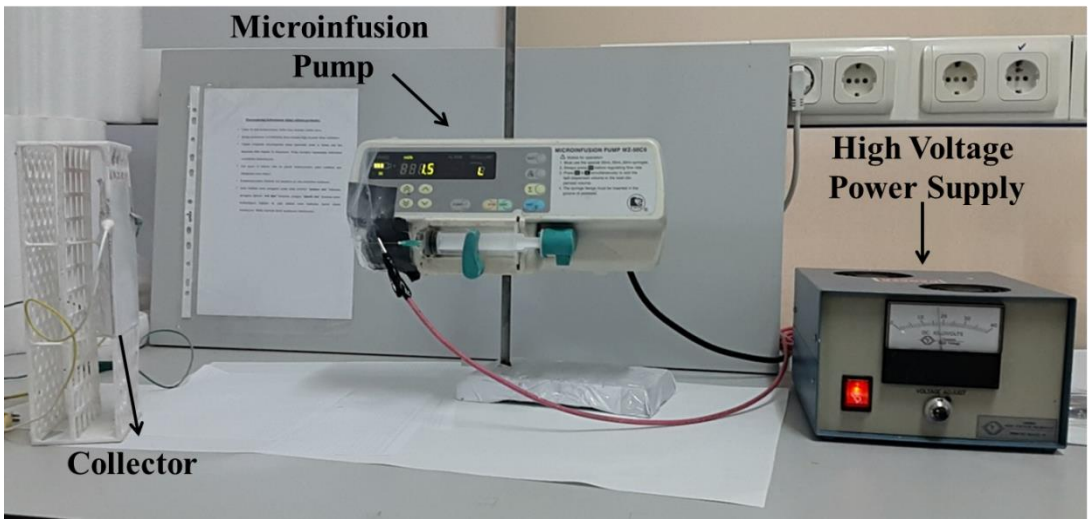

Figure 1.1. Electrospinning setup in our laboratory

1.2. Scope and Structure of the Thesis

This thesis study proposes to investigate glucose sensing efficiency of polyvinyl alcohol (PVA) electrospun nanofibers as a supporting material for the fabrication of different types of sensor electrodes enhanced with carbon nanotubes (CNTs). Structural design and the composition of the nanocomposite membranes were defined as the decisive aspect for the comperative study of five different sensor electrodes. Disposable pencil graphite electrode was used as the working electrode for electrochemical characterization of the nanocomposite membranes. Glucose sensing activities of the electrodes were amperometrically measured.

Structurally, this thesis study consists of six chapters. *Chapter 1*, gives an introduction to the basic concepts of the research. *Chapter 2* includes a background information based on the fundamental aspects of the research including electrochemical biosensor systems, reaction mechanism of glucose oxidase, polyvinyl alcohol and carbon nanotubes. *Chapter 3* presents a literature review in glucose biosensing systems. *Chapter 4* describes the detailed experimental stages of the study. In *Chapter 5* results of the study were given and discussed. In *Chapter 6* concluding remarks were explained.

CHAPTER 2

BACKGROUND

Diabetes (Diabetes mellitus) is a metabolic disease in normal blood glucose level changing outside the normal range of 4-8 mM. As per 2013 reports of International Diabetes Federation (IDF), there are 382 million diabetes patients worldwide and it is expected that this number will reach to 471 million by 2035 (Danaei et al.). According to World Health Organization (WHO), 5.1 million diabetes related death occurred in 2013 and there are 200 million people who have undiagnosed diabetes around the world (Soni and Jha 2015). Continuous control of the blood glucose level has vital importance for patients' life quality and avoiding the complications as blindness, heart disease, kidney and circulatory problems. Detection of abnormal glucose level is a requirement to determine the used insulin dosage. Monitoring of blood glucose level is the widely used implementation for the management of diabetes. Currently available glucose meters require pricking of the skin periodically to get blood sample and this invasive process is painful for the patients. It also carries contamination risk for the disease as Human Immunodeficiency Virus (HIV) and Hepatitis (Yadav et al. 2015). In addition, the cost of these devices is a limiting factor for the people in underdeveloped countries. Hence, there is a need for developing of non-invasive and low cost glucose monitoring devices.

As an alternative to the blood, the other body fluids such as saliva, tears, sweat and urine can provide vital information about diabetes (Tripathi et al. 2010). For a healthy individual, the normal blood glucose level is ranged between 4-8 mM (72–144 mg dL^{-1}) and this value varies between 2–30 mM (36–540 mg dL^{-1}) for pathophysiological conditions. Lane et al (2006) define the normal and diabetic tear glucose concentration as 0.35± 0.04 mmol/L and 0.16± 0.03 mmol/L respectively (Peng et al. 2013). Within this context, improving the sensitivity, selectivity, reliability, and time response of biosensors is the main requirement to progress the diagnosis systems that can be applicable for the alternative body fluids. Many types of glucose detection methods developed in recent years including fluorescence and absorption spectroscopy and electrochemistry. As an electrochemical approach, amperometric biosensors are

more appealing because of their potential of miniaturization that is mandatory for the implantable medical device fabrication (Carrara et al. 2012).

Sensitivity of an amperometric biosensor is a controlled parameter by the several factors as diffusion ability of the substrate, redox mediator characteristics and the electrical communication between the recognition element and the other device components. In the case of enzyme based biosensing systems, electrical communication between the transducer (working electrode interface etc.) and the biomolecule recognition element is a challenging aspect because of the amino acid shell of the enzyme which reduces the direct electron transfer between enzyme and the electrode (Cortez et al. 2015). To enhance the electron transfer efficiency and to preserve the native structural and functional characteristics of the enzyme, a large variety of surface modification methods have been explored such as hydrogels (Heller 1990), self-assembled monolayers (Putzbach and Ronkainen 2013), proteic coatings (Lisdat et al. 2009) and polymers (Baba et al. 2010). Protein immobilization on polymeric materials is a widely used method. Especially fibrous form of the polymer structures constitute desirable supporting stage because of their high surface area, inter-fiber porosity, flexibility and mechanical strength. High surface to volume ratio of the fibers ensures the binding of large amount of enzymes and secondly porosity of the surface decreases the substrate diffusion resistance thus enhance the enzyme activity (Wan, Ke, and Xu 2008).

Carbon nanotubes (CNTs) are the carbon based nanomaterials. They are extensively applied to the construction of biosensing systems because of their chemical and dimensional concurrency with the biomolecules. This concurrency enhance the catalytic ability of the biomolecule and promote the electron transfer efficiency between the electrode interface and the biomolecule (Kurkina et al. 2011).

2.1. Definition of the Term “Biosensor”

The term of “ biosensor ” was firstly introduced by Cammann in 1977 (Cammann 1977). A biosensor is a device that is used to identify and quantify a targeted analyte from a sample matrix. According to IUPAC definition, “ A biosensor is a self-contained integrated device which is capable of providing specific quantitative or semi-quantitative analytical information using a biological recognition element (biochemical

receptor) which is in direct spatial contact with a transducer element." (Thevenot et al. 1999). A biosensor consists of two main elements such as,

1. *A bioreceptor* : immobilized biological element (antibody, enzyme, DNA probe etc.) that recognizes the targeted analyte (antigen, enzyme substrate, complementary DNA etc).

2. *A transducer* : converts the (bio) chemical signal to a quantifiable physical signal caused by the analyte- bioreceptor interaction. The intensity of the resulted signal is directly or inversely proportional to the analyte concentration.

Biosensors can be categorized as electrochemical, piezoelectric, thermal and optical sensors according to the transducing element. There are three types of electrochemical biosensors such as amperometric, conductometric and potentiometric (Thevenot et al. 1999). Biosensors have a wide variety of application area ranging from medical applications to the military defense industry (Liu and Lin 2005). Figure 2.1 shows a schematic of a typical biosensor system.

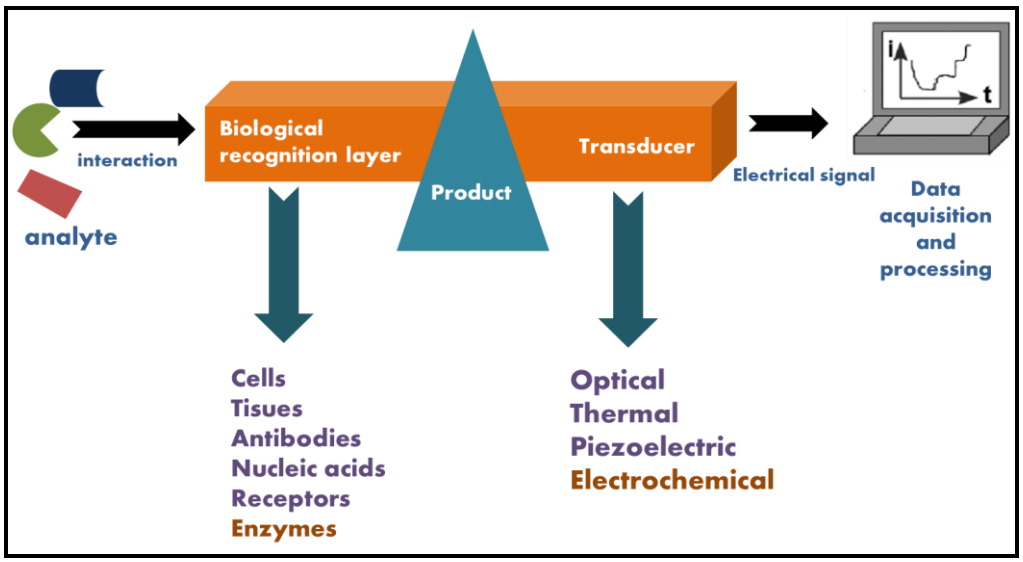

Figure 2.1. Typical biosensor set up

2.2. Electrochemical Biosensors

Bio electroanalytical sensor systems are convenient for the analysis of the species with high specificity and selectivity. These systems can be used in in vivo studies, on-line control processes and clinical analysis (Dixon, Lowry, and O'Neill 2002). In a electrochemical biosensing system, a bio electrochemical reaction is occurred and this reaction would produce a measurable current (amperometric biosensor), a measurable charge accumulation or potential (potentiometric biosensor) or measurable conductivity change (conductometric biosensor) in sensing medium. If the current is measured at a potential value, these kinds of systems are referred as amperometry, correlatively, if the electrical current is measured as form of the potential, this method is called as voltammetry. Amperometric sensor systems measures the current change caused by the electroactive species when a constant potential is applied; the concentration of the target species (analyte) is represented as the change at the current (Arora et al. 2011). Factors that define the performance of a electrochemical biosensor are sensitivity range, selectivity, solution conditions, accuracy, recovery time and life time of the biosensor. Electrochemical cell systems are used to perform electrochemical biosensor studies.

2.2.1. Electrochemical Cells

In consideration of the performance of an electrochemical biosensor, electrodes play an important role. Surface modification characteristics and dimensions of the electrodes effects the detection capability of the biosensor. An electrochemical cell system consists of three different types of electrodes as working electrode, reference electrode and counter (auxilary) electrode. Figure 2.2 shows a typical electrochemical cell system.

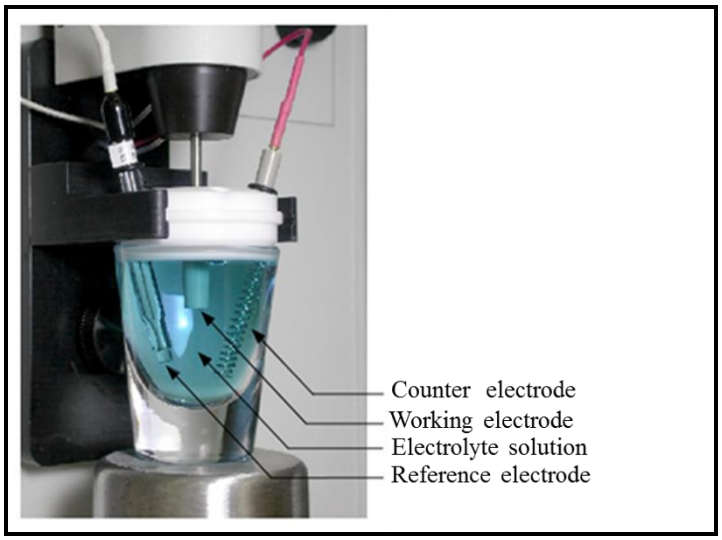

Figure 2.2. Electrochemical cell system
(Source: Adesokan et. al. 2016)

2.2.1.1. Reference Electrode

There are two types of reference electrodes commonly used and commercially available;

1. Ag/AgCl Electrode: It is composed of a Ag wire that coated with AgCl and immersed into a NaCl solution.

$$AgCl + e^{-} \longrightarrow Ag + Cl \qquad (E^{0} = +0.22\ V) \tag{2.1}$$

2. Saturated Calomel Electrode: Working principle is based on the reaction between elemental mercury and mercury (I) chloride. Calomel is the other name of mercurous chloride (Hg_2Cl_2). Figure 2.3 shows a schematic of reference electrode.

$$Hg_2Cl_2 + 2e^{-} \longrightarrow 2Hg + 2Cl^{2} \qquad (E^{0} = +0.24\ V) \tag{2.2}$$

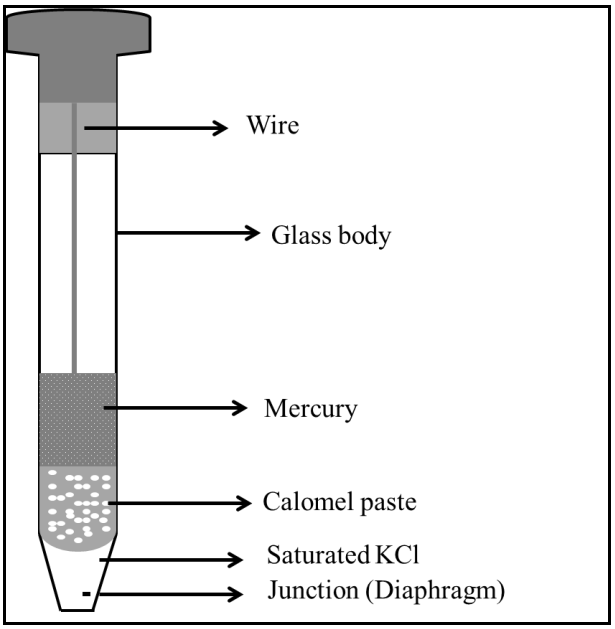

Figure 2.3. Reference (calomel) electrode
(Reproduced from Adesokan et al. 2016)

2.2.1.2. Working Electrode

In an electrochemical system with three electrodes, electrochemical reaction occurs at the working electrode (Wohlfahrt et al. 1999). Depending on the reaction type on the working electrode is an oxidation or reduction, it is referred as anodic or cathodic. There are many types of working electrodes such as glassy carbon electrode, gold electrode, Pt electrode and indium tin oxide coated glass electrode etc.

2.2.1.3. Counter (Auxilary) Electrode

Counter electrode works as a cathode while the working electrode is serving as an anode and vice versa. The counter electrode has larger surface area than the working electrode and half-reaction processing at the counter electrode should be fast enough not to slow the process at the working electrode. Counter electrode potential is not measured against the reference electrode, it just regulated to balance the reaction processing at the working electrode. This electrochemical connection provides the

measuring of the working electrode potential against a known reference electrode. Inert materials such as carbon, gold or platinum are used to fabricate counter electrodes.

2.2.2. Cyclic Voltammetry (CV)

2.2.2.1 Basics of Amperometric and Voltammetric Analysis

All electrochemical reactions are versant in part by the Nernst equation**.** This fundamental equation expresses the relationship between the potential of an electrode and the concentrations of oxidized and reduced species.

$$O + ne^- \longleftrightarrow R \tag{2.3}$$

$$E = E^0 + \frac{RT}{nF} ln\left(\frac{C_0}{C_R}\right) \tag{2.4}$$

E^0 refers to the redox potential of the couple of oxidized and reduced species, C_0 is the concentration of the oxidized "half" of the couple and C_R refers to the reduced half. For instance, in the consideration of Fe $^{3+/2+}$ redox couple, Fe^{3+} subtends to oxidize and Fe $^{2+}$ to reduced species. Nerst equation is applicable for the conditions that the solution is directly adjacent to the surface of the electrode (Adesokan et al. 2016).

In cyclic voltammery, system sweeps the potential of the working electrode at a defined sweep rate (in volts/second) and generates a current versus time curve. Since the sweeping rate is constant and switching and initial potentials are defined, finally current versus applied potential is recorded. Figure 2.4 illustrates the common concept.

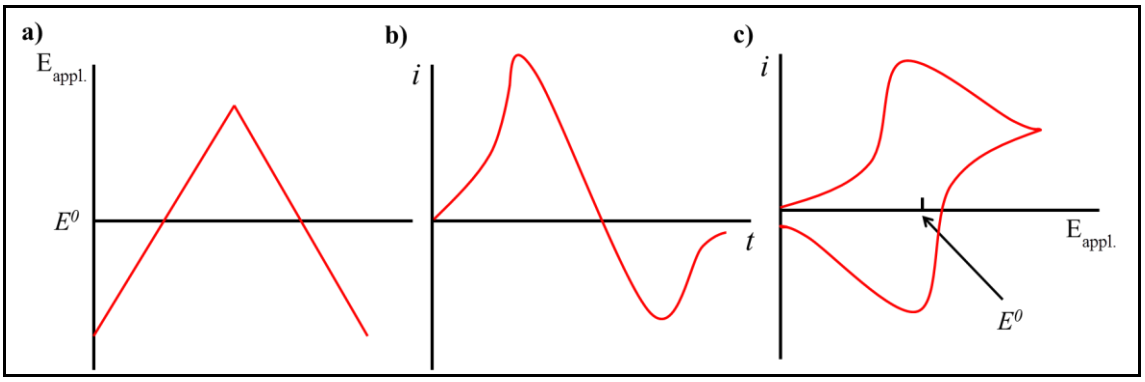

Figure 2.4. Cyclic voltammograms of a) $E_{appl.}$ versus time, b) current versus time, c) current versus $E_{appl.}$ (Reproduced from Adesokan et al. 2016)

Current versus applied potential curve (Figure 2.4.c) is estimated for an ideal reversible system and the peak current I_p is expressed as;

$$i_p = (2.69\times10^5)\, n^{3/2} A D^{1/2} v^{1/2} C \qquad (2.5)$$

In the equation, i_p is the peak current (ampere), n is the number of electrones passed per molecule of reduced or oxidized analyte, A is the area of the electrode (cm^2), D is the diffusion coefficient of analyte (cm^2/sec), v is the potential sweep rate (volts/sec) and C is the concentration of analyte in bulk solution (moles / cm^3). Midpoint potential of the two peaks in the voltammogram is expressed as;

$$E_{midpoint} = \left(\frac{E_{p,anodic} + E_{p,cathodic}}{2}\right) = E^{0'} + \frac{RT}{nF} ln \frac{D_R^{1/2}}{D_0^{1/2}} \qquad (2.6)$$

$E^{0'}$ refers to the redox potential, D_0 and D_R are the diffusion coefficients of the oxidized and reduced half of the redox couple. It is generally conceivable to assume that D_0 and D_R are almost equal and with this assumption, the redox potential is nearly equal to the midpoint potential. And, the separation between the two peaks of the voltammogram is expressed as:

$$\Delta E_p = \left|E_{p,anodic} - E_{p,cathodic}\right| = 2.3\frac{RT}{nF} = \frac{59}{n} mV \quad \text{(at 298 K)} \qquad (2.7)$$

Finally, for a single experiment, depending on the already known parameter, it is possible to determine the diffusion coefficient; the number of electrons per molecule of analyte oxidizing or reducing concentration, and the redox potential for the analyte (Adesokan et al. 2016).

2.2.3. Chronoamperometry

Chronoamperometry is a quantitative electrochemical technique that used to analysis nucleation processes. This technique provides to obtain information about nucleation and growth mechanism of the working system. (Mei et al. 2016) Basic concept of the technique based on the measuring the steady state current of the working electrode (exposed to a potential), as a function of time. Between the electrode surface and the solution, there is a diffusion layer. Analyte transfer from the high concentration solution to the electrode surface is controlled by diffusion phenomena. There is a concentration gradient from solution to electrode surface. Cottrell equation explains this diffusion concept: It states the current-time dependence for linear diffusion control for an electrode.

$$I = nFAc_0 \sqrt{\frac{D}{\pi t}} \tag{2.8}$$

In the equation, I is current, F is Faraday's constant, n is the number of transferred electrons, A is the surface area of the electrode, c_0 is the concentration of analyte, D is diffusion coefficient and t is the time (Marozzi, Gennero de Chialvo, and Chialvo 2013).

2.2.4. Electrochemical Impedance Spectroscopy

Electrochemical Impedance Spectroscopy (EIS) is an effective technique that used to characterize the electrical characteristics of materials and their interfaces with conducting electrodes. Also it can be used to study dynamics of mobile charge or bound

or interfacial area of solid and liquid materials such as insulators, semi-conducting, ionic and mixed electronic-ionic (Suni 2008).

Electrical resistance generally has been described as the capability of a material to resist the flow of current as explained with Ohm's law for DC conditions:

$$E = I \times R \tag{2.9}$$

However, this equation is eligible for the ideal circuits that all voltage, current and resistance value independent from frequency.

In electrochemical impedance spectroscopy, an AC potential is applied to an electrochemical cell and it measures the current through the cell. When a sinusoidal potential is applied to a circuit, response that corresponds to this potential is an AC signal. This signal is evaluated as a sum of sinusoidal functions (Fourier serie). Considering the AC conditions:

$$I \times Z \tag{2.10}$$

Z represents the impedance of the system. The impedance is calculated by setting the input potential and measuring the induced current (Eggins 2002).

2.3. Glucose Oxidase

Fungi produce different enzymes that provides them to process different organic compounds as nutrition source (Gouka, Punt, and vandenHondel 1997). In consideration of non-hydrolotic enzymes produced by fungi, glucose oxidase (EC 1.1.3.4) has a largest application area since 1950's (Fiedurek and Gromada 1997). Glucose oxidase is commonly purified from the genus *Aspergillus and Penicillium* but *Aspergillus niger* is the most used species for GOx production (Pluschkell, Hellmuth, and Rinas 1996).

GOx (β-D-glucose:oxygen 1-oxidoreductase) catalyzes the oxidation of β-D-glucose to gluconic acid by using molecular oxygen with the production of hydrogen peroxide (H_2O_2) (Hatzinikolaou and Macris 1995). GOx has large variety of commercial applications such as canned beverages, removal of oxygen from fruit juices, glucose removal from dried egg, improvement of flavor, color, and shelf life of food

materials. Also it has been used in glucose assay kit in conjugated with catalase and in biosensor applications for detection of glucose in body fluids such as urine and blood (Petruccioli et al. 1999). It is reported that GOx has the best antagonistic efficiency against food-borne pathogens such as *Listeria monocytogens, Clostridium perfringens, Bacillus cereus, Salmonella infantis, Campylobacter jejuni, Staphylococcus aureus* (Kapat, Jung, and Park 1998).

2.3.1. Structure of Glucose Oxidase

GOx that produced by ascomycetes is a homodimeric glycoprotein structure consist of two polypeptide subunits and this subunits are covalently linked by disulfide bonds (Rando, Kohring, and Giffhorn 1997). Figure 2.5 shows the FAD moiety and conserved active sites of GOx from *P. amagaskiense*. Each subunit contains one mole of FAD as co-factor and entire structure is glycosylated with mannose-rich carbohydrate of 11-13 % (Witt et al. 2000) Conserved active site residues are His-563, His-520, Arg-516, Asn-518, Tyr-73, Trp-430 and Phe-418. Witt et al. (2000) suggested that Arg-516 is a critical amino acid for effective binding of GOx to β-D-glucose. Aromatic residues Trp-430, Tyr-73 and Phe-418 are important for the accurate orientation of the substrate to reach the maximum velocity of glucose oxidation. His-563 and His-520 bind to the 1-OH of glucose during oxidation.

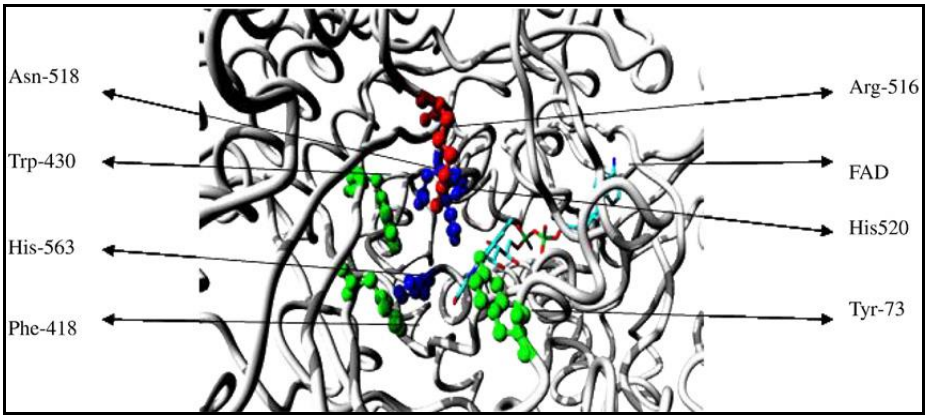

Figure 2.5. Glucose oxidase from *P. amagasakiense*
(Source: Wohlfahrt et al. 1999)

2.3.2. Characteristics of Glucose Oxidase

Molecular weight of GOx changes in a range of 130 to 175 kDa (Kalisz, Hendle, and Schmid 1997). GOx shows high specificity to the β- anomer of D- glucose, conversely α- anomer is not a suitable substrate for GOx. Lower GOx activity was observed when using D-galactose, D-mannose and 2-deoxy-D-glucose as a substrate. Sodium bisulphate, pchloromecuribenzoate, hydrazine, phenylhydrazine, hydroxylamine, dimedone and Cu^{2+}, Ag^{+}, Hg^{2+} ions inhibit the GOx activity (Kusai et al.,1960). Fujiki and Nakamura (1968) made a comparative studies on molecular weights of *Aspergillus niger* and *Penicillium amagasakiense.* They found their molecular weights as 150 and 152 kD respectively. P. amagasakiense contains more glucose than *A. niger*, but mannose and hexosamine contend of *A. niger* is more than *P. amagasakiense*. Carbohydrate contents of A. niger and *P amagasakiense* was found as 16% and 11% respectively. Optimal pH range of GOx from *A. niger* is 3.5-6.5 and its ranging between 4.0-5.5 for the GOx from *P. amagasakiense.* eventually, GOx from *A. niger* shows broader pH range than from *P. amagasakiense* (Nakamura and Fujiki, 1968).

2.3.3. Reaction Mechanism of Glucose Oxidase

GOx catalyzes oxidation of β-D-glucose to D-glucono-δ-lactone and H_2O_2 is used as an electron acceptor during the reaction. This oxidation reaction can be evaluated into two steps as reductive and oxidative step. In the reductive half reaction step, β-D-glucose is oxidized to D-glucono-δ-lactone. D-glucono-δ-lactone is non-enzymatically hydrolyzed to gluconic acid. Afterwards, flavine adenine dinucleotide (FAD) group of GOx is reduced to $FADH_2$. In the oxidative half reaction, reduced GOx is reoxidized via molecular oxygen to yield H_2O_2 (Witt et al. 2000). Figure 2.6 represents the GOx catalysis reaction.

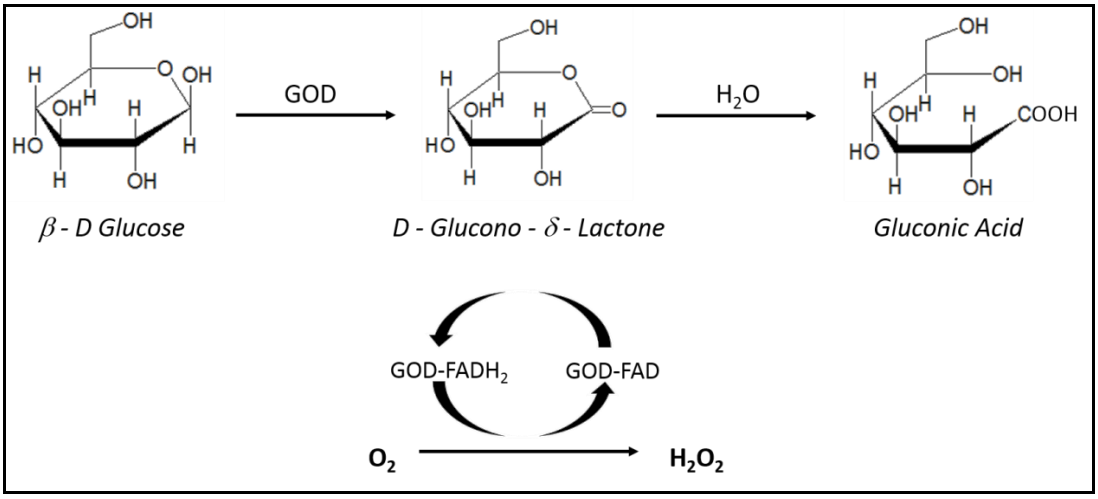

Figure 2.6. Schematic representation of GOx catalysis reaction

2.3.4. Glucose Oxidase Activity Analysis

In literature, there are different types of analytical methods used to determine GOx activity. Tongbue et al. (1996), studied on titrimetric method to determine the GOx activity. In this titrimetric method, glucose oxidase solution was added into sodium acetate buffer solution including 2% β-D-glucose and reaction was stopped by adding sodium hydroxide solution. Final solution was titrated with hydrochloric acid to measure the added volume of hydrochloric acid and hereby to define GOx activity.

The most used analytical method for GOx activity determination is based on the oxidation of β-D-glucose to β-D-glucono-δ-lactone and H_2O_2 in the presence of molecular oxygen. In a secondary reaction step, produced H_2O_2 is used to oxidase a chromogenic substrate in the presence of horseradish peroxidase (HRP) and occurred colour change is monitored spectrophotometrically. 2,2′-Azino-di-[3-ethylbenzthiazolin-sulfonate] (ABTS) (Witt, Singh, and Kalisz 1998) and o-dianisidine (Bergmeyer, Horder, and Rej 1986) are the mostly used chromogenic substrates. ABTS generates a green-blue product can be measured spectrophotometrically at 420 nm. Figure 2.7 represents the GOx reaction with ABTS.

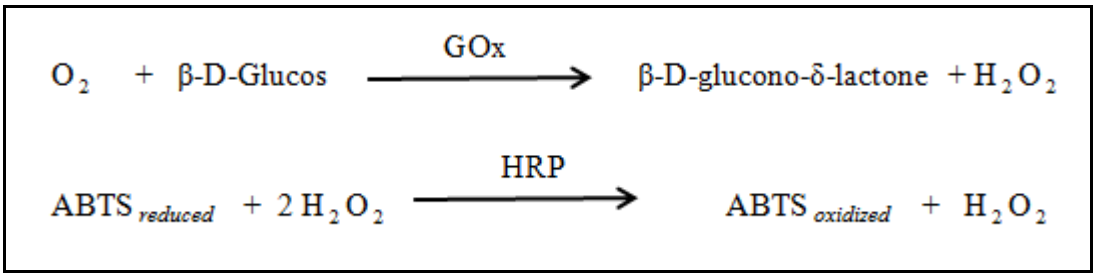

Figure 2.7. Schematic representation of GOx reaction with ABTS
(Reproduced from Witt et al., 1998)

Oxidation of o-dianisidine generates a quinoneimine dye and it is measured at 500 nm spectrophotometrically (Figure 2.8). Petruccioli et al. (1999) studied with benzoquinone for spectrophotometric determination of GOx activity. This spectrophotometric method was based on the reduction of benzoquinone by hydroquinone and measurement of the rate of absorbance increase at 290 nm (Petruccioli et al. 1999).

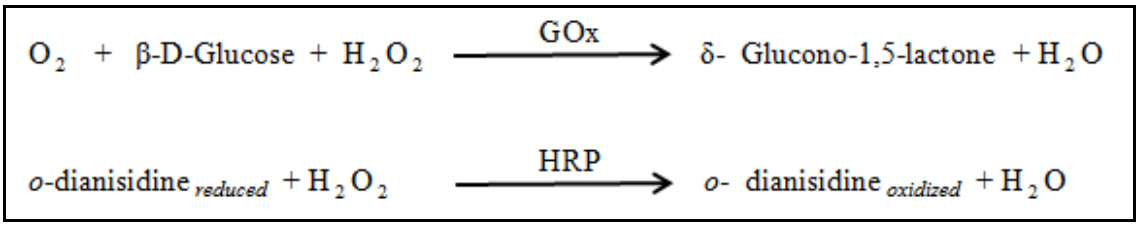

Figure 2.8. Schematic representation of GOx reaction with *o*-dianisidine
(Reproduced from Bergmeyer et al., 1974)

Karmali et al. (2004) developed a new assay for GOx by using Fourier transform infrared spectroscopy. This new method was considered more appropriate to study the kinetic characteristics of Gox, because the substrate and the product absorbs at different frequency values. Other advantages of this assay were reaction speed and smaller amount of enzyme and substrate requirement.

2.4. Polyvinyl alcohol (PVA)

Polyvinyl alcohol (PVA) is the first synthetic colloid produced by Herrmann and Haehnel in 1924 (Finch 1973). PVA is produced by polymerization of vinyl acetate monomer to polyvinyl acetate (PVAc) and hydrolyzing of the acetate groups to PVA (Li et al. 2004). Figure 2.9 shows the chemical structure of PVA.

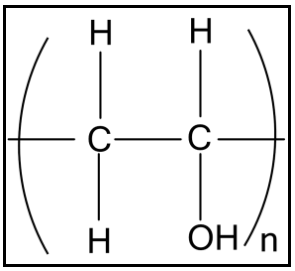

Figure 2.9. Chemical structure of PVA

There are three different hydrolysis methods that can be used for the production of PVA as acidolysis, alkaline hydrolysis, and aminolysis (Finch 1973). On the industrial scale production of PVA, alkaline alcoholysis method is used for the conversion of PVAc to PVA in which acetate groups are hydrolyzed by methanol interchanged ester in the presence of sodium hydroxide (Saini, Saxena, and Bansil 2010). Figure 2.10 shows the production stage of PVA.

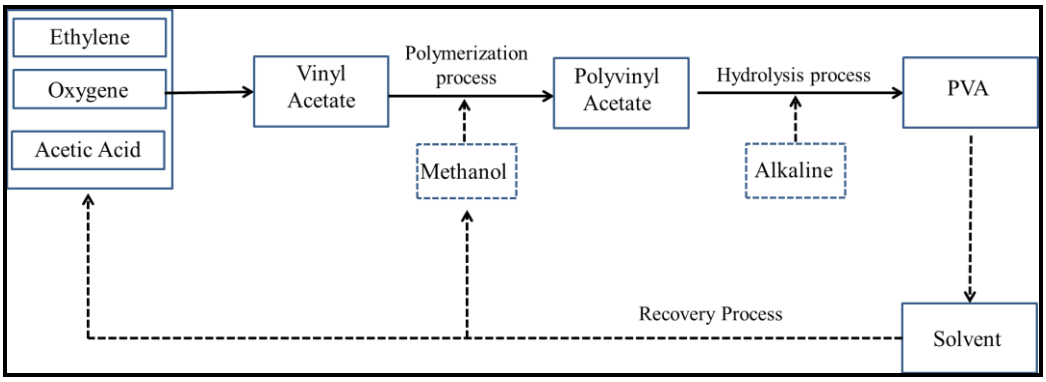

Figure 2.10. Production stages of PVA
(Reproduced from Thong, Teo, and Ng 2016)

Because of the chemical resistance and physical properties, PVA has a wide range of application areas in different industries such as textile sizing, protective colloids for emulsion polymerization, adhesives, PVA fiber and polyvinyl butyral production, paper sizing (Hamielec, Gomezvaillard, and Marten 1982). It is also used in food and medical applications (DeMerlis and Schoneker 2003), for soil stabilizing and as wood preservatives against the termite attack and fungal decay (Mohareb et al. 2011).

High volumes of PVA is used in building industry as building binding material such as thickening agent for latex paint and seals, aggregate surface pretreatment agent, modifier and fiber reinforcement in cement based materials. It is interpreted as hydroxyl groups of the PVA have a potential to defeat the surface bond between the matrix, aggregate and fiber reinforcement (Ahmed and Mihashi 2011).

2.4.1. Physical Properties of PVA

PVA is a synthetic and water soluble polymer. It is in the class of water soluble, non-ionic, vinyl containing polymers (Moukwa, Youn, and Hassanali 1993). It is nonhazardous, thus considered safe to handle and environmental friendly. PVA is a tasteless, odorless and diaphanous polymer and available in powder form (Saini, Saxena, and Bansil 2010). Physical properties of PVA depend on the degree of hydrolysis and polymerization.

There are two different classes of PVA in commercial grades. Depending on the degree of hydrolysis and polymerization, they classified as fully hydrolyzed group and

partially hydrolyzed group. In fully hydrolyzed group PVA, 98% of acetate groups are replaced by alcohol groups. This group is soluble in hot water and shows good film forming properties (Chan, Hao, and Heng 1999). Partially hydrolyzed group is soluble in water at room temperature, nearly soluble in ethanol but insoluble in other organic solvents. PVA is converted to water insoluble form by using cross-linking agents such as glutaraldehyde, formaldehyde and boric acid (Feldman 2016).

2.4.2. Cross-linking of PVA

Because of its water-soluble nature, PVA is modified to decrease the swelling in water for the aqueous media applications. In literature, stability of cross-linked PVA in highly alkaline or highly acidic medium has been verified (Peter, Hese, and Stefan 1976). PVA membranes have been extensively used in water treatment processes (Katz and Wydeven 1981). In pharmaceutical and biotechnological studies, PVA hydrogels have been studied to incorporate bio-active materials because of their similarities to living tissues. For example, hydrophilicity and water swelling degree of modified PVA can be regulated for the controlling of drug delivery quotient in human body and this provides a preventing mechanism for the overdosing and rejection problems. Also, it is possible to immobilize cells or biomolecules in this life-mimicking systems to study their function in non-living media (Ferraz et al. 2007) . PVA is extensively studied as biomaterials for glucose sensors, artificial cartilage, contact lenses, artificial pancreas and kidney, protein recovery and drug delivery systems (Amanda and Mallapragada 2001).

Non-crosslinked PVA structures are not stable in water. Aquatic medium damages the integrity of the structure and reduce its performance. Cross-linking of PVA decreases the hydrophilicity of the membrane and provides a resistant supporting network for immobilization of biomolecules. The major techniques that are used to cross-link the polymers based on the chemical, physical and heat treatment. In heat treatment, supplied heat energy is utilized for the modifying the spatial organization of chains and to assemble stronger hydrogen bonds among the hydroxyl groups. In physical cross-linking process, crystalline regions are introduced to the structure that perform as cross-linker (Hickey and Peppas 1995). Physical crosslinking is not stable and strong as chemical cross-linking, because the increasing crystallinity causes a

decrease on the water content of the polymer (Ofstead and Poser 1989). Chemical cross-linking is based on the reaction between cross-linker and hydroxyl groups on PVA. There are different crosslinking agents that can be used for PVA such as glutaraldehyde (GA), formaldehyde and maleic acid. By using specific cross-linker and controlling the process conditions, intra- and inter-molecular modes of cross-linking reaction can be adjusted (Han et al. 2003).

GA is the commonly used cross-linking agent for the PVA cross-linking because of the absence of heat treatment to drive the reaction. In addition, GA could bind to the biomolecules nonspecifically such as proteins; for example, for production of artificial blood, in polymerization of hemoglobin, GA joins the polypeptide backbone. Because GA has two active sites, it can bind both PVA and protein. This property of GA allows to develop specific structures to be used in biosensing systems (Buehler et al. 2005).

General cross-linking procedure is based on the immersion of the polymer membrane into an alcoholic solution consisting of a cross-linker and a mineral acid such as hydrochloric acid or sulfuric acid (Guo et al. 2007). Alcoholic environment causes the swelling of the membrane and swelling permits the diffusion of the protonic ions and dialdehyde molecules which are utilized to catalyze the reaction (Yeom and Lee 1996a). Figure 2.11 shows the proposed crosslinking reaction mechanism between PVA and GA.

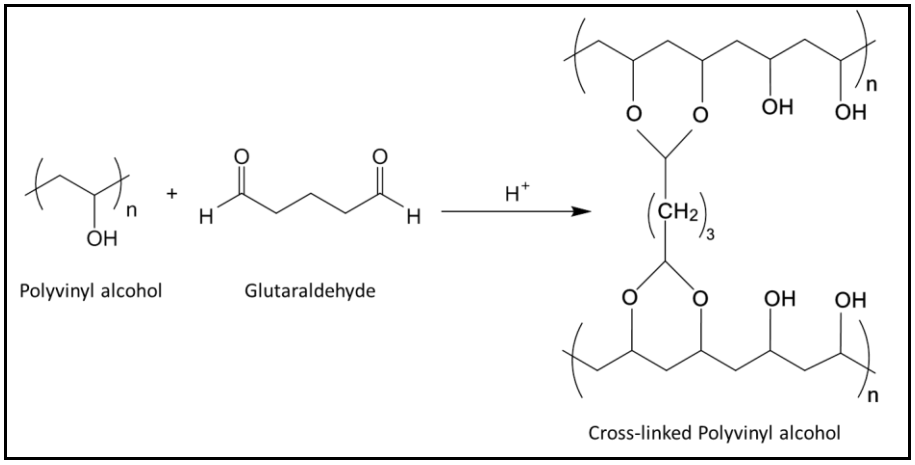

Figure 2.11. Mechanism of the cross-linking reaction between PVA and GA

2.5. Carbon Nanotubes (CNTs)

Carbon nanotubes (CNTs), discovered in 1991 by Sumio Iijima. They constitute an important group of nanoscale materials because of their unique mechanical, electronic and structural properties. They are formed from sp^2 carbon units and they exhibit a seamless structure with a hexagonal honeycomb lattices which is several nanometers in diameter and microns in length (Zhao, Gan, and Zhuang 2002). CNTs are classified in two groups as single-walled carbon nanotubes (SWCNTs) and multi-walled carbon nanotubes (MWCNTs). SWCNTs are formed of one layer rolling graphene sheet. Their length and diameter distribution are at the range of 1-50 μm and 0.75-3 nm respectively. MWCNTs are formed of more than two layers of rolled graphene sheet and their diameter is ranged between 2-100 nm and the distance between each graphene layer is approximately 0.42 nm (Popov 2004). Figure 2.12 (a) and (b) schematically represents the structures of SWCNT and MWCNT respectively.

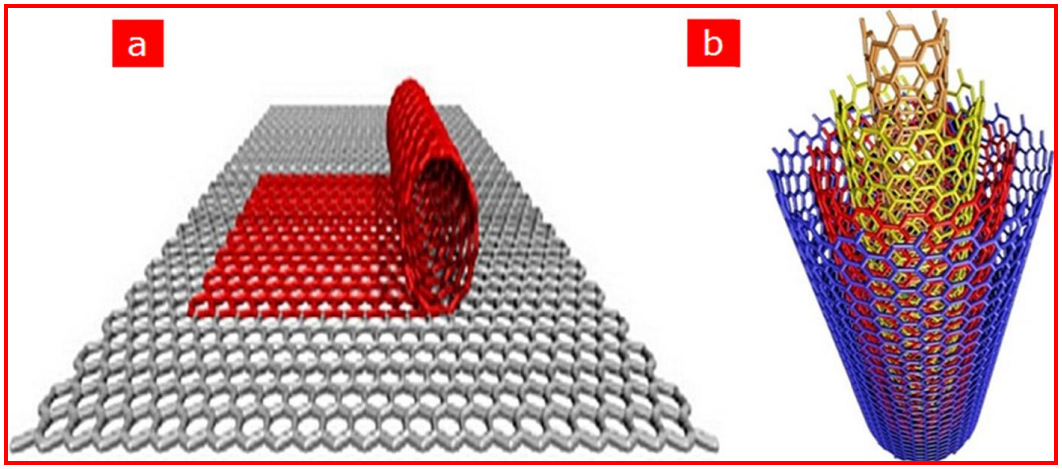

Figure 2.12. (a) Schematics of SWCNTs (b) Schematics of MWCNTs
(Source: Yang et al. 2015)

SWCNT graphene plane can be mapped into a cylinder hexagonal graphene layer (Figure 2.13). Vector from A to A' can be defined as in Eq. (10),

$$\hat{C}_h = n\overline{a_1} + m\overline{a_2} \tag{2.11}$$

C_k and a_1 are the lattice basis vectors and n and m are positive integers, which refer the chiral indices. When the graphene sheet is rolled on, carbon atom A overlaps the carbon atom A' and CNT is formed. When the integers n and m are defined, all structural parameters of CNT can be determined (Dresselhaus 2004), (Terrones 2003).

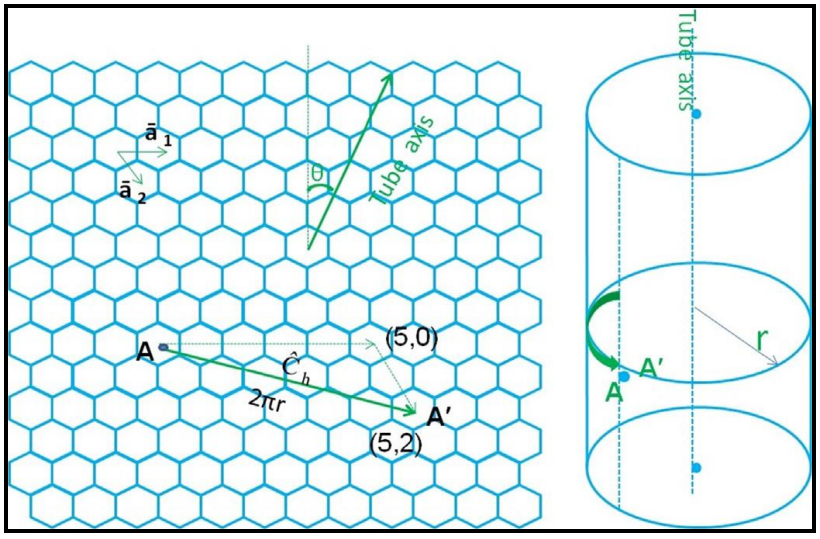

Figure 2.13. Structural schematic diagram of SWCNTs
(Source: Dresselhaus 2010)

Depending on the direction of the winding, SWCNTs are divided into three different structural types such as armchair, zigzag and chiral type (Golberg et al. 2003). Figure 5.3 shows the different types of SWCNTs. These structural types are related to the spiral angle θ and chiral vectors (n,m). If n=m, spiral angle θ equals to 30^0, the types of CNT is called arm-chair. If n=0, θ equals to 0 and CNT is called zig-zag. In the case of $0 < \theta < 30^0$, types of CNT is called chiral. Electrical characteristic of SWCNTs widely depends on the chirality and diameter of the structure (Dresselhaus et al. 1998). As given in Eq (2.12), d is the diameter of the CNT and a is the distance between the two adjacent carbon atoms.

$$d = \frac{|C|}{\Pi} = a\,(n^2 + nm + m^2)^{1/2} \qquad (2.12)$$

When *n-m= 3r* (*r* is integer) all of the CNTs have metallic attribute or they shows semiconductor properties. Energy gap of a semi-conductive SWCNT is inversely proportional to the diameter of the nanotube. Energy gap is approximately zero If d is too large, thus metallic attribute of CNT turns into semiconductor. Arm-chair types SWCNTs are most stable types with the metallic attribute (Odom et al. 1998).

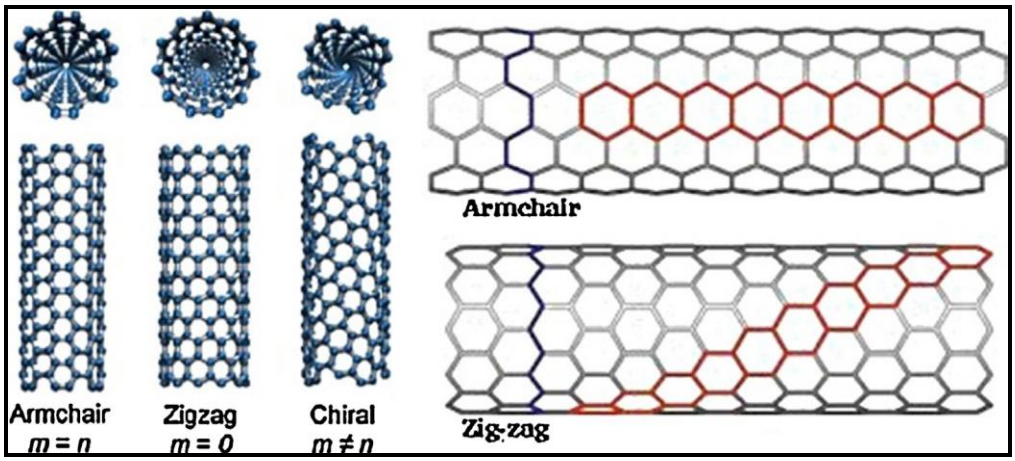

Figure 2.14. Types of SWCNTs
(Source: Golberg et al. 2003)

2.5.1. Raman Spectroscopy of Carbon Materials

Raman spectroscopy is a technique which used to characterize carbon based materials showing different characteristic spectra for sp, sp^2, sp^3 carbons, fullerenes and CNTs (Dresselhaus et al. 2002). Raman spectroscopy is inelastic scattering of light, generally associated with emission (stokes process) or absorption (anti-Stokes process) of light (Calleja, Vogt, and Cardona 1982). By observing the energy shift of scattered light relative to the incident light, which is yield Raman spectra in cm^{-1} (Figure 2. 15), phonon frequency is obtained and this frequency value can be used to identify the unknown structure of the material.To define the defect density of a material, a ratio of

the intensity of disorder induced D band to the one of symmetry allowed G band (I_D/I_G) metric is used (Dresselhaus, Dresselhaus, and Saito 1992).

Mono-layer graphene is the fundamental sp^2 carbon material which shows the simplest and most fundamental form of Raman spectral features which named the first order G and the second order symmetry G' bands. The former symbol refers the term "graphitic". The second commonly observed feature is the D- band, which is a defect activated Raman mode. D band is observed at about 1350 cm^{-1} at 2.41 eV laser excitation *(E_{laser})*. Since the melting point of graphene is at over 4200 K, the D/G band intensity ratio provides a sensitive metric for the degree of disorder in sp^2 carbon materials for the over wide temperature ranges. In consideration of carbon nanotubes, the atoms around the circumference of a single wall carbon nanotube (SWCNT) are vibrating in a breathing mode in the radial direction, Raman-active radial breathing mode (RBM) which is cylindrical specific is used to check the presence of nanotubes in a sample. This vibrational mode is commonly used to identify the presence of carbon nanotubes in a given sample (Rao et al. 1997). In addition, RBM frequency ω_{RBM} is inversely proportional to the diameter of the carbon nanotube (d_t) diameter distribution of nanotubes in a sample can be estimated (Jorio et al. 2001). For the observation of isolated carbon nanotube, Raman spectrum can be used to obtain detailed structural information such as spatial orientation, diameter and chiral angle of the nanotube.

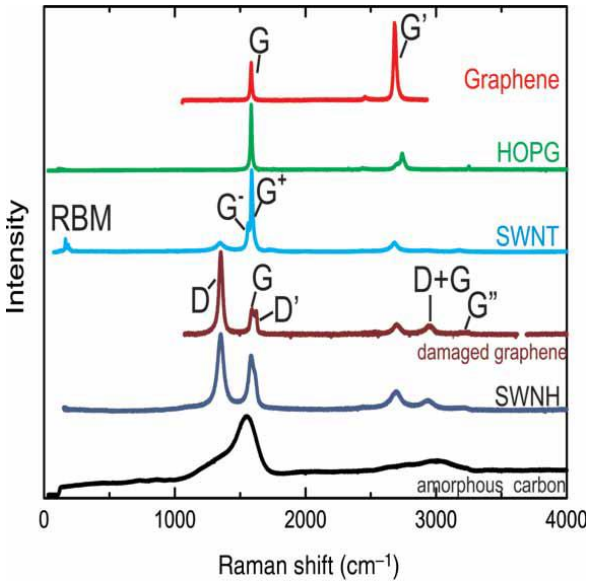

Figure 2.15. Raman spectrum of different carbon based materials
(Source: Jiang et al. 2004)

2.6. Scanning Electrochemical Microscopy (SECM) Analysis of Polymer Fibers

2.6.1. Basics of SECM

Scanning electrochemical microscopy (SECM) is a scanned probe microscopes that is used for the characterization of various heterogeneous surfaces such as conducting, semiconducting and insulating in solutions (Bard et al. 1989). Technique employs an ultra-micro electrode (UME) probe that is immersed in a solution close to the sample surface. Mass transfer between electrode-interface and chemical reaction which occurs on the surface of the sample, defines the response of the electrode (Figure 2.16). In condition of the probe is at a large distance from the sample surface, the response of the UME is the steady state current under semi-infinite diffusion conditions. When the distance between the sample surface and the probe is decreased, diffusion layer interacts with the sample and UME current changes. If the surface is insulator, UME current decreases while it is approaching to the sample, because the surface hinders the diffusion of the reacting species thus produce a negative feedback. Above a conductive surface, when the probe-sample distance is small, it is able to regenerate the species reacting and resulted in a positive feedback (Kwak and Bard 1989)

SECM can locally characterize the reactivity and electrical properties of a surface. Resolution is directly correlated with the UME's diameter (typically 1-25 μm in diameter).

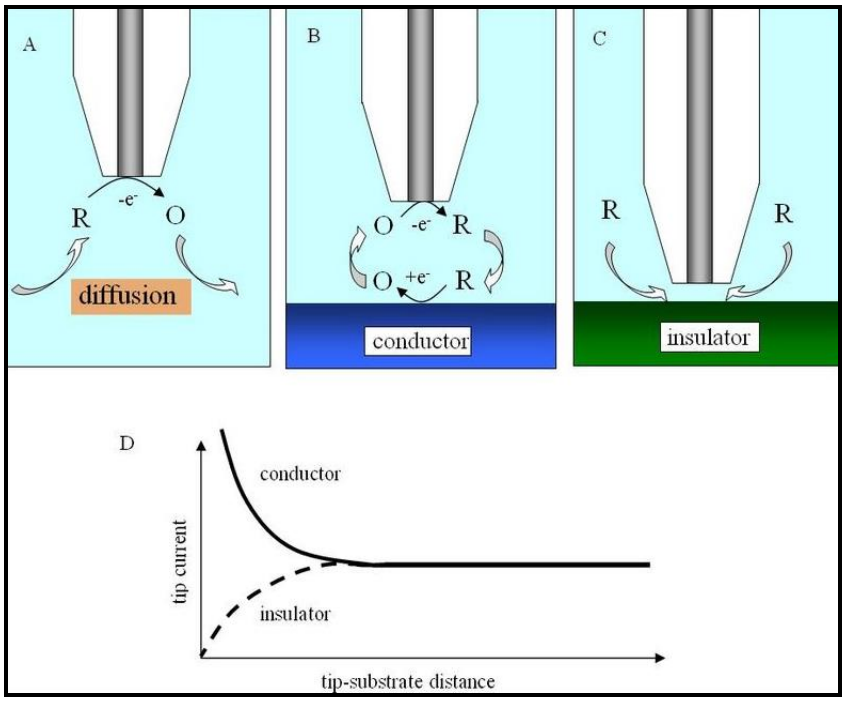

Figure 2.16. Scanning electrochemical microscope working principle
A) Semi- infinite diffusion conditions distent from the surface,
B) diffusion on conducting surface,
C) diffusion on non-conducting surface,
D) Current response of the UME.
(Source: Husser, Craston, and Bard 1989)

CHAPTER 3

LITERATURE REVIEW

Diabetes is a serious health problem that causes 4 million deaths every year in worldwide (Wild et al. 2004). There is not an efficient treatment yet for diabetes and avoiding the potential complications, thus, blood glucose level of diabetic patients should be periodically monitored. Due to the critical importance of continuous monitoring of blood glucose level, fabrication of sensitive and accurate glucose detection devices for personal and clinical diagnosis have gained a significant attention (Li et al. 2009).

In this manner, there is a significant increase in glucose biosensing related publication number during the last few decades. Many strategies have been developed for the fabrication of glucose biosensing systems such as chemiluminesence, acoustic, optical, fluorescent nanogels, field effect transistors based on glucose boronic acid chemistry, near infrared spectroscopy and transdermal approaches (Malin et al. 1999). However, these technologies are required complicated and costly device designing. Conversely, electrochemical glucose biosensor technologies allows to construct low cost, easy operation, miniaturization for portable glucose sensing device fabrication with high sensitivity, selectivity and lower response time (Zaidi and Shin 2016).

Electrochemical enzyme biosensors are classified into enzymatic and non-enzymatic groups. In enzymatic biosensors, electrode surface is functionalized with a glucose sensitive enzyme which generates hydrogen peroxide by reducing molecular oxygen and this reduction is monitored amperometrically (Lerner et al. 2013). Non-enzymatic glucose biosensing systems based on the oxidation or reduction of glucose on metal electrode which is modified with nanomaterials to provide enhanced electron transfer and high surface area. Different types of nanomaterials such as carbonaceous materials (graphene and carbon nanotubes), metal oxides, doped metal oxides and their nanocomposites have been utilized in designing of glucose biosensors because of their unique properties. In addition, nanoscale design of biosensor electrode surface controls the architecture of these nanomaterials (Cash and Clark 2010).

Different types of enzymes such as glucose dehydrogenase (GDH), isoenzyme 2 of hexokinase (HK) and glucose oxidase (GOx) have been utilized for the fabrication of

glucose biosensors. Glucose Oxidase is the most used candidate for glucose biosensor applications.

Chen *et al.* designed an oxygen reduction-based electrochemical glucose biosensor. In this work, glassy carbon electrode surface was modified by nanodendrite poly[meso-tetrakis(2-thienyl) porphyrinato] cobalt(II), single walled carbon nanotubes (SWCNTs), nafion and GOx. Sensitivity and linear concentration range of the biosensor were estimated to be 16.57 mAM $^{-1}$ cm $^{-2}$ and 0-1 mM respectively. Michaelis–Menten constant (Km^{app}) was defined as 0.98 mM.

Che *et al.* modified gold electrode with chitosan-prussian blue-multi walled carbon nanotubes (MWCNTs)-hollow PtCo nanochains film. GOx containing nafion was then immobilized on to the composite film. Glucose concentration was estimated by measuring the generated hydrogenperoxide. Linear range of the electrode was 1.5 µM –1.12mM which is not effective for the detection of diabetic blood glucose level (2–30 mM).

Yuan group (2011) modified glassy carbon electrode with hollow nanostructured Pt decorated MWCNTs by casting. For the covalent attachment of GOx onto the nanostructure layer, negatively charged L-cysteine (L-cys) and gold nanoparticles modified with positively charged poly(diallydimethylammonium) chloride (PDDA) were used (Figure 3.1). Linear concentration range of the sensor was 1.2 µM–8.4 mM and estimated detection limit was 0.4 µM.

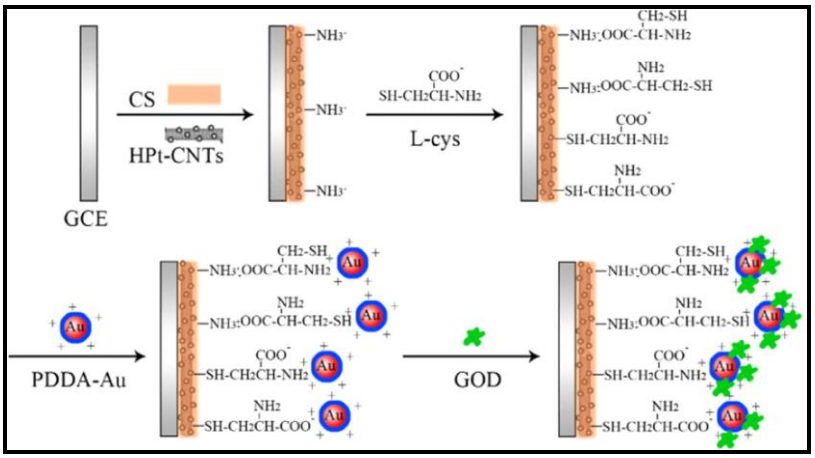

Figure 3.1. Fabrication steps of glucose biosensor
(Source: Wang et al. 2011)

Chauhan *et al.* constructed a reusable real time monitoring glucose biosensor by using CV. In this method, indium tin oxide (ITO) coated glass plate was modified with GOx immobilized nanostructured polyaniline (NSPANI). Liner concentration range of the sensor was 0.5–10 mM and it displayed Km^{app} value of 0.28mM.

Luo *et al.* designed a copper oxide based amperometric biosensor by synthesizing CuO nanocubes-graphene over GCE. Linear concentration range of the electrode was 2 μM–4 mM and detection limit was defined as 0.7 μM.

Li *et al.* prepared an interface to immobilize GOx. Pt nanopartical- chitosan composite film electrodeposited on GCE and than GOx was mechanically spreaded over the composite film surface. By using CV and Electrochemical Impedance Spectroscopy (EIS), they charactherized the PtNP effect on sensor sensitivity and selectivity. The proposed sensing system showed Km^{app} value of 2.4mM.

Qiu *et al.* designed a simple electrode system containing GOx adsorbed physically on to gold nanostructured film on GCE. This thin composite film provided a biocompatible, porous and conductive surface for GOx immobilization and effective electron transfer between the active center of GOx and the electrode. Generated hydrogen peroxide amount was measured to detect the glucose concentration. However, linear glucose concentration range of the proposed sensor was in micro molar range (2.5– 32.5 μmol L^{-1}) which is not effective for the determination of diabetic blood glucose level.

In another work, Hui group immobilized GOx onto nafion protected reduced graphene (rGO) over Au disk electrode. The linear glucose concentration range of the electrode was 2-14 mM which is better but not effective in order to diagnose diabetes.

Yue *et al.* performed GOx immobilization on graphene/MWCNTs nanocomposite functionalized with PDDA-wrapped AuNPs over GCE. Km^{app} value of the sensor was 2.09mM and linear glucose concentration was 5–175 mM and the detection limit was 4.8 mM which is not more sufficient.

In a simple methodology developed by Gao *et al.*, a nanocomplex prepared by mixing GOx and hydroxyl fullerenes (HFs) casted on GCE and coated with chitosan membrane for protection. Km^{app} value of the electrode was 694 ± 8μM and linear glucose concentration range was 0.05-1 mM.

Balakrishnan group developed a non-invasive, label free and high sensitive glucose biosensor for the detection of low level of salivary glucose. They design a

nanogap system by using (3-aminopropyl) triethoxysilane (APTES) and GOx modified polysilicon. Nanogap size effect was used to analyse the concentration of glucose. Linear glucose concentration range of the sensor was 5µM- 50mM. In consideration of the diabetic level of glucose in saliva (30 to 80 µM) proposed biosensor perfectly meets the desired criteria for the non-invasive detection of glucose. Figure 3.2 shows the sensor mechanism. Generated hydrogen ions by the GOx catalysis reaction donates as transduced signal.

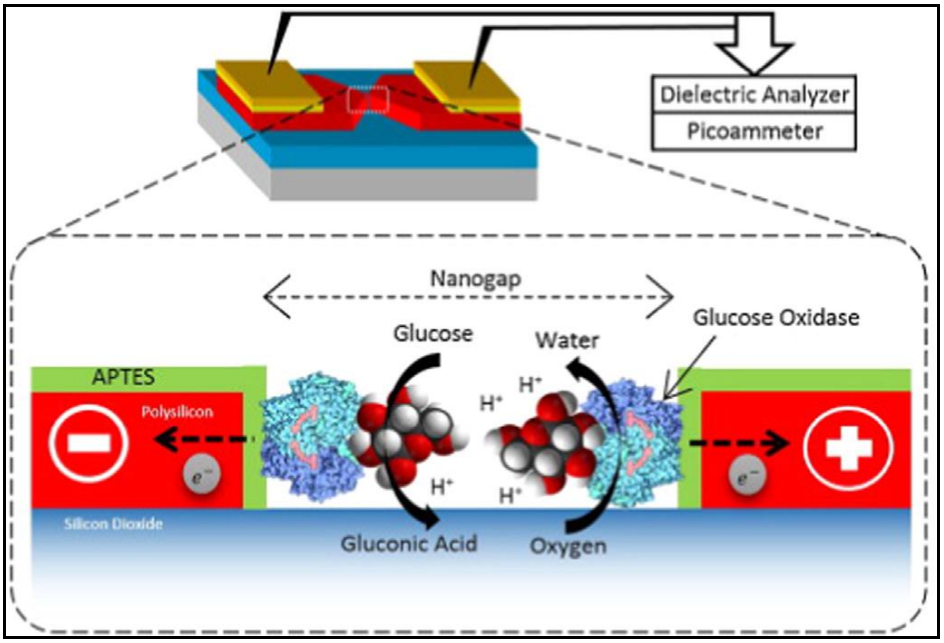

Figure 3.2. Glucose detection mechanism on PSNG electrode
(Source: Balakrishnan et al. 2014)

Table 3.1 Different glucose biosensor schemes and their analytical performances

Sensor Fabrication Scheme	Sensitivity ($mAM^{-1}cm^{-2}$)	Limit of detection (LOD, μM)	References
Pt decorated MWCNTs/GCE	20.1	0.4	(Wang et al. 2011)
CuO-G-GCE	1360	0.7	(Luo, Zhu, and Wang 2012)
GOx-PtNs-CS/GCE	—	0.4	(Li et al. 2012)
GOx-Au-GCE	—	0.32	(Qiu et al. 2012)
GOx-rGO/Au disk	—	40	(Hui et al. 2013)
GOx-AuNPs-G-MWCNTs	29. 72	4800	(Yu et al. 2014)
GOx-fullerenes/GCE	—	5	(Gao et al. 2014)
APTES-GOx/ polysilicon nanogap chip	—	0.6	(Balakrishnan et al. 2014)
GOx–Pd-HCNF/GCE	13	30	(Jia et al. 2013)
GOx-PtNPs-PANI Hydrogel heterostructure	96.1	0.7	(Zhai et al. 2013)
CuO nanoflowers/ Cu foil electrode	—	789.3	(Song et al. 2013)
CuO NPs	—	1.43	(Huang et al. 2013)
CuO NPs modified Ag electrode	2762.5	~0.5	(Ahmad et al. 2013)
CuO nanowires on Cu	1800	10	(Espro et al. 2014)

CHAPTER 4

EXPERIMENTAL SECTION

4.1. Materials

Polyvinyl alcohol (PVA, 87-90 % hydrolyzed, Mw = 30 – 70 kg mol^{-}, Sigma-Aldrich), D(+)-Glucose (99%, AppliChem), glucose oxidase (GOx, EC 1.1.3.4 *Aspergillus niger*, 50 KU, Sigma), Poly (diallydiamethylammonium) chloride solution (PDDA, Mw= 400000-500000, Sigma-Aldrich), Glutaraldehyde (25%, Alfa Aesar), Ethyl Alcohol (99.5%, Tekkim), Acetone (99.5%, Honeywell) were used without any further purification. MWCNTs (9-10 nm in diameter, NC7000™) and SWCNTs (2 nm in diameter, NC1100™) were purchased from Nanocyl. Nitric acid (HNO_3, 65%, Merck) and Sulfuric acid (H_2SO_4, 95.0-98.0%, Sigma-Aldrich) were used for the purification and functionalization of CNTs. Phosphate Buffer Saline (PBS, Sigma) were used for preparation of glucose and glucose oxidase aqueous solutions. Potassium hexacyanoferrate (II) trihydrate ($K_3Fe(CN)_6 \cdot 3\ H_2O$, 98.5-102.0%, Sigma-Aldrich) and Potassium chloride (KCl, Sigma-Aldrich) were used for the electrochemical measurements. Double-distilled water was used throught the experiments. Pencil graphite (0.9 mm in diameter, Tombow) was used for making sensor electrode.

Cyclic Voltammetry and Chronoamperometry experiments were conducted using Gamry Instrument Reference 600-Potentiostat/Galvanostat/ZRA. Electrochemical Impedance Spectroscopy (EIS) experiments were conducted using the AUTOLAB PGSTAT204 Compact and modular potentiostat/Galvanostat. Three-electrode system including of the pencil graphite electrode (GE) as the working electrode, a reference electrode (Ag/AgCl) and platinum wire as the auxiliary electrode was used in connection with Gamry Echem Analyst software.

4.2. Purification and Functionalization of CNTs

0,3 g of pristine CNTs were refluxed in 200 mL, 2.6 M aqueous solution of HNO_3 at 70 ^{0}C for 45 h. After that, nanotube suspension was diluted with double-distilled water until the pH 7.0 was reached and filtered with a 0.22 μm pore sized cellulose acetate membrane. Obtained residue dried at 50 ^{0}C for 1 h under vacuum.

For the oxidative functionalization of CNTs, 0.2 g of purified CNTs immersed in 32 mL of H_2SO_4/ HNO_3 in 3:1 volume ratio and sonicated for 3h at room temperature. Subsequently, solution was neutralized with ammonium hydroxide until the pH 7.0 was reached and filtered with a 0.22 μm pore sized cellulose acetate membrane. Filtered CNTs were washed with double-distilled water to remove the salt residues and dried in oven at 80 ^{0}C for 1 h. Pristine and oxidized CNTs analyzed with Raman spectrometry (Horiba, Xplora Plus).

4.3. Preparation of Neat and CNT Modified PVA Nanofibers

For the fabrication of neat PVA nanofiber membrane, PVA powder was added into distilled water adjusting the mass content 20 %. Prepared mixture was stirred at room temperature for 24 h to obtain homogeneous solution.

For the fabrication of CNT modified PVA nanofiber membrane, purified and oxidized CNTs added into the PVA solution (20 wt %). Mass ratio of PVA: CNT was fixed to 100:2. Prepared mixture was stirred at room temperature for 24 h to obtain a homogeneous solution.

In electrospinning process, polymer solution was placed in a 20 mL plastic syringe with steel needle and the needle was connected to a high voltage supply with a potential difference 25 kV. Flow rate was adjusted as 4 mL/h by using a micro syringe pump and distance between needle and collector was 20 cm. Nearly dry, mat like PVA fibers were collected on the grounded aluminum collector. The fiber mat on the collector was dried at room temperature for 24 h and then detached from the collector surface. The morphology of electrospun membranes was observed using Scanning Electron Microscope (FEI Quanta250 FEG, Oregon, USA). For the determination of

average fiber diameters, the fibers were randomly selected from each SEM micrographs and the diameter of each was measured using Image-J software.

4.3.1. PVA Coating of Pencil Graphite Electrode

Pencil graphite electrode surface was coated with the PVA electrospun nanofiber by using two different coating set-up as a home made rotating system and a stable coating system to get a homogeneous fiber mat thickness. In home made rotating system, firstly, pencil graphite was fixed on a 2 cm diameter and 1 mm thickness sized styrofoam. Then, it was placed on a 50 mL beaker half-filled with water and beaker located between the tip and the collector. Circulating of water via magnetic stirrer provided a rotation to pencil graphite upon itself (Figure 4.1). In this set-up, Gamma High Voltage Research Ormond Beach, FL, US high voltage supply and LION WZ-50C6 micro syringe pump combined electrospinning system was used.

In the stable coating system, pencil graphite was fixed from the edge surface of it on to the drum collector and in stable condition (no rotation on collector), fiber coating process was performed. In this set-up, Inovenso Ne 300 electrospinning device was used. Figure 4.2 shows the schema of stable coating set-up.

The thickness of PVA fiber mat on the graphite electrode was controlled with electrospinning time. At a fixed 25 kV potential difference, 4 mL/h flow rate and 20 cm tip to graphite electrode distance, three different spinning time was processed: 1,2 and 5 min. Coating homogenity and fiber thickness on the electrode surface was observed by using SEM.

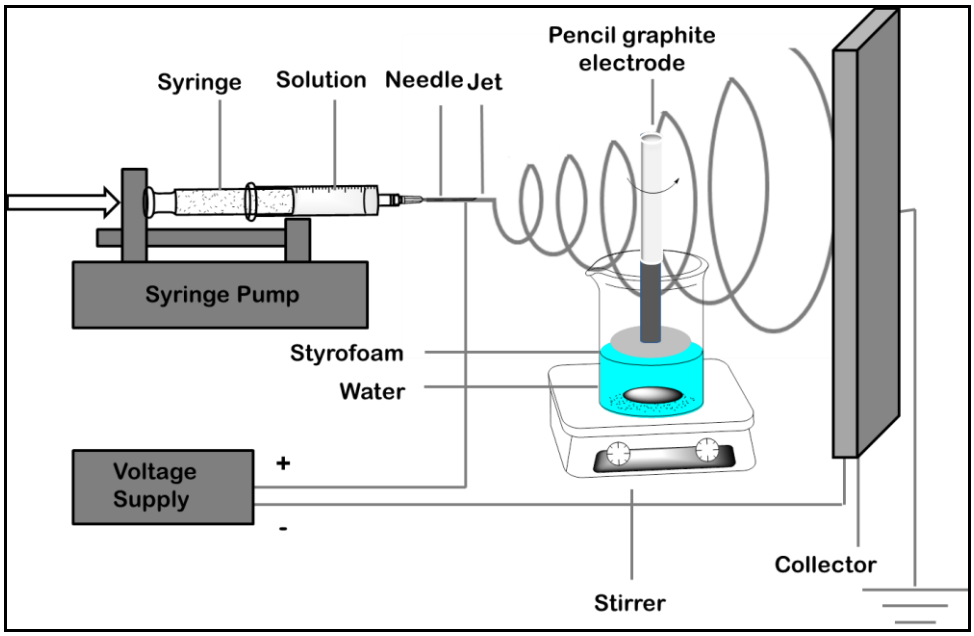

Figure 4.1 Schematic representation of graphite electrode fiber home-made coating set up

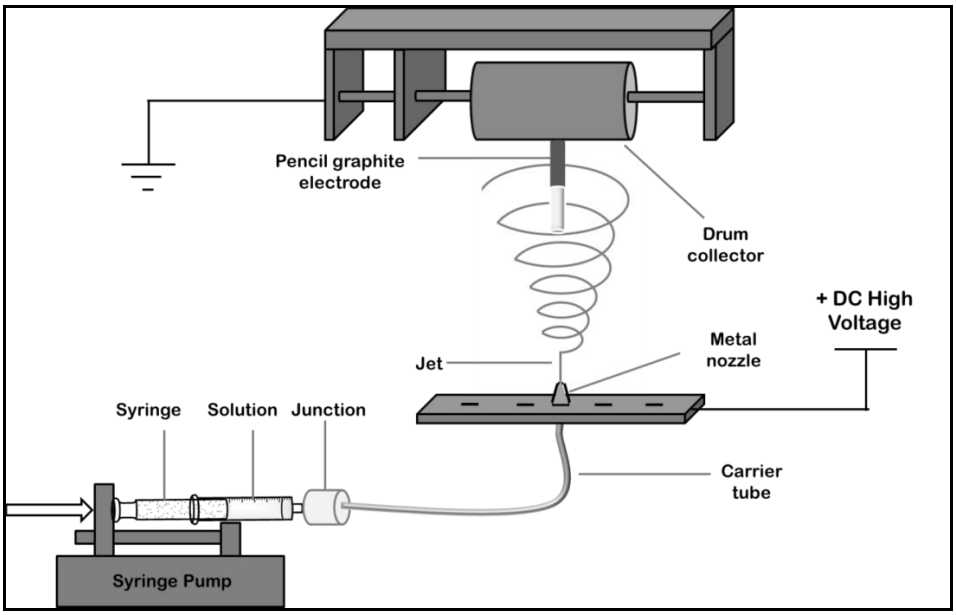

Figure 4.2 Schematic representation of graphite electrode fiber coating stable set-up

4.4. Cross-linking of PVA Electrospun Fiber Membranes

PVA molecules in fiber scale were cross-linked by using gluteraldehyde (GA). 0.3 M GA and 0.05 M HCl containing acetone solution was prepared. Neat and CNT modified electrospun membranes were immersed in crosslinking GA solution (10 mL/g). To investigate the effect of cross-linking time on fiber morphology and to define the optimal cross-linking time, 1, 3 and 24 h cross-linking results were employed. After cross-linking, membranes were removed from the solution and washed with ethyl alcohol and PBS buffer (pH 7.0) respectively. Cross-linked membranes were dried at room temperature for 24 h. The morphology of electrospun membranes were observed by using SEM and fiber diameter distributions were obtained by statistical analysis of SEM micrographs using ImageJ software. FTIR-ATR measurements were performed before and after cross-linking of the membranes.

4.5. Interfacial Cross-linkingof the PVA Nanofiber Mat

As well as in-situ cross-linking of the PVA nanofiber mats, in another process, to observe the glucose sensing efficiency of the nanofiber electrode, neat PVA fiber mats cross-linked with GA solution containing oxidized MWCNT. By using the dispersive phase of the CNTs in GA containing acetone solution, cross-linking of the PVA fiber mat and CNT immobilization on to the PVA fiber surface were achieved simultaneously.

In this process, 200 mg of oxidized MWCNT was immersed into 100 mL of GA solution and it was sonicated for 1 h at room temperature. After that, neat PVA nanofiber coated pencil graphite electrode immersed into the cross-linking solution. After 1 h cross-linking, graphite electrode washed with ethanol and PBS (pH 7) respectively and dried at room temperature for 1 h. Figure 4.3 shows the experimental steps of interfacial cross-linking.

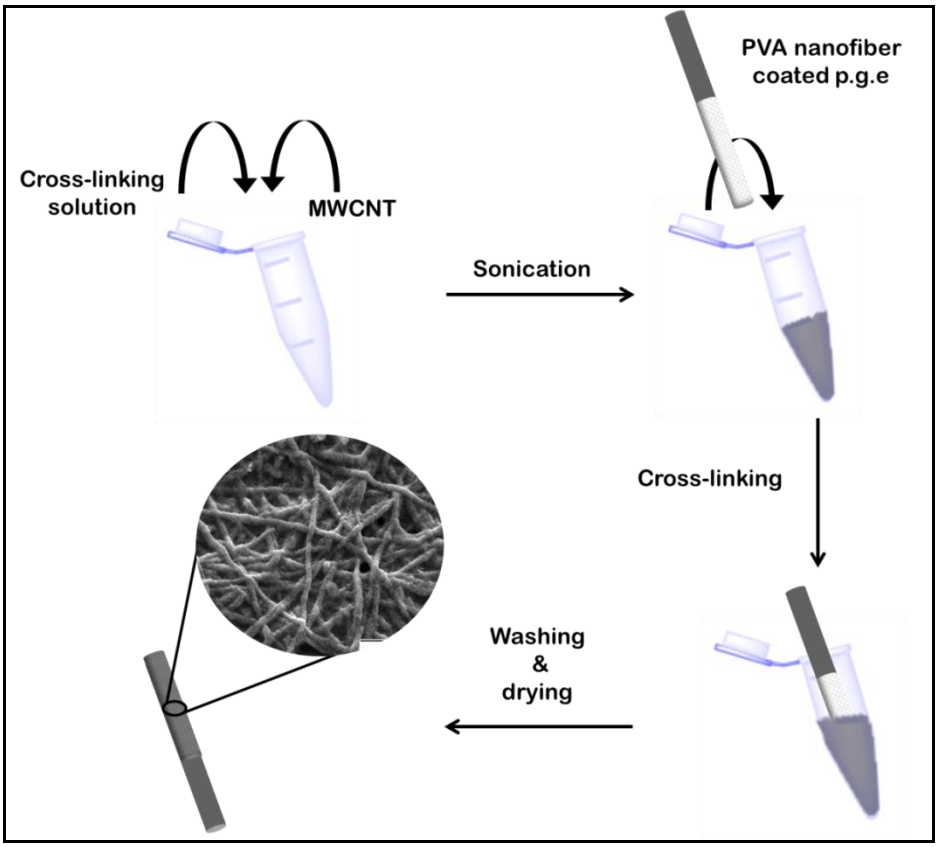

Figure 4.3. Schematic representation of interfacial cross-linking process

4.5.1. SECM Characterization of PVA Nanofiber Mats

In order to determine electrical conductivity of the neat and CNT immobilized PVA nanofiber mats, four different types of fiber mat samples were prepared and coded as S-1, S-2, S-3 and S-4. Sample S-1 was neat PVA fiber mat cross-linked with GA cross-linking solution. S-2 was neat PVA fiber mat cross-linked with GA cross-linking solution containing oxidized MWCNT, S-3 was PVA fiber mat containing MWCNT and cross-linked with GA cross-linking solution and S-4 was PVA fiber mat containing MWCNT and cross-linked with GA cross-linking solution containing MWCNT. S-1, S-2 and S-3 were also used in enzyme electrode preparation. In section 5.6.1, S-1 was named as **a)** *GOx immobilized PVA electrospun electrode*, S-2 was named as **e)** *Interfacially cross-linked PVA electrospun electrode containing PDDA functionalized MWCNT* and S-3 was named as **c)** *GOx immobilized PVA electrospun electrode containing PDDA*

functionalized MWCNT. Table 4.1 shows the SECM coding of the samples. Figure 4.4 shows the preparation steps of the samples.

Table.4.1. Sensor electrodes and SECM releated sample codes

Sensor electrode	**Sample code**
a) Glucose oxidase (GOx) immobilized PVA electrospun electrode	S-1
b) Glucose oxidase (GOx) immobilized PVA electrospun electrode containing multi- walled carbon nanotube (MWCNT)	None
c) Glucose oxidase (GOx) immobilized PVA electrospun electrode containing Poly(diallyldimethylammonium chloride) (PDDA) functionalized multi-walled carbon nanotube (MWCNT)	S-3
d) Glucose oxidase (GOx) immobilized PVA electrospun electrode containing Poly(diallyldimethylammonium chloride) (PDDA) functionalized single-walled carbon nanotube (SWCNT)	None

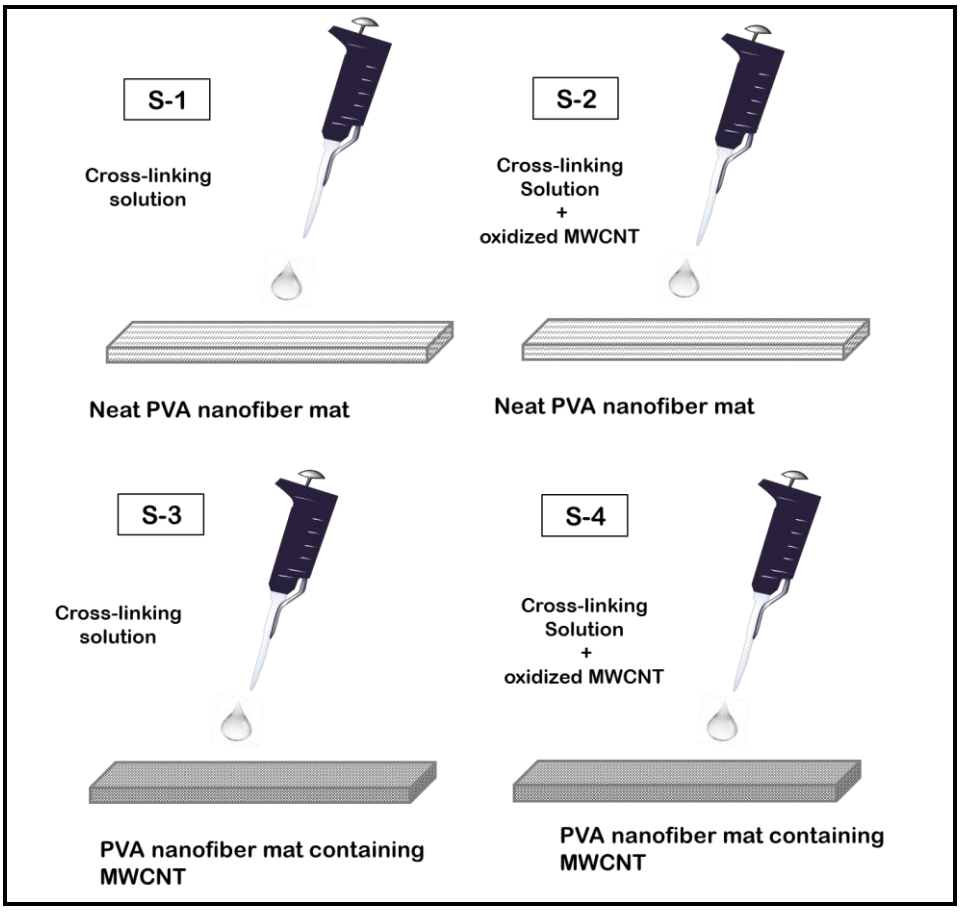

Figure 4.4. Preparation steps of the samples S-1, S-2, S-3, S-4

To perform the SECM measurements, 5×5 mm^2 of each sample was fixed with double side scotch onto a glass surface. Fixed sample was placed into a three-electrode electrochemical cell including platinum wire as counter electrode, silver wire as reference electrode and ultra- micro electrode as working electrode. All measurements were performed in 2 mM solution of FcMeOH in 0.1 M KCl. Soft probe SECM and standard probe SECM were performed. In soft probe SECM, printed graphite plastic microelectrode was used as working electrode. In standard SECM, platinum micro-electrode (25 μm diameter sized) was used as working electrode (Figure 4.5).

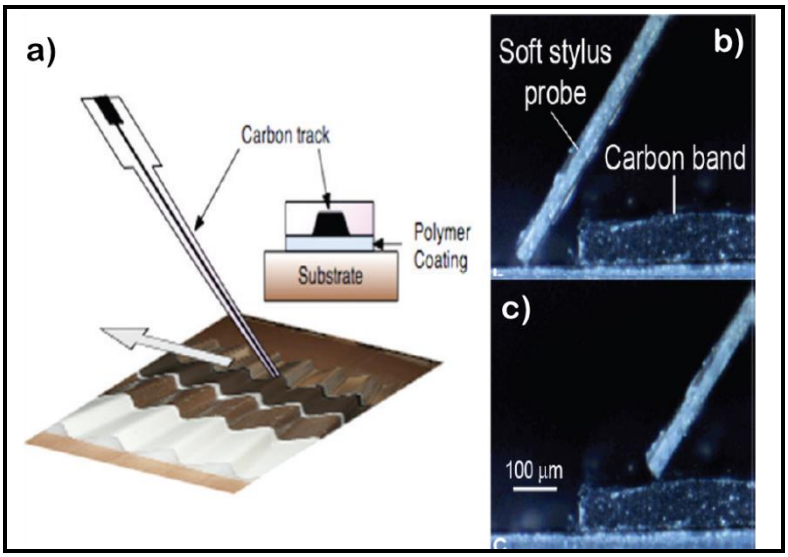

Figure 4.5. a) Schematic representation of a soft stylus probe used as a working electrode for SECM in a contact regime. b-c) Optical image of the soft stylus probe scanning in a contact regime above an unbiased substrate (Source: Cortes-Salazar et al. 2011)

4.6. Preparation of CNT-(PDDA/GOx)$_2$ Conjugate

(PDDA/GOx)$_2$ conjugate was generated on carbon nanotubes which were modified on PVA fiber structure. Immobilization steps were processed on pencil graphite electrode. 10 wt % aqueous solution of PDDA was dispersed by ultra-sonication for 1 h. Enzyme solution containing 2560 unit/mL GOx in 0.1M PBS (pH 7) was prepared. For the layer by layer immobilization of positive charged PDDA and negative charged GOx respectively onto the oxidized CNT, immobilization process was performed step by step (Figure 4.6) Firstly, pencil graphite electrode immersed in 5 mL PDDA solution and immobilization process took 15 min on an orbital shaker +4 ^{0}C. Then graphite electrode washed with PBS to remove the free PDDA. Secondly, PDDA immobilized pencil graphite electrode immersed in 5 mL of GOx solution during 15 min on orbital shaker at +4 ^{0} C. Using the same procedure, immobilization process was repeated two times to obtain two layers of PDDA/GOx conjugate. On the final step, pencil graphite electrode which is immersed in GOx solution incubated +4 ^{0} C for 24 h. Figure 4.7 shows the steps of layer by layer immobilization GOx/PDDA conjugate on oxidized CNT.

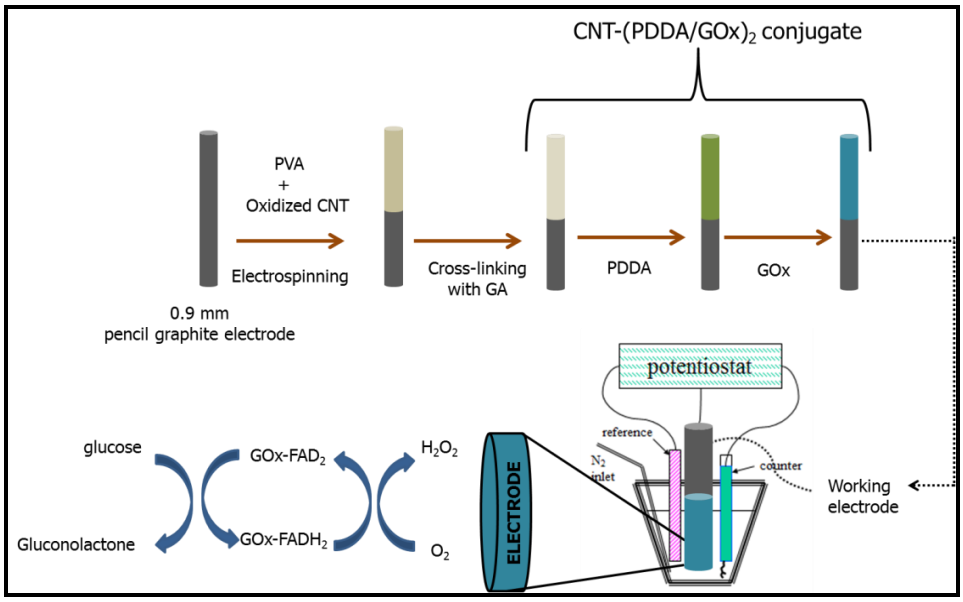

Figure 4.6. Glucose sensing electrode preparation steps

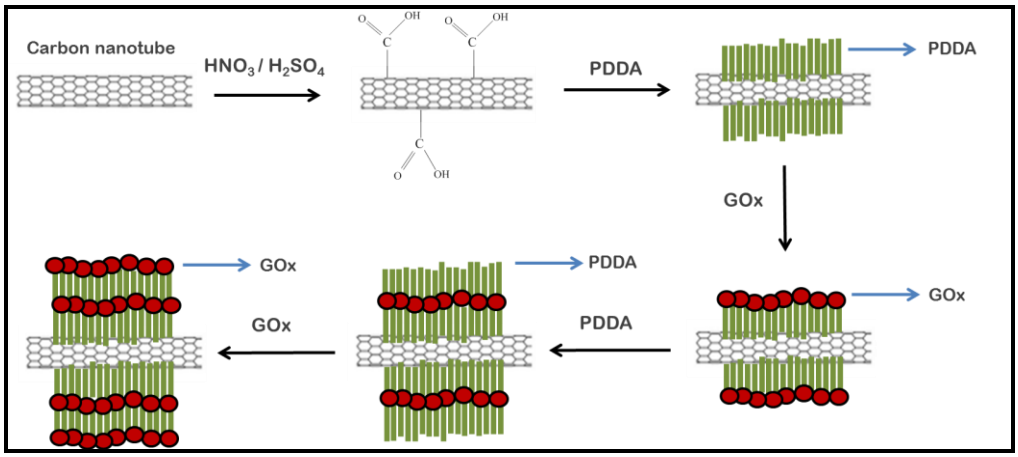

Figure 4.7. CNT-(PDDA/GOx)$_2$ conjugate preparation steps

4.7. Electrochemical Measurements

Cyclic Voltammetry and Chronoamperometry experiments were conducted using Gamry Instrument Reference 600-Potentiostat/ Galvanostat/ZRA.Three- electrode system including of the pencil graphite electrode (GE) as the working electrode, a reference electrode (Ag/AgCl) and platinum wire as the auxiliary electrode was used in

connection with Gamry Echem Analyst software. Cyclic Voltammetry was performed in air saturated solutions of 5 mM $Fe(CN)_6^{3-}$ / $Fe(CN)_6^{4-}$ redox couple in 0.1M KCl at a scan rate of 100 mV s^{-1}. Chronoamperometry measurements were performed in stirred 0.1 M PBS at -0.5 V. *i-t* curve technique was used to detect glucose in PBS. The detection of varying concentration of glucose was processed by injection of varying volumes of 20 mM glucose solution into stirred PBS.

Electrochemical Impedance Spectroscopy (EIS) experiments were conducted using the AUTOLAB PGSTAT204 Compact and modular potentiostat/Galvanostat. Measurements were performed in a mixture of 2.5 mM (1:1) $Fe(CN)_6^{3-}$ / $Fe(CN)_6^{4-}$ in 0.1 M KCl solution and between the frequency range of 10^{-1} -10^5 Hz. A potential +0.23 V DC voltage versus Ag/AgCl and 10 mV of AC signal was applied through the EIS measurements. All the EIS measurements were performed in faraday cage.

CHAPTER 5

RESULTS AND DISCUSSION

5.1. Characterization of Polyvinyl Alcohol Electrospun Nanofibers

Three processing variables, applied voltage, solution flow rate and tip-collector distance were studied for the fabrication of sensitive electrospun mat for the biosensing of glucose. Electrospinning conditions were fixed at 25 kV applied voltage, 4 mL/h flow rate and 20 cm tip to collector distance. The concentration of spinning solution was kept at 20 wt % and smooth and continuous fiber formation was observed. Figure 5.1 shows the photographic image of PVA electrospun nanofibers, SEM micrograph and fiber diameter distribution of the PVA electrospun nanofibers. The average diameter of the electrospun PVA fibers was 115 nm and no beat formation on fiber surface was observed.

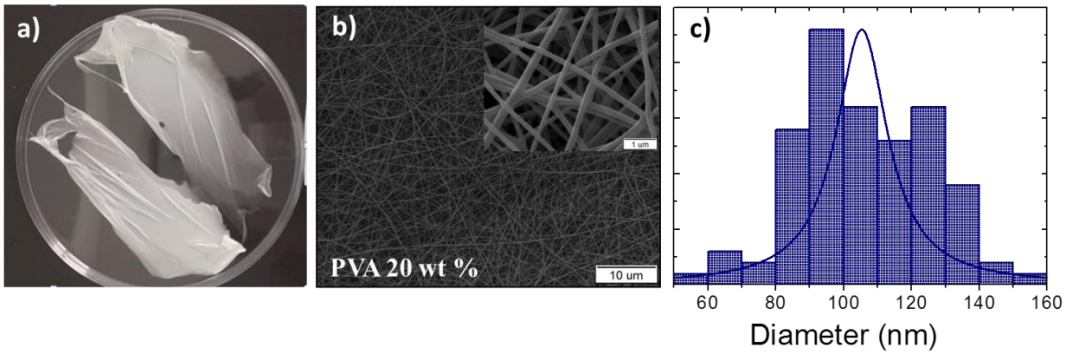

Figure 5.1. (a) Photographic image of PVA electrospun nanofibers, (b-c) SEM micrograph and fiber diameter distribution of the PVA electrospun nanofibers

After crosslinking, the smooth fibrous morphology of nanofibers did not significantly change but the average fiber diameter was increased. Fiure 5.2 shows the SEM micrograph and fiber diameter distribution of time dependent cross-linking of PVA electrospun fibers a) PVA pristine, b) 1 h c) 3 h d) 24 h cross-linked. Table 5.1 shows the diameter distributions of the fibers for defined cross-linking times.

After 1 hour cross-linking, the average fiber diameter reached to 122 nm, this value increased to 136 nm after 3 hours cross-linking time and for the 24 hours cross-linking average fiber diameter was observed as 190 nm. This increase in fiber diameter after cross-linking is due to the swelling of the nanofibers during the GA crosslinking process.

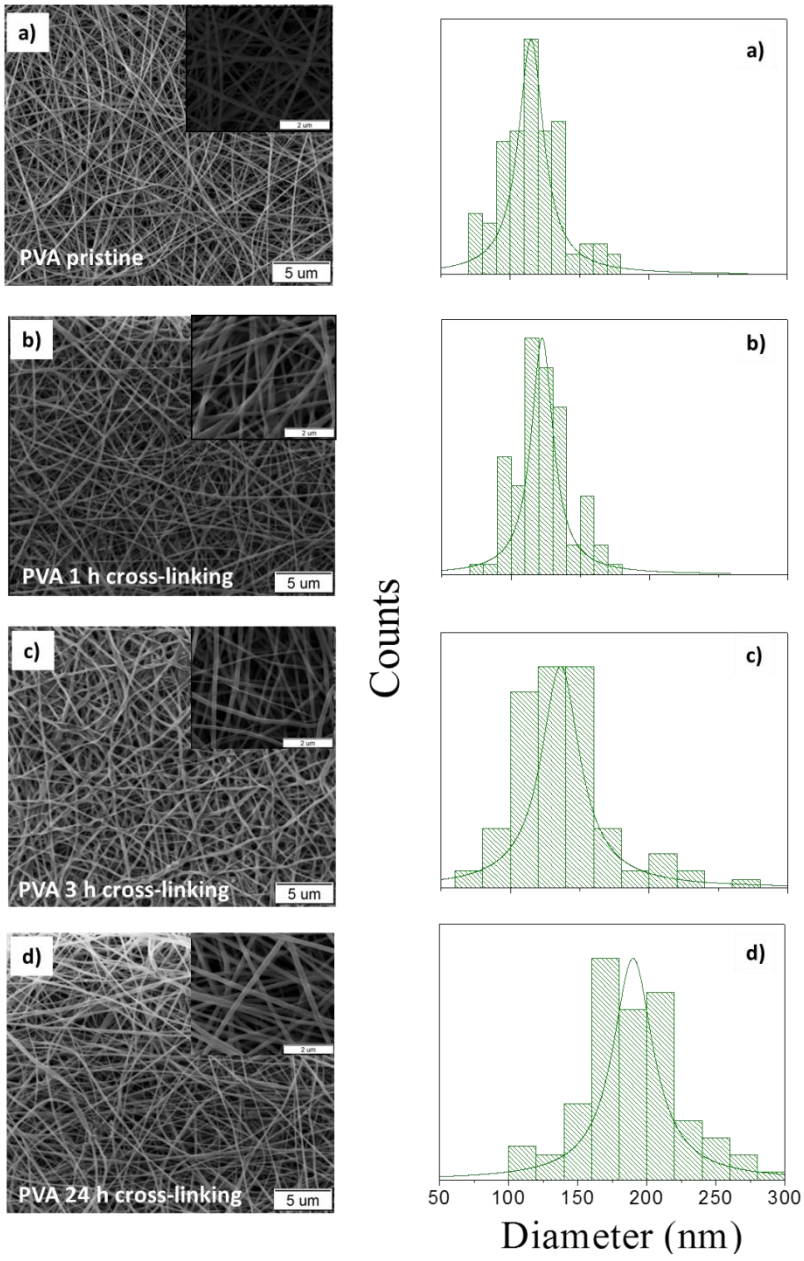

Figure 5.2. SEM micrograph and fiber diameter distribution of time dependent cross-linking of PVA electrospun fibers a) PVA pristine, b) 1 h c) 3 h d) 24 h cross-linked.

Table 5.1. Characteristics of PVA fiber membranes before and after crosslinking

Cross-linking time	**Average fiber diameter ± SD (nm)**
Pristine PVA	115 ± 22
1 h	122 ±19
3 h	136 ± 34
24 h	190 ± 35

Figure 5.3 shows the ATR FT-IR spectra of neat and 1-3-24 hours cross-linked PVA nanofibers. Neat PVA shows characteristic bands at 3300 cm^{-1} that refers the hydroxyl groups on the polymer chain. After cross-linking, intensity of hydroxyl group at 3565-3000 cm^{-1} was relatively decreased compared with the neat PVA nanofibers, which is due to the interaction between –OH group in PVA and -CHO in glutaraldehyde. Also it is observed that there is no remarkable difference on the intensity of hydroxyl groups between 1, 3 and 24 hours cross-linked PVA nanofibers. The absorbance at 1720, 2731, and 2866 cm^{-1} attributes the aldehyde groups. The increase in the absorbance between 970 and 1385 cm^{-1} causes from the generation of acetal ring and ether linkage as a results of the reaction between the hydroxyl groups and the aldehydes (Yeom and Lee 1996b).

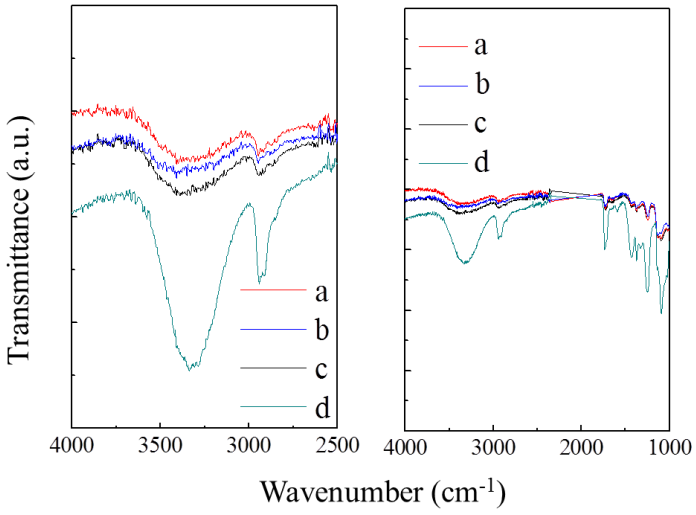

Figure 5.2. ATR FT-IR spectra of PVA nanofibers, a) 3h, b) 24 h c) 1 h cross-linked PVA fibers, d) neat PVA fibers

5.2. PVA Coating of Pencil Graphite Electrode

Figure 5.4 shows the photographic image of PVA coated (a) and bare (b) pencil graphite electrode. Depending on the conductive characteristic of the graphite, pencil electrode surface was coated with the PVA electrospun nanofiber by electrospinning process. To determine the time dependent PVA coting thickness on the surface, three different fiber coating time processes were performed as 1,2 and 5 min at 25 kV applied voltage, 4 mL/h flow rate and 20 cm tip to collector distance. Fiber thickness on the electrode surface was examined on SEM. Figure 5.5 shows the SEM images of the PVA coated pencil graphite electrodes for 1, 2 and 5 min fiber coating time. 1, 2 and 5 min PVA spinning times were resulted in 9, 24 and 30 μm fiber thickness on the graphite surface, respectively. It was observed that, there is not a linear correlation between the fiber coating time and the fiber mat thickness (Figure 5.6) because of the non-conductive nature of the PVA. Increased surface thickness decreases the conductivity of the graphite and fiber deposition amount decreases.

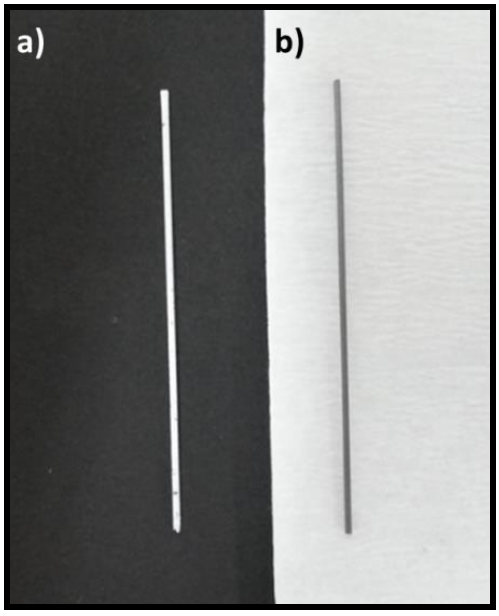

Figure 5.4. Photographic image of a) PVA coated pencil graphite electrode
b) bare pencil graphite electrode

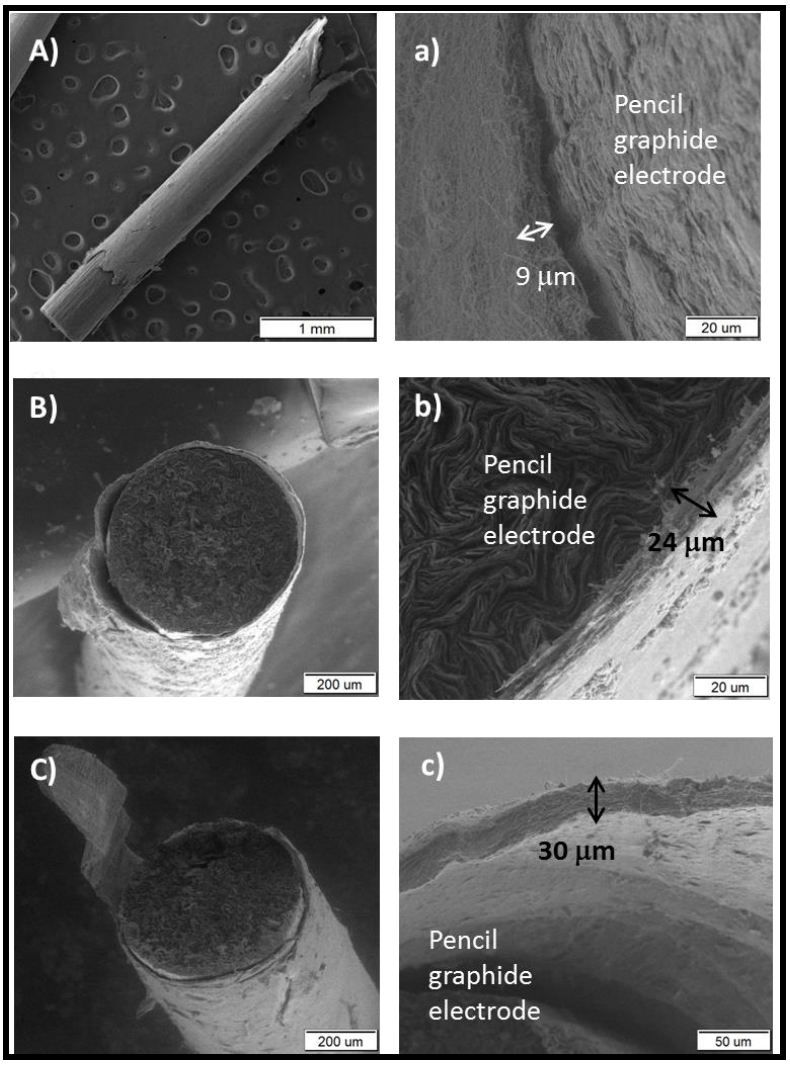

Figure 5.5. SEM micrograph of pencil graphite electrodes with PVA fiber coating in various spinning times. A) 1 min, B) 2 min C) 5 min

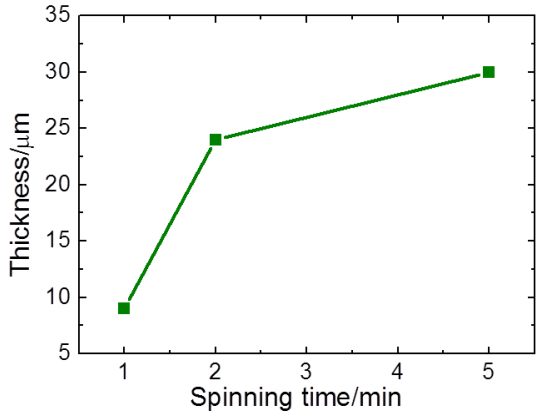

Figure 5.6. Relationship between the thickness of the fiber mat on the electrode surface and PVA spinning time

5.3. Electrochemical Characterization

PVA coating uniformity and fiber thickness dependent electro activity of the modified electrodes was evaluated by using the cyclic voltammetry (CV) method. CV responses of the electrodes were investigated in a solution including 5 mM $Fe(CN)_6^{3-/4-}$ in 0.1M KCl and cyclic voltammograms were obtained by scanning the potentials between 650 mV and -100 mV at 100 mV/s scan rate. Considering the electrode reaction as ferricyanide is reduced to ferrocyanide (Eq.5.2), the peak current, I_p is governed by the Randle-Sevcik equation; where the $k = 2.72 \times 10^5$, n is the number of moles of electrons transferred, A is the area of the electrode in cm^2, D is the diffusion coefficient in cm^2/s, C^b is the solution concentration in M and v is the scan rate of the potential in volts/s.

$$Fe^{III}(CN)_6^{3-} + e^- \longleftrightarrow Fe^{II}(CN)_6^{4-} \quad (5.1)$$

$$I_p = k\, n^{3/2} A\, D^{1/2} C^b v^{1/2} \quad (5.2)$$

Figure 5.7 shows the cyclic voltammograms of bare and PVA nanofiber modified pencil graphite electrodes. A well-defined redox peak pairs was obtained on the bare pencil graphite electrode at 76.8 µA and -76.8 µA current values. After 1 min coating of PVA nanofiber mat on the graphite electrode surface, redox peak currents were decreased to 0.3 µA and -0.3 µA. After 2 min coating, redox peak current values were decreased to 0.27 µA and -0.27 µA and 5 min PVA coating was resulted in 0.027 µA and -0.027 µA peak current values. The current decrease indicates the obstructed electron transfer process induced by the non-conductive PVA fiber surface. Referring to Randle-Sevcik equation (2), number of moles of electrons transferred (n) is the one of the distinctive parameter for the PVA modified species. Another parameter is the area of the electrode surface (A). Since the PVA nanofibers which have 115 nm average diameter distribution blockade effective electron transfer to the graphite surface through the nanofiber network with respect to unmodified graphite electrode. Thus, the peak potential decreases dramatically. Figure 5.8 summarizes the relationship between the thickness of the fiber mat on the electrode surface, PVA spinning time and peak current.

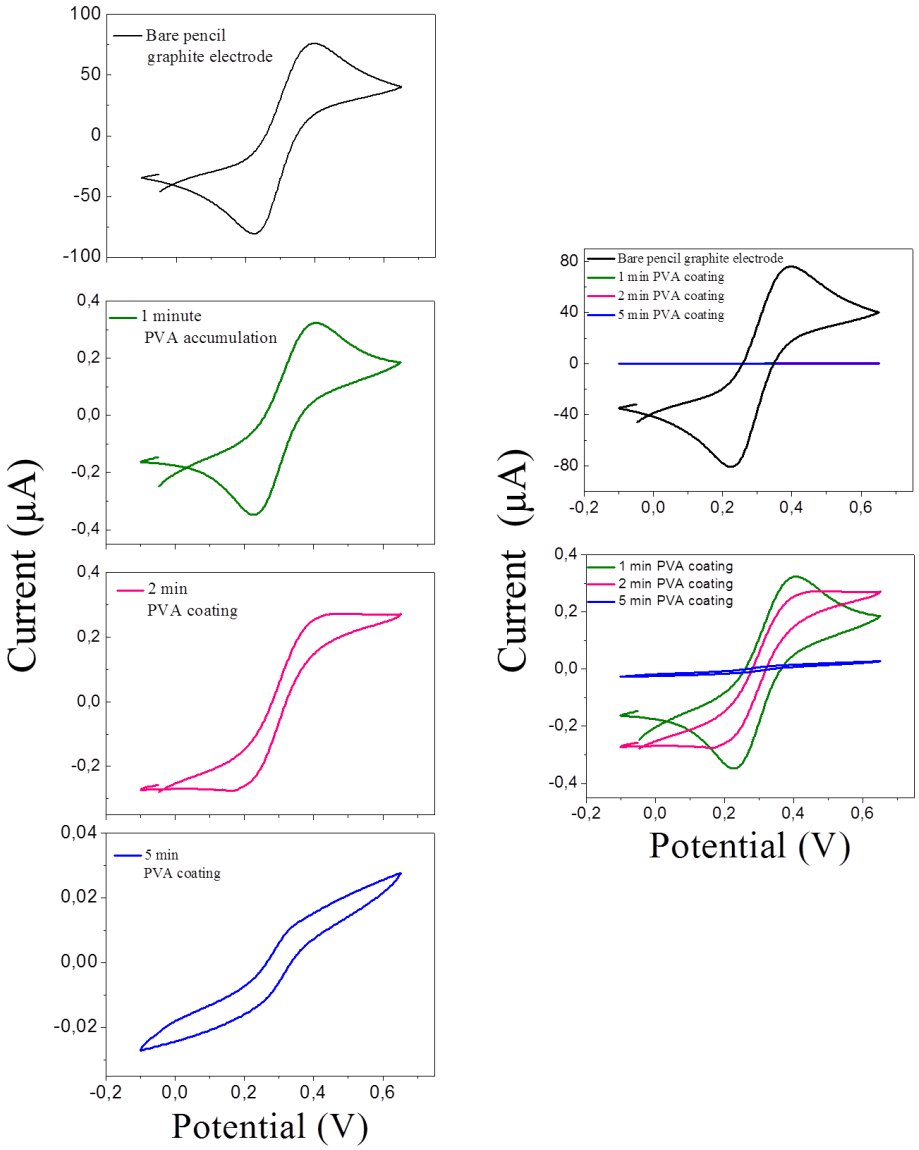

Figure 5.7. Cyclic voltammograms of bare and PVA nanofiber modified pencil graphite electrodes in 5 mM $Fe(CN)_6^{3-/4-}$ solution in 0.1M KCl

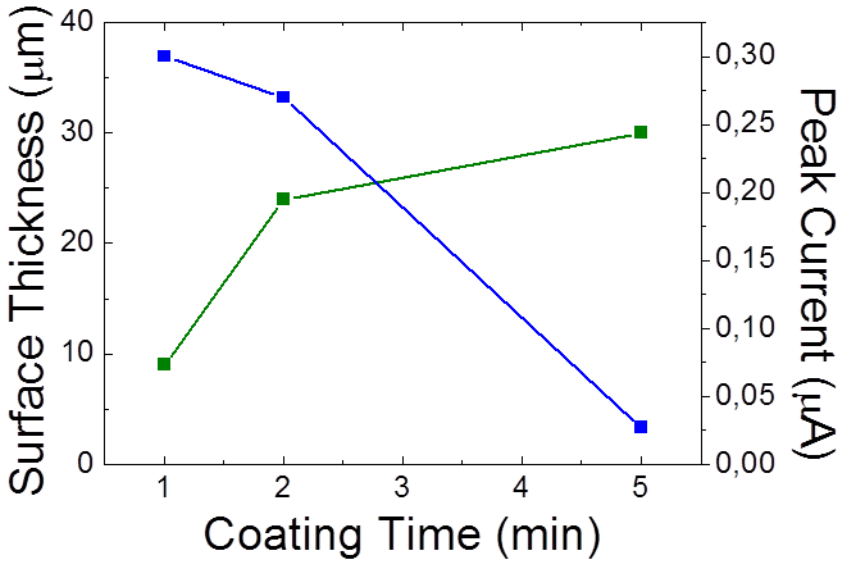

Figure 5.8. Relationship between the thickness of the fiber mat on the electrode surface, PVA spinning time and peak current.

Electrochemical Impedance Spectroscopy (EIS) is an effective method for evaluating the interface characteristics of modified electrodes. The value of electron transfer resistance R_{ct} (semicircle diameter), depends on the insulating and dielectric properties of the electrolyte/electrode system. Increased R_{ct} value verifies a hindrance or resistance of electron flow caused by addition of a substance on the surface of the electrode and that results an increase in R_{ct} value. Figure 5.9 compares the Nyquist plots of the impedance spectroscopy of blank and PVA modified pencil graphite electrodes. On the graph, Z'' is the real variable and Z' is the negative value of the imaginary variable of impedance. In Figure 5.9 (a), 1 minute PVA coated graphite electrode shows greater semicircle compared to the blank graphite electrode that verify the largest electron transfer resistance due to the insulating effect of non-conductive PVA layer. PVA nanofiber layer prevents the electron motion of redox couple Fe $(CN)_6^{3-/4-}$ through the graphite surface. With the further coating of graphite electrode (Fig 5.9. b-c) the graphite surface turned more resistive thus there was an increase at R_{ct} values in the order of 5 min > 2 min > 1 min > blank.

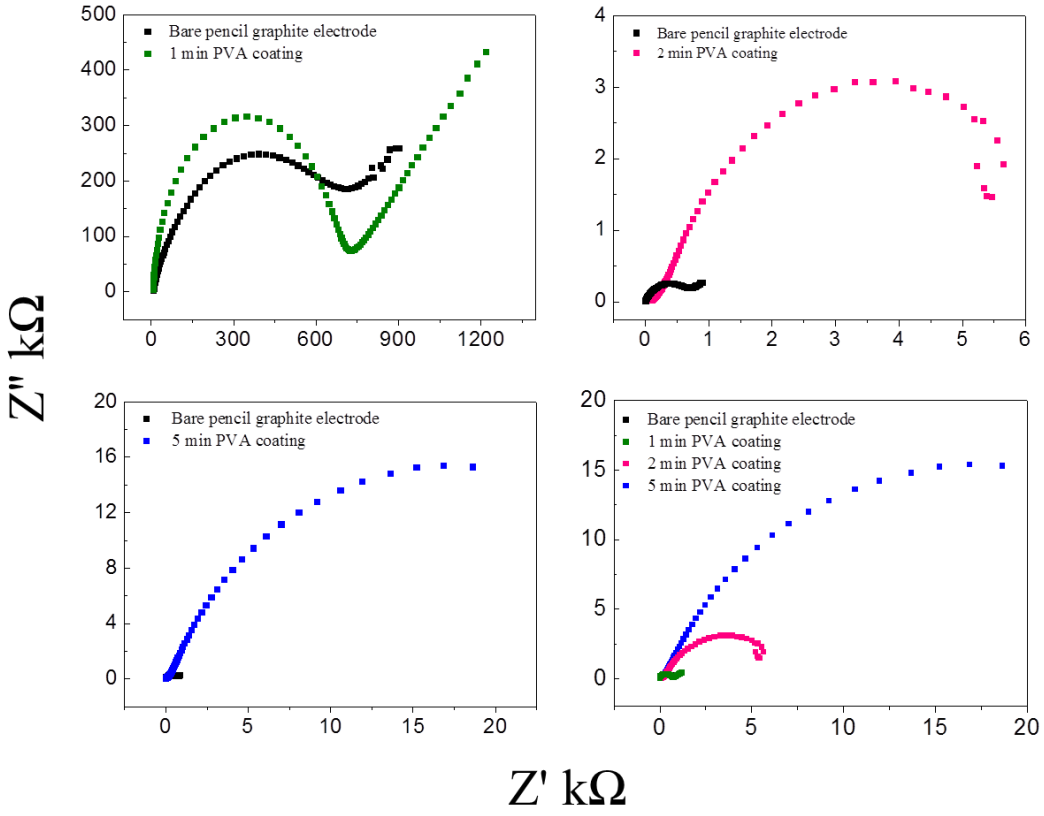

Figure 5.9. Electrochemical impedance spectra of bare and PVA modified pencil graphite electrodes in 5 mM $Fe(CN)_6^{3-}$ / $Fe(CN)_6^{4-}$ in 0.1M KCl

5.4. Characterization of Functionalized CNTs

5.4.1. Effect of CNT Surface Modification

Oxidative surface modification of carbon nanotubes (CNTs) changes the physical morphology of the pristine CNT. This process creates defect sites and incorporates carboxyl groups (COOH) to the sidewall at this defect sites. Modified carboxyl groups (COOH) decreases the degree of agglomeration thus provides a dispersion state for the nanotubes and by constituting of atomic spaces or reactive regions, reinforces their chemical reactivity for covalent bonding of functional groups along the surface or on the side walls of the nanotubes. Oxidation decreases the length of CNTs in a degree of more than half its normal length, decreases the diameter, dissipates the amorphous carbon (Rosca et al. 2005) and increases the number of CNTs

with open end region which provides reactive sites for the secondary functional group addition.

5.4.2. Raman Spectroscopy

In the high frequency region of Raman Spectra (1000-3500 cm^{-1}), three characteristic bands are observed which is specific for CNTs. These bands refers the graphite band (G band) at 1580 cm^{-1}, the disorder/defect band (D band) at 1330 cm^{-1} and G' band at 2674 cm^{-1} . The ratio of the D and G band peak intensities ($I_{D/G}$) is related with the degree of disorder or defect of the nanotube surface. Increased $I_{D/G}$ ratio refers the high proportion of sp^3 carbon and the presence of sp^3 carbon is attributed to structural defects. And G' band predicates the over tone of D band of the structure. Figure 5.10.a shows the Raman spectra of pristine and functionalized single- walled carbon nanotubes (SWCNTs). Characteristic D and G peaks of CNTs can be observed for the pristine SWCNTs at 1336 and 1583 cm^{-1} respectively. G' band location is observable at 2674 cm^{-1} that refers the double value of the D band intensity. After oxidative surface modification was performed, these characteristic peaks were still observable which means that surface modification process does not change the structural geometry of the nanotube. Evaluating the $I_{D/G}$ values for pristine and functionalized species, the $I_{D/G}$ value for non-functionalized SWCNT is 0.113 and it is 0.667 for functionalized SWCNT (Table 5.2). This increase in $I_{D/G}$ value can be interpreted as oxidation process breaks some bonds on the nanotube surface and inserts chemical groups to these regions. The results indicate that oxidative surface functionalization is achieved by the acid treatment process.

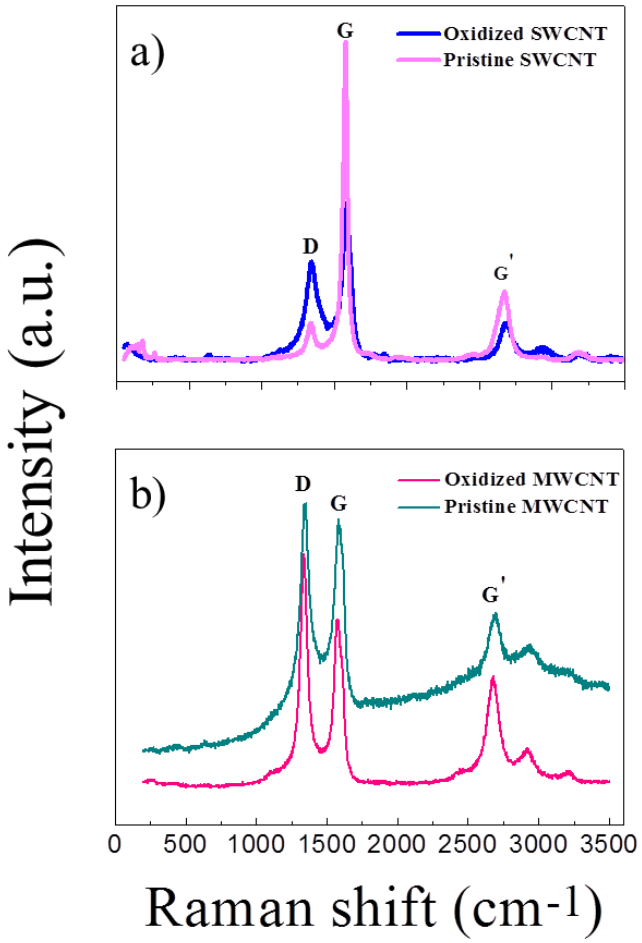

Figure 5.10. Raman spectra of pristine and oxidized a) SWCNT, b) MWCNT

Table 5.2. The values of D band intensity and D/G ratio for pristine and carboxy-functionalized SWCNTs

Type of SWCNTs	D band intensity	D/G ratio
Pristine	350	0.113
Functionalized	926	0.667

Figure 5.10.b shows the Raman spectra of pristine and functionalized multi-walled carbon nanotubes (MWCNTs). Three strong peaks are identified at 1345, 1581, 2674 cm^{-1} which refers to D, G and G' bands, respectively. D band refers the

defect/disorder characteristic and G band refers the graphitic characteristic of the surface. As shown in Table 5.3, $I_{D/G}$ value for non-functionalized MWCNT is 1.06 and it is 1.393 for functionalized MWCNT. The other parameter that identified the nanotube surface defect is ($W_{G,1/2}$), which defines the full width at half height of G band also an increase in this value identify the nanotube surface defect. This value is 83.5 for pristine MWCNT and it is 85 for the modified MWCNT.

Table 5.3. The values of D band intensity, full width at half height of G band ($W_{G,1/2}$), and D/G ratio for pristine and carboxy-functionalized MWCNTs

Type of MWCNTs	**D band intensity**	**D/G ratio**	**$W_{G,1/2}$ (cm^{-1})**
Pristine	918	1.06	83.5
Functionalized	1104	1.393	85

5.5. Characterization of PVA- Carbon Nanotube (CNT) Composite Nanofiber Mats

5.5.1. SEM Characterization

Figure 5.11 shows the SEM micrograph of S-1, S-2, S-3 and S-4 For the fixed electrospinning process parameters, average diameter of the S-1 is 119 nm and average diameter of S-3 is found as 164 nm. As shown in the diameter distribution diagram, carbon nanotube addition to the PVA solution leads an increase in fiber diameter. This increase can explaned by the volume effect of the nanotubes located on the fiber. Another reason could be the increase of conductivity which decreases the flow resistance of the polymer solution and this state mimics the increased flow rate condition which causes the higher diameter fiber formation. Average diameter of S-4 was found as 347 nm. Considering 119 nm average fiber diameter of the pristine PVA membrane, approximately 30 nm MWCNT coating was processed on the PVA fiber surface. Also, MWCNT's dispersed state distribution can be observed on the fiber surface.

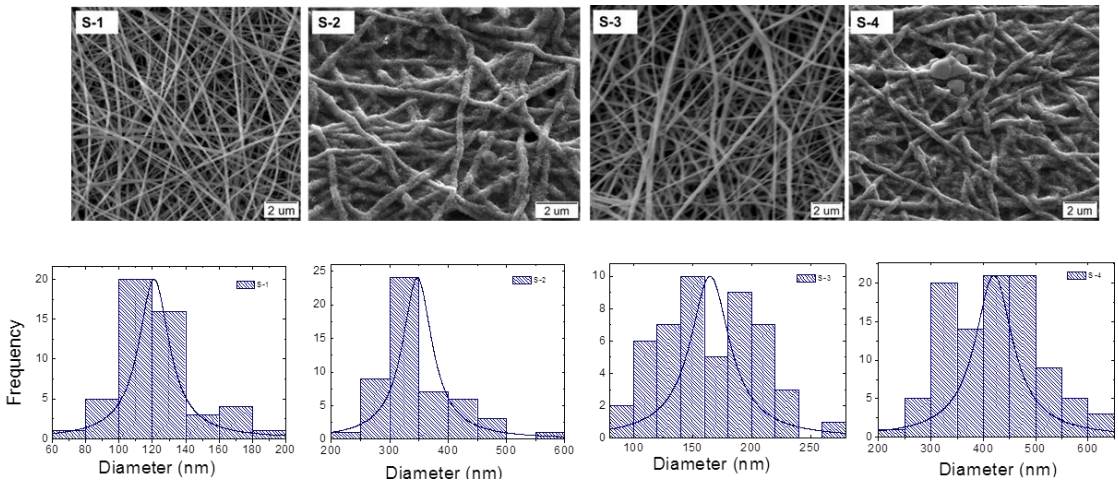

Figure 5.11. SEM micrograph and diameter distribution graph of S-1, S-2, S-3, S-4

5.5.2. SECM Characterization

Figure 5.12. shows typical SECM line scans of S-1, S-2, S-3 and S-4 recorded above a border region between the clean glass slide and the sample surfaces. Current increments, due to the positive feedback effect were recorded when the microelectrode travelled above the regions from -8900 to -6700 for S-1, S-2 and from -5000 to -2900 for S-3, S-4. Lower current values were recorded as long as the microelectrode was travelled above the glass slides (from -5000 to -6000 and from 0 to -3000). Line scans with approximately similar features and relatively different current changes were obtained above the different nanofiber surfaces. The unstable current changes were essentially due to the roughness topography of the samples which could affect the tip-current responses (Battistel, Daniele, and Fratter 2012). In consideration of the local current responses of the samples, lower current response was observed for the sample S-4. Current response of S-4 fluctuates between 8 and 9 nA. Current responses of S-3 and S-1 change between 9 -11 nA and 9-12 nA respectively. The higher current response was obtained for the sample S-2 that changes between 9 and 13 nA.

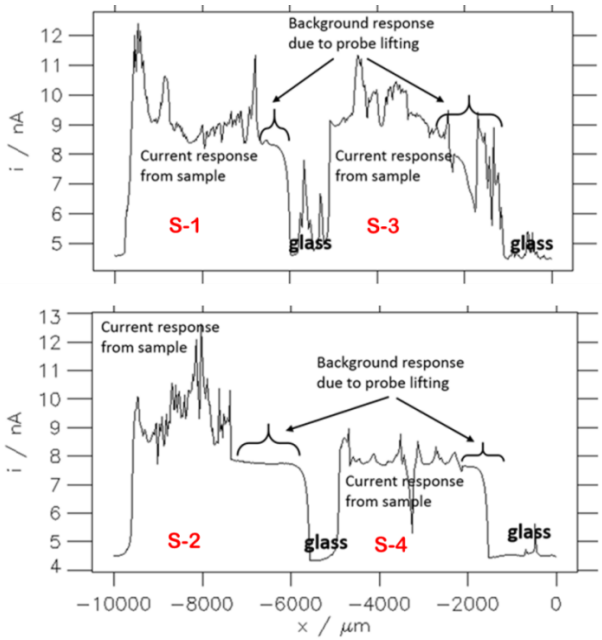

Figure 5.12. Soft probe SECM profile for S-1, S-2, S-3 and S-4. Scan rate 100 µm/s. 2mM FcMeOH in 0.1 M KCl, E tip = 0.5V vs Ag.

Figure 5.13 shows the current against distance plots recorded while the microelectrode approaching to the surface and passing through the samples S-1, S-2, S-3 and S-4. In consideration of the surface conductivity, the distance between the micro-electrode and the sample surface was approached to zero, tip current responses of the species were observed as 6.1, 12, 5.9 and 4.8 nA for S-1, S-2, S-3 and S-4 respectively. Only S-2 exibits detectable surface conductivity as 12 nA.

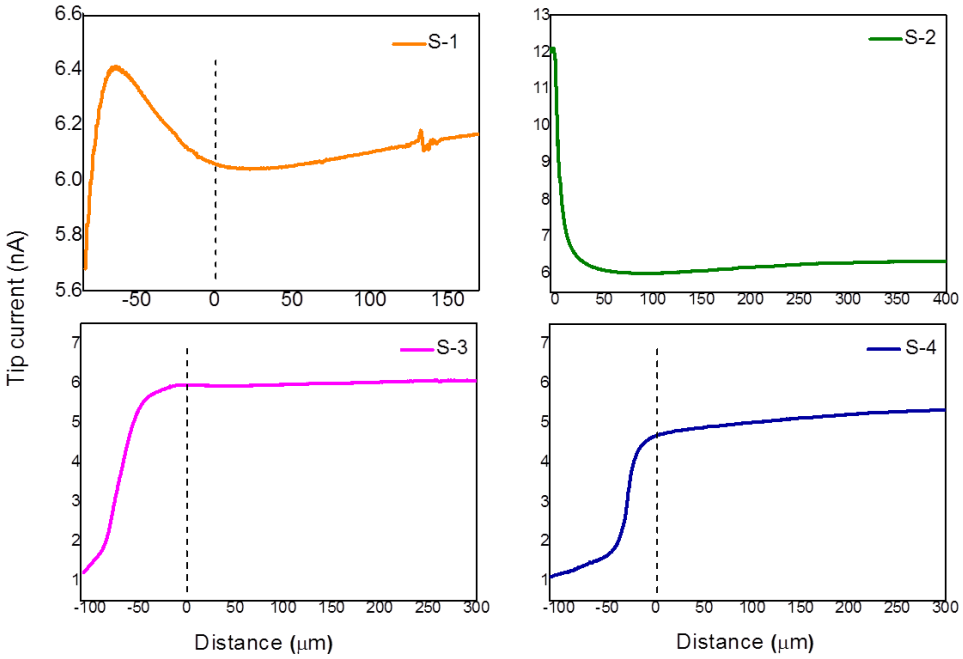

Figure 5.13. Approach curves recorded for the samples S-1, S-2,S-3 and S-4. 2 mM FcMeOH in 0.1 M KCl, E tip = 0.5V vs Ag

5.5.3. Electrochemical Characterization

Electrochemical characterizations of bare pencil graphite electrode (PGE), PVA nanofiber coated pencil graphite electrode (PGE/PVA), MWCNT enhanced PVA nanofiber coated pencil graphite (PGE/PVA-MWCNT) and Interfacial cross-linked PVA/MWCNT coated nanocomposite electrodes were performed by using cyclic voltammetry (CV). CV measurements were performed in 4.8 mM K_3 [Fe $(CN)_6$] and 0.1 M KNO_3 for reversible redox couple reaction at a potential range of −0.2 to 0.5 V versus Ag/AgCl at scan rate of 100 mV/s. When the oxidation current response was 25 μA at PGE/PVA, at the PGE/PVA-MWCNT current response increased to 45 μA. This relatively stronger electroactive state of PGE/PVA-MWCNT interpreted to the presence of MWCNTs on/in the PVA nanofiber (Figure 5.14) During the nanofiber fabrication process, carbon nanotubes show two phase separation as the inside and the outside (surface) of the fiber. Inside located carbon nanotubes are insulated by the non-conductive PVA layer. Therefore, total mass effect of used 2 wt % MWCNT does not contribute to the conductive characteristic of the nanofiber. On the other hand,

increasing carbon nanotube content limits the electrospinning efficiency of the PVA solution. Interfacial cross- linked PVA/MWCNT coated nanocomposite electrode shows approximately two times higher current response than PGE/PVA-MWCNT electrode. Coating the fiber surface by the dispersed carbon nanotube stack enhances the electron transfer efficiency between the redox couple and the pencil graphite electrode surface.

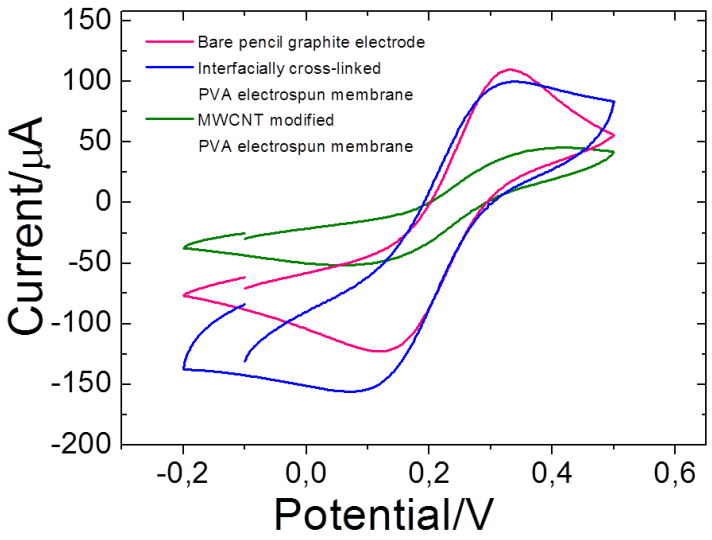

Figure 5.14. Cyclic voltammograms of bare, PVA/MWCNT modified (2 wt %) and interfacially cross- linked PVA/MWCNT PGE

5.6. Enzyme Electrodes

PDDA wrapping of MWCNT surface enhanced the dispersion of the oxidatively functionalized carbon nanotubes in the PVA matrix. Positive charges on protonated nitrogen in PDDA chains generates electrostatic repulsive forces between PDDA wrapped MWCNTs and prevents the nanotube aggregation. Secondly, at pH 7.4, GOx is negatively charged. Thus, GOx electrostatically binds to the surface of the carbon nanotubes.

Figure 5.15.a shows the SEM image of pencil graphite electrode wrapped with two layers of PDDA/GOx modified PVA/MWCNT electrospun membrane. Proceeding of the PVA fiber surface with PDDA and GOx has no defective effect on fiber network on PG. PDDA/GOx modified PVA/MWCNT electrospun membrane

fibers (Figure 5.15.b) shows conserved fibrous morphology and no bead formation is observed on the surface inflicted on the residual PDDA and GOx. Thickness of the two layers of PDDA/GOx modified PVA/MWCNT electrospun membran was defined as 8.7 μm (Figure 5.15.c). To identify the effect of PDDA/GOx layer number on the sensing properties of the electrode, five layers assembling was processed. Three layers (PDDA/GOx) addition caused approximately three times increasing on the thickness of the membrane (Figure 5.15.d).

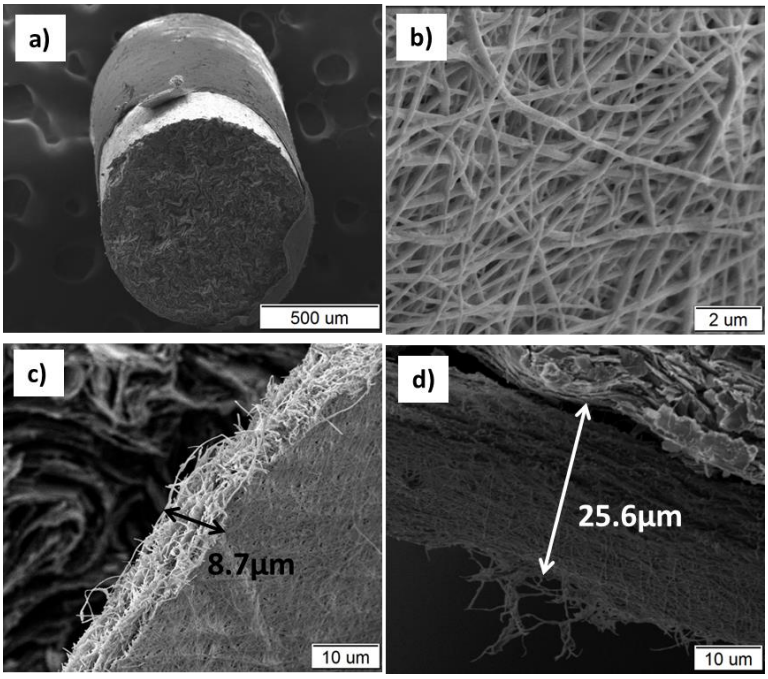

Figure 5.15. SEM micrograph of a) Two layers of PVA(MWCNT)/ GOx/ PDDA immobilized pencil graphide electrode, b) PVA(MWCNT)/ GOx/ PDDA membrane c) Surface thickness for two layers PVA(MWCNT)/ GOx/ PDDA membra d) Surface thickness for five layers PVA(MWCNT)/ GOx/PDDA membrane

5.6.1. Glucose sensing activities of the enzyme electrodes

Comparative glucose sensing property studies were performed for the six different electrodes as; a) *bare pencil graphite electrode,* b) *GOx immobilized PVA electrospun electrode,* c) *GOx immobilized PVA electrospun electrode containing MWCNT,* d) *GOx immobilized PVA electrospun electrode containing PDDA functionalized MWCNT,* e) *GOx immobilized PVA electrospun electrode containing PDDA functionalized SWCNT,* f) *Interfacially cross-linked PVA electrospun electrode containing PDDA functionalized MWCNT.* For the all species, glucose sensing activity of the electrodes were measured amperometrically at an applied voltage -0.5 V with the successive addition of glucose.

The *bare pencil graphite electrode* was used as control electrode to check the physical stability of three electrode electrochemical cell system. Thus there was no GOx immobilization on the surface of the bare graphite electrode. Figure 5.17.a. shows the steady state amperometric response of the bare pencil graphite electrode to the successive addition of glucose and resulting current increment versus glucose concentration profile (Figure 5.16.b) and calibration curve (Figure 5.16.c). In consideration of the reaction between glucose and the FADs in glucose oxidase (reactions 5.3-5.5), glucose addition leads to the reduction of FAD (forward of reaction 5.4) and increases the concentration of $FADH_2$ and in turn, oxidation of $FADH_2$ (reverse of reaction 5.2) occurs during chronoamperometry measurements. Presence of glucose in a GOx containing medium, results in increased peak current. This increment is directly propotional to the concentration of the added glucose. For the bare graphite glucose sensing electrode, the current response was increased non-linearly (Figure 5.16.c). Linear function of the obtained calibration curve does not show a correlation between the current response and the glucose concentration. Thus, the regression value of the linear function is 0.0204 indicating that there is not a an agreement between the concentration of glucose and the resulting current response. This non-linear and random distribution of the current response caused by the absence of GOx in the reaction medium. Increasing current drift between -16 μA and -21μA can arise from the physical unstabilitiy of our three electrode electrochemical system.

$$Glucose \rightarrow 2H^{+} + 2e^{-} + Gluconolactone \quad (5.3)$$

$$GOx\ (FAD) + 2H^{+} + 2e^{-} \rightarrow GOx\ (FADH_2) \quad (5.4)$$

$$Overall : Glucose + GOx\ (FAD) \rightarrow GOx\ (FADH_2) + Gluconolactone \quad (5.5)$$

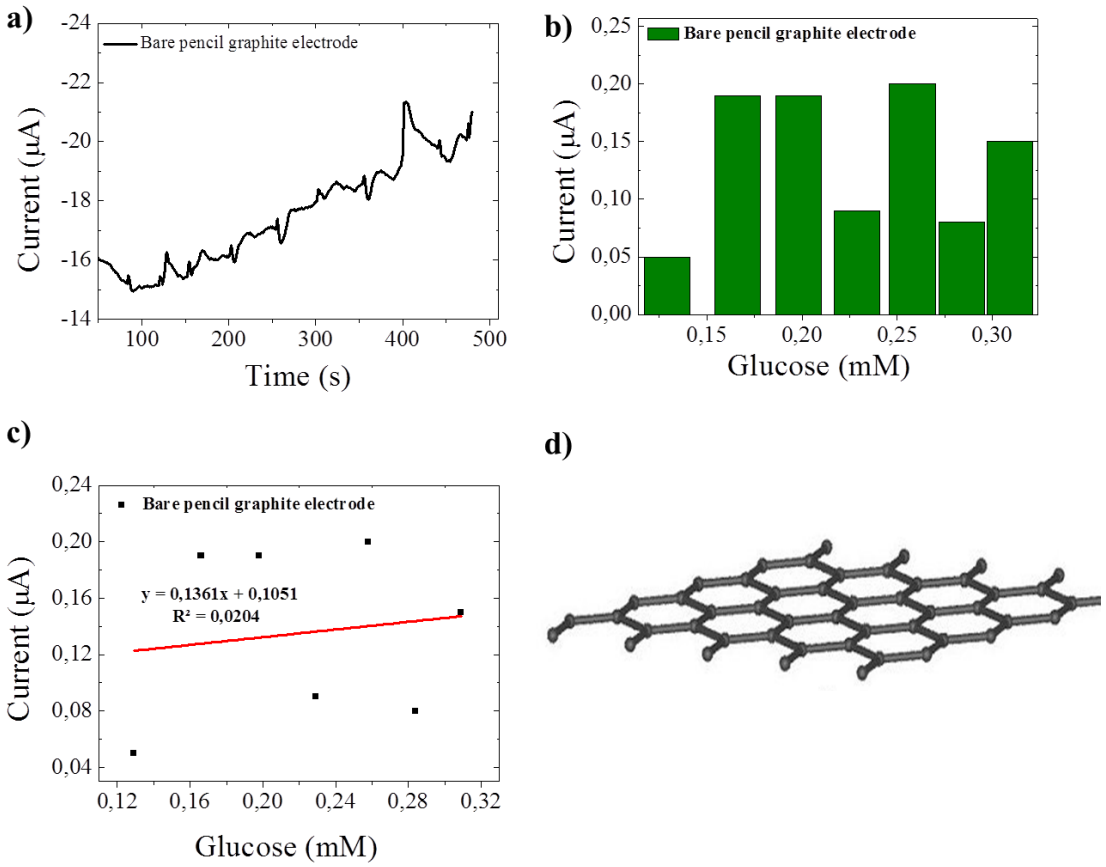

Figure 5.16. a) Amperometric response of bare pencil graphite electrode b)Relationship between current increment versus glucose concentration,c) Calibration curve, d) Schematic of the electrode surface

Figure 5.17 shows the chronoamperometric response of the *GOx immobilized PVA electrospun electrode* to the successive addition of glucose (a), resulting current increment versus glucose concentration profile (b), calibration curve (c) and schematic of the electrode surface (d). For the each injection of glucose, a smooth increase (~ 1 µA) in current response was observed momentarily and then current response showed a

decrease showing difference with 0.50 µA . The decrease on the current value might arise from two effects- detaching of GOx molecules from the PVA fiber surface in stirring aquous medium and the non-conductive PVA membrane repress the consistent electron transfer between the enzyme and the electrode. Linear function of the calibration curve does not show a correlation between the current response and the glucose concentration. The regression value of the linear function is 0.6121. However, glucose detection limit of the electrode was defined as 0.0476mM.

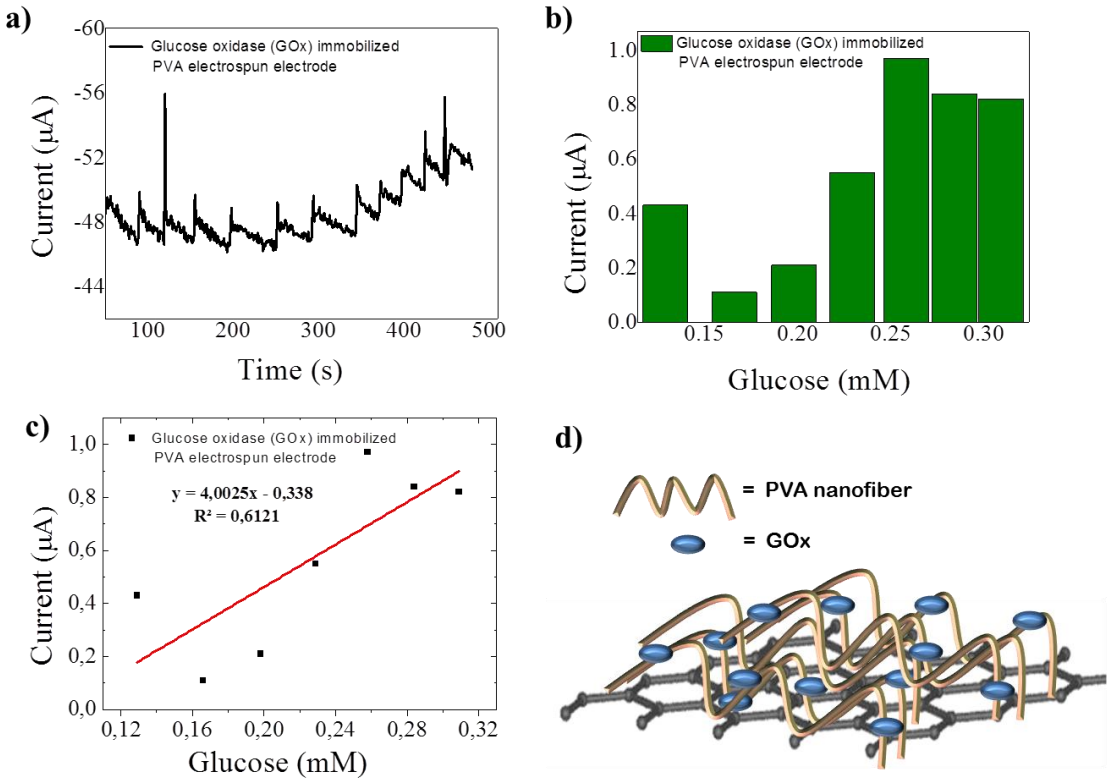

Figure 5.17. a) Amperometric response of GOx immobilized PVA electrospun electrode
b) Relationship between current increment versus glucose concentration
c) Calibration curve, d) Schematic of the electrode surface

To evaluate the effect of CNT on GOx catalytic reactivity, chronoamperometry measurements of *GOx immobilized PVA electrospun electrode containing MWCNT* were carried out. Figure 5.18 shows the amperometric response of the electrode to the successive addition of glucose (a), resulting current increment versus glucose concentration profile (b) and calibration curve (c). For the each addition of glucose

solution, current response shows an increase approximately 2 µA and than it reached a final and stabile value with difference ~ 1 µA. In consideration of the previous electrode system which does not contain CNT, MWCNT addition does not effectively enhance the catalytic reactivity of the enzyme electrode. Detection limit of the electrode was 0.0476mM and the response time was approximately 10 s. Current increment does not show a correlation with the increasing glucose concentration values and linear function regression value of the electrode is 0.7498. Even though the precence of MWCNT, enzyme electrode shows an analogy with the previous *GOx immobilized PVA electrospun electrode*. Inefficiency of the MWCNT addition can arise from the weak adsorbtion ratio of the GOx molecules onto the surface of CNTs. Negative charges on the carboxylated surface of the CNTs can cause a repulsive effect on GOx which is negatively charged at pH 7 thus decreasing the binding efficiency of the GOx onto the CNT surface.

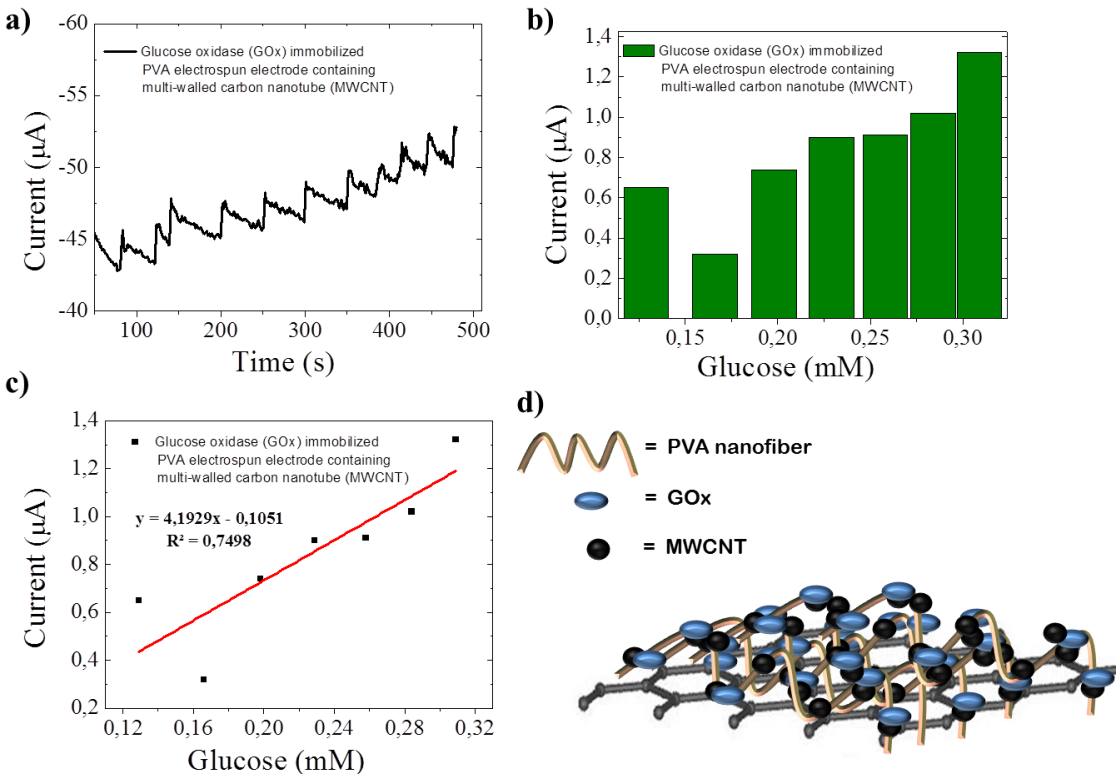

Figure 5.18. a) Amperometric response of GOx immobilized PVA electrospun electrode containing MWCNT, b) Relationship between current increment versus glucose concentration c) Calibration curve, d) Schematic of the electrode surface.

In order to enhance the binding efficiency of GOx onto the CNT surface, oxidized CNTs functionalized with the cationic polymer Poly (diallydiamethylammonium) chloride (PDDA) (See section 4.5). Figure 5.19 shows the chronoamperometric response of *GOx immobilized PVA electrospun electrode containing PDDA functionalized MWCNT* to the successive addition of glucose (a), resulting current increment versus glucose concentration profile (b) and calibration curve (c). For the each addition of glucose solution, current response increases approximately 1μA. The current response reached its steady state value with in 32s. Glucose detection limit of the electrode is observed as 0.0243 mM. Linear function regression value of the electrode is 0.8995 which shows more correlative behavior for the current response versus increasing glucose concentration.

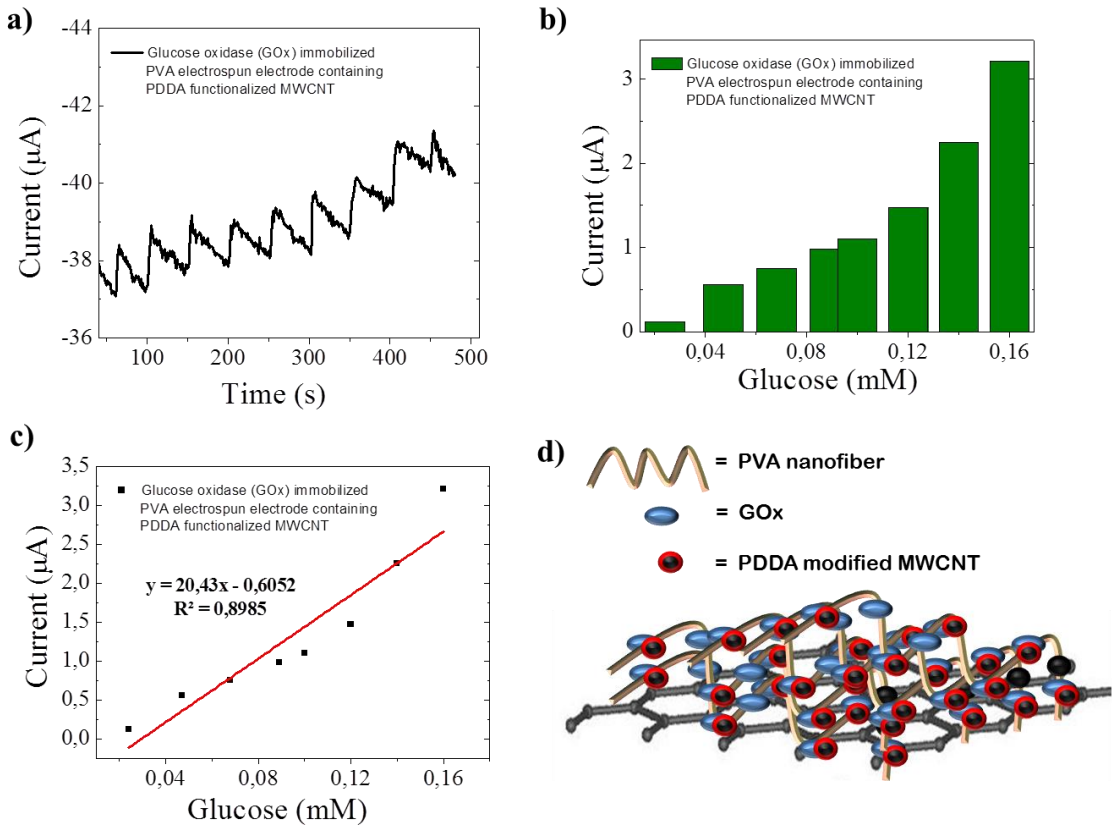

Figure 5.19. a) Amperometric response of GOx immobilized PVA electrospun electrode containing PDDA functionalized MWCNT, b) Relationship between current increment versus glucose concentration, c) Calibration curve, d) Schematic of the electrode surface

To identify the effect of the CNT types on the GOx catalysis efficiency, SWCNTs functionalized with PDDA were used. Figure 5.20 shows the amperometric response of *GOx immobilized PVA electrospun electrode containing PDDA functionalized SWCNT* to the successive addition of glucose (a), resulting current increment versus glucose concentration profile (b) and calibration curve (c). For the each addition of glucose solution, current response increases approximately 1μA. With the difference of the previously observed four electrode, current response does not show a decrease and it reached to its steady state value with in approximately 25 s and glucose detection limit of the electrode is observed as 0.0243 mM. In addition, linear function regression value of the electrode is 0.9305 indicating that there is an agreement between the current response and glucose concentrations.

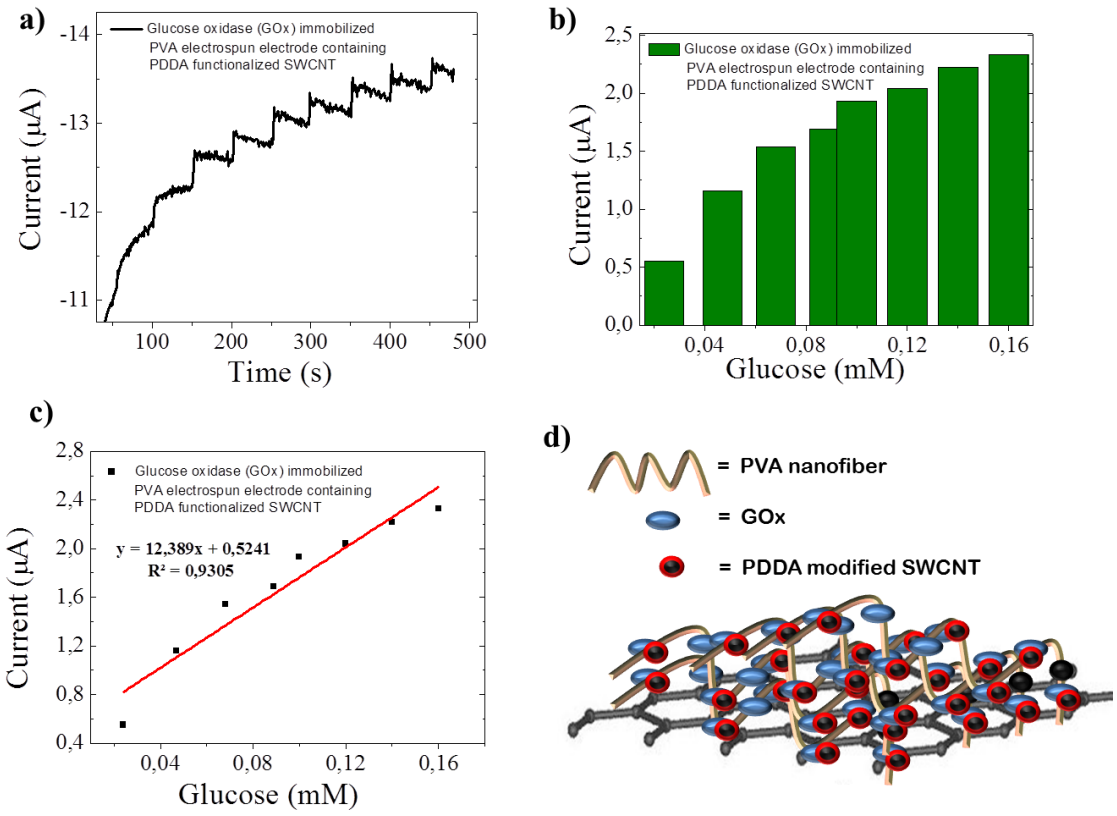

Figure 5.20. a) Amperometric response of GOx immobilized PVA electrospun electrode containing PDDA functionalized, b) Relationship between current increment versus glucose concentration, c) Calibration curve, d) Schematic of the electrode surface.

The final glucose sensing electrode is designed to identify the effect of CNT immobilization method on PVA electrospun fiber structure. Referring to the CV and SECM results, it is observed that the interfacially cross-linked PVA membranes show more conductive properties than the in-situ CNT immobilized PVA membranes. Figure 5.21 shows the chronoamperometric response of *Interfacially cross-linked PVA electrospun electrode containing PDDA functionalized MWCNT* to the successive addition of glucose (a), resulting current increment versus glucose concentration profile (b) and calibration curve (c). For the each injection of glucose solution, a sharp increase in the current was observed and the response reached to its steady state value within 9 s and glucose detection limit of the electrode is observed as 0.1 mM. The current response shows a gradual increase with the increased glucose concentration (Figure 5.21.b). The regression value of the linear function reached to 0.963.

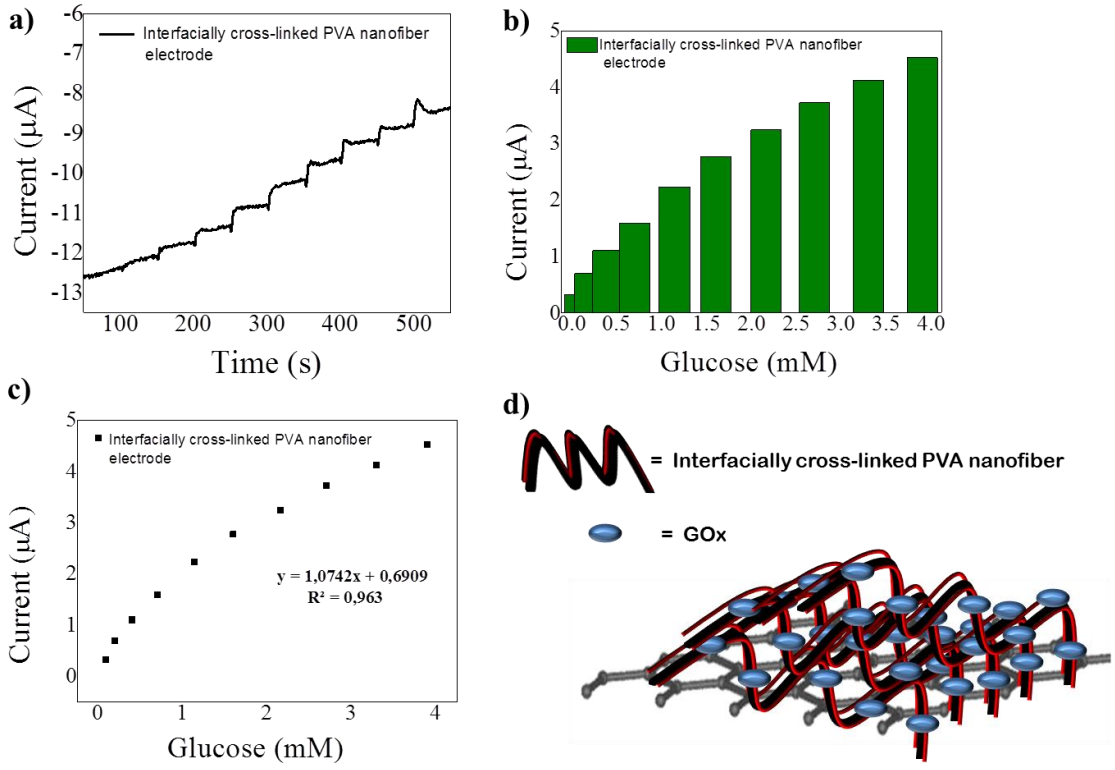

Figure 5.21. a) Amperometric response of Interfacially cross-linked PVA electrospun electrode containing PDDA functionalized MWCNT, b) Relationship between current increment versus glucose concentration
c) Calibration curve, d) Schematic of the electrode surface

The correlation between the current response and glucose hints about the glucose sensitivity (μA mM^{-1} cm^{-2}) of the enzyme electrodes. Electrode surface area exposed to the catalytic reaction was calculated based on the dimensions of a cylinder which has 0.9 mm diameter size and 10 mm height. Calculated sensitivities of electrodes are given in Table 5.4.

Table 5.4. Calculated sensitivities of enzyme electrodes

Type of electrode	**Sensitivity (μA mM^{-1} cm^{-2})**
PVA/GOx electrode	19.6
PVA(MWCNT)/GOx electrode	27.7
$PVA(MWCNT)_{PDDA}$/GOx electrode	67.5
$PVA(SWCNT)_{PDDA}$/GOx electrode	44.4
$PVA(MWCNT)_{PDDA}$/GOx electrode Intefacial X-linking	4.0

The sensitivity of *PVA/*GOx electrode was calculated as 19.6 μA $mM^{-1}cm^{-2}$. The addition of oxidized MWCNT into the *PVA/*GOx membrane increased the sensivity to 27.7 μA $mM^{-1}cm^{-2}$. In the preparation stage of the PVA/GOx electrode, GOx was physically immobilized in neutral conditions which the GOx was negatively charged on to the cross-linked pristine PVA fiber. Probably, GOx binding efficiency was repressed due to the unmodified feature of the pristine fiber surface and electron transfer was prevented because of the non-conductive PVA fiber layer. Carboxylated MWCNT addition might not be efficient effect on the increment of enzyme binding efficiency, because carboxylated MWCNT surface exibits a negatively charged layer that prevents the GOx adsorbtion. However, for the adsorbed GOx molecules, CNT might has a promoting effect on electrone transfer efficiency of the electrode. Based on this, for the **(c)** *GOx immobilized PVA electrospun electrode containing PDDA functionalized MWCNT* electrode, it was observed that the sensing ability of the sensor increased approximately 2 and half times as 67.5 μA $mM^{-1}cm^{-2}$. This sensitivity increment can be explained as higher binding efficiency of the GOx on to the CNT surface promoted by

the electrostatic interactions between the negatively charged GOx molecules (at pH 7) and the cationic polymer PDDA, modified on carboxylated MWCNTs. On the other hand, **(d)** *GOx immobilized PVA electrospun electrode containing PDDA functionalized SWCNT* shows lower sensitivity (44.4 μA $mM^{-1}cm^{-2}$) than the *GOx immobilized PVA electrospun electrode containing PDDA functionalized MWCNT* (67.5 μA $mM^{-1}cm^{-2}$). In consideration of the electrical properties of CNTs, our results are agree with literature. Banks et al (Banks et al. 2005) reported that the surface based activity and electron transfer efficiency of the graphite-like materials, constitutively occurs at edge-plane region. Moreover, Davies et. al (Davies, Hyde, and Compton 2005) studied on highly oriented pyrolytic graphite (HOPG) and they reported that surface defects of pyrolytic graphite in form of exposed edge plane nanobands have higher electron transfer rate constant (*k*) (approximately 7 orders of magnitude) than its basal plane and *k* constant of defect-free regions of the graphitic surface is around zero. Considering the electrical properties of the used carbon nanotubes, based on the Raman spectroscopy results, I_D/ I_G ratio of oxidized single-walled and multi-walled carbon nanotubes (Table 5.2 and Table 5.3) was 0.667 and 1.393, respectively. Increased defect ratio refers to the open ends of carbon nanotube surface, which had an enhanced charge transfer rate therefore inceased electrocatalytic activity (Miller et al. 2012). Higher glucose sensing efficiency of *GOx immobilized PVA electrospun electrode containing PDDA functionalized MWCNT* might be attributed to the higher charge transfer rate of oxidized MWCNTs.

Altough the detected surface conductivity of interfacially cross-linked electrode shows higher surface conductivity, interfacially cross-linkined glucose electrode (**e)** exibits the lowest glucose sensitivity as 4.03 μA $mM^{-1}cm^{-2}$. Herein, it was observed that the average fiber diameter was 119 and 347 nm for the pristine and interfacially cross-linked PVA electrospun mats respectively (See section 5.5.2). In consideration of the high surface to volume ratio of the fiber formed materials, decreased surface area - depending on the increased fiber diameter- might cause a reduced surface area for the GOx adsorption on to electrode surface. Limited GOx molecule adsorbtion on the high diameter sized fiber surface might be the decisive effect for the inefficient sensing ability of the interfacially cross-linked sensor electrode.

CHAPTER 6

CONCLUSION

Electrospinning, a nanoscale fiber fabrication technique promises a large variety of potential applications results from their high surface to volume ratio, porosity and competence to manipulate to get desired functions and properties. This thesis, proposes an electrospun membrane based nanocomposite biosensor system for the detection of glucose.

A vinyl-based, non-toxic polymer PVA was utilized for the electrospun membrane fabrication. PVA nanofiber membranes were obtained with 115 nm average diameter size by using electrospinning process. Effect of cationic polymer PDDA, CNT type and CNT modification proceeding were defined as the control parameters on glucose sensing efficiency of the sensor electrode. Depending on the sensor electrode design, nanofiber membranes modified with carboxylic acid-functionalized CNTs via in-situ addition and interfacial cross-linking. GOx was physically adsorped on CNT using cationic polymer PDDA. Chronoamperometric response of the electrodes to the successive addition of glucose was measured at an applied voltage -0.5 V (vs. Ag/AgCl) .

All in all, we concluded that, MWCNT modified sensor electrodes show higher glucose sensitivity than the neat PVA/GOx composite electrode interpreted to the enhanced direct electron transfer between GOx and the working electrode provided by the CNTs unique electron conductivity. In a second concern, it was also showed that PDDA modification on oxidized MWCNTs increased the sensor sensitivity, results from the higher binding efficiency of the GOx on to the CNT surface promoted by the electrostatic interactions between the negatively charged GOx molecules (at pH 7) and the cationic polymer PDDA, modified on carboxylated CNTs. In spide of the higher surface conductivity, interfacially cross-linked sensor electrode shows lower glucose sensing efficiency. However, the regression value of the linear function was 0.963 that refers to a more gradual increase with the glucose addition. In addition, the response time of the electrode was 9 s which is shorter than the another glucose sensing electrodes. In consideration of the diabetic blood glucose level ranging from 4 mM to 8mM, for the electrodes containing PDDA modified single-walled and multi-walled carbon nanotubes, 0.02 mM glucose detection limit was observed. In this manner, the

proposed electrospun nanofiber based glucose sensing electrodes exhibit appropriate properties for the sensitive determination of glucose in diabetic human blood samples and it can be used for improving the efficiency of new generation glucose sensing systems.

REFERENCES

Adams, Freddy C., and Carlo Barbante. 2013. "Nanoscience, nanotechnology and spectrometry." *Spectrochimica Acta Part B: Atomic Spectroscopy* 86:3-13. doi: http://dx.doi.org/10.1016/j.sab.2013.04.008.

Adesokan, B. J., X. Quan, A. Evgrafov, A. Heiskanen, A. Boisen, and M. P. Sørensen. 2016. "Experimentation and numerical modeling of cyclic voltammetry for electrochemical micro-sized sensors under the influence of electrolyte flow." *Journal of Electroanalytical Chemistry* 763:141-148. doi: http://dx.doi.org/10.1016/j.jelechem.2015.12.029.

Agarwal, Seema, Joachim H. Wendorff, and Andreas Greiner. 2010. "Chemistry on Electrospun Polymeric Nanofibers: Merely Routine Chemistry or a Real Challenge?" *Macromolecular Rapid Communications* 31 (15):1317-1331. doi: 10.1002/marc.201000021.

Ahmad, Rafiq, Mohammad Vaseem, Nirmalya Tripathy, and Yoon-Bong Hahn. 2013. "Wide Linear-Range Detecting Nonenzymatic Glucose Biosensor Based on CuO Nanoparticles Inkjet-Printed on Electrodes." *Analytical Chemistry* 85 (21):10448-10454. doi: 10.1021/ac402925r.

Ahmed, Shaikh Faiz Uddin, and Hirozo Mihashi. 2011. "Strain hardening behavior of lightweight hybrid polyvinyl alcohol (PVA) fiber reinforced cement composites." *Materials and Structures* 44 (6):1179-1191. doi: 10.1617/s11527-010-9691-8.

Amanda, A., and S. K. Mallapragada. 2001. "Comparison of protein fouling on heat-treated poly(vinyl alcohol), poly(ether sulfone) and regenerated cellulose membranes using diffuse reflectance infrared Fourier transform spectroscopy." *Biotechnology Progress* 17 (5):917-923. doi: 10.1021/bp0100631.

Arora, Pooja, Annu Sindhu, Neeraj Dilbaghi, and Ashok Chaudhury. 2011. "Biosensors as innovative tools for the detection of food borne pathogens." *Biosensors & Bioelectronics* 28 (1):1-12. doi: 10.1016/j.bios.2011.06.002.

Baba, Akira, Prasad Taranekar, Ramakrishna R. Ponnapati, Wolfgang Knoll, and Rigoberto C. Advincula. 2010. "Electrochemical Surface Plasmon Resonance and Waveguide-Enhanced Glucose Biosensing with N-Alkylaminated Polypyrrole/Glucose Oxidase Multilayers." *Acs Applied Materials & Interfaces* 2 (8):2347-2354. doi: 10.1021/am100373v.

Balakrishnan, Sharma Rao, U. Hashim, G. R. Letchumanan, M. Kashif, A. R. Ruslinda, W. W. Liu, P. Veeradasan, R. Haarindra Prasad, K. L. Foo, and P. Poopalan. 2014. "Development of highly sensitive polysilicon nanogap with APTES/GOx based lab-on-chip biosensor to determine low levels of salivary glucose." *Sensors and Actuators A: Physical* 220:101-111. doi: http://dx.doi.org/10.1016/j.sna.2014.09.027.

Banks, C. E., T. J. Davies, G. G. Wildgoose, and R. G. Compton. 2005. "Electrocatalysis at graphite and carbon nanotube modified electrodes: edge-plane sites and tube ends are the reactive sites." *Chemical Communications* (7):829-841. doi: 10.1039/b413177k.

Bard, A. J., F. R. F. Fan, J. Kwak, and O. Lev. 1989. "Scanning electrochemical microscopy - introduction and principles." *Analytical Chemistry* 61 (2):132-138. doi: 10.1021/ac00177a011.

Battistel, Dario, Salvatore Daniele, and Davide Fratter. 2012. "A scanning electrochemical microscopy procedure for micropatterning Al2O3-thin films deposited on a platinum substrate." *Electrochimica Acta* 78:557-562. doi: 10.1016/j.electacta.2012.06.066.

Bergmeyer, H. U., M. Horder, and R. Rej. 1986. "International-federation-of-clinical-chemistry scientific committee analytical section expert panel on enzymes - approved recommendation (1985) on ifcc methods for the measurement of catalytic concentrations of enzymes .3. ifcc method for alanine aminotransferase (l-alanine - 2-oxoglutarate aminotransferase, ec 2.6.1.2)c." *Annales De Biologie Clinique* 44 (3):321-334.

Bhardwaj, Nandana, and Subhas C. Kundu. 2010. "Electrospinning: A fascinating fiber fabrication technique." *Biotechnology Advances* 28 (3):325-347. doi: http://dx.doi.org/10.1016/j.biotechadv.2010.01.004.

Boland, E. D., J. A. Matthews, K. J. Pawlowski, D. G. Simpson, G. E. Wnek, and G. L. Bowlin. 2004. "Electrospinning collagen and elastin: Preliminary vascular tissue engineering." *Frontiers in Bioscience* 9:1422-1432. doi: 10.2741/1313.

Buehler, P. W., R. A. Boykins, Y. P. Jia, S. Norris, D. I. Freedberg, and A. I. Alayash. 2005. "Structural and functional characterization of glutaraldehyde-polymerized bovine hemoglobin and its isolated fractions." *Analytical Chemistry* 77 (11):3466-3478. doi: 10.1021/ac050064y.

Calleja, J. M., H. Vogt, and M. Cardona. 1982. "Absolute raman-scattering efficiencies of some zincblende and fluorite-type materials." *Philosophical Magazine a-Physics of Condensed Matter Structure Defects and Mechanical Properties* 45 (2):239-254.

Cammann, K. 1977. "Bio-sensors based on ion-selective electrodes." *Fresenius Zeitschrift Fur Analytische Chemie* 287 (1):1-9. doi: 10.1007/bf00539519.

Carrara, Sandro, Sara Ghoreishizadeh, Jacopo Olivo, Irene Taurino, Camilla Baj-Rossi, Andrea Cavallini, Maaike Op de Beeck, Catherine Dehollain, Wayne Burleson, Francis Gabriel Moussy, Anthony Guiseppi-Elie, and Giovanni De Micheli. 2012. "Fully Integrated Biochip Platforms for Advanced Healthcare." *Sensors* 12 (8):11013-11060. doi: 10.3390/s120811013.

Cash, Kevin J., and Heather A. Clark. 2010. "Nanosensors and nanomaterials for monitoring glucose in diabetes." *Trends in Molecular Medicine* 16 (12):584-593. doi: 10.1016/j.molmed.2010.08.002.

Chan, L. W., J. S. Hao, and P. W. S. Heng. 1999. "Evaluation of permeability and mechanical properties of composite polyvinyl alcohol films." *Chemical & Pharmaceutical Bulletin* 47 (10):1412-1416.

Che, Xin, Ruo Yuan, Yaqin Chai, Jingjing Li, Zhongju Song, Wenjuan Li, and Xia Zhong. 2011. "A glucose biosensor based on chitosan–Prussian blue–multiwall carbon nanotubes–hollow PtCo nanochains formed by one-step electrodeposition." *Colloids and Surfaces B: Biointerfaces* 84 (2):454-461. doi: http://dx.doi.org/10.1016/j.colsurfb.2011.01.041.

Chen, Wei, Yu Ding, Joshua Akhigbe, Christian Brückner, Chang Ming Li, and Yu Lei. 2010. "Enhanced electrochemical oxygen reduction-based glucose sensing using glucose oxidase on nanodendritic poly[meso-tetrakis(2-thienyl)porphyrinato]cobalt(II)-SWNTs composite electrodes." *Biosensors and Bioelectronics* 26 (2):504-510. doi: http://dx.doi.org/10.1016/j.bios.2010.07.062.

Cortes-Salazar, Fernando, Dmitry Momotenko, Hubert H. Girault, Andreas Lesch, and Gunther Wittstock. 2011. "Seeing Big with Scanning Electrochemical Microscopy." *Analytical Chemistry* 83 (5):1493-1499. doi: 10.1021/ac101931d.

Cortez, M. Lorena, Marcelo Ceolín, Omar Azzaroni, and Fernando Battaglini. 2015. "Formation of redox-active self-assembled polyelectrolyte–surfactant complexes integrating glucose oxidase on electrodes: Influence of the self-assembly solvent on the signal generation."*Bioelectrochemistry* 105:117-122. doi: http://dx.doi.org/10.1016/j.bioelechem.2015.06.001.

Danaei, Goodarz, Mariel M. Finucane, Yuan Lu, Gitanjali M. Singh, Melanie J. Cowan, Christopher J. Paciorek, John K. Lin, Farshad Farzadfar, Young-Ho Khang, Gretchen A. Stevens, Mayuree Rao, Mohammed K. Ali, Leanne M. Riley, Carolyn A. Robinson, and Majid Ezzati. "National, regional, and global trends in fasting plasma glucose and diabetes prevalence since 1980: systematic analysis of health examination surveys and epidemiological studies with 370 country-years and 2·7 million participants." *The Lancet* 378 (9785):31-40. doi: http://dx.doi.org/10.1016/S0140-6736(11)60679-X.

Davies, T. J., M. E. Hyde, and R. G. Compton. 2005. "Nanotrench arrays reveal insight into graphite electrochemistry." *Angewandte Chemie-International Edition* 44 (32):5121-5126. doi: 10.1002/anie.200462750.

DeMerlis, C. C., and D. R. Schoneker. 2003. "Review of the oral toxicity of polyvinyl alcohol (PVA)." *Food and Chemical Toxicology* 41 (3):319-326. doi: http://dx.doi.org/10.1016/S0278-6915(02)00258-2.

Dixon, B. M., J. P. Lowry, and R. D. O'Neill. 2002. "Characterization in vitro and in vivo of the oxygen dependence of an enzyme/polymer biosensor for monitoring

brain glucose." *Journal of Neuroscience Methods* 119 (2):135-142. doi: 10.1016/s0165-0270(02)00170-x.

Dresselhaus, M., G. Dresselhaus, P. Eklund, and R. Saito. 1998. "Carbon nanotubes." *Physics World* 11 (1):33-38.

Dresselhaus, M. S. 2004. "Nanotubes - A step in synthesis." *Nature Materials* 3 (10):665-666. doi: 10.1038/nmat1232.

Dresselhaus, M. S., G. Dresselhaus, and R. Saito. 1992. "Carbon-fibers based on c-60 and their symmetry." *Physical Review B* 45 (11):6234-6242. doi: 10.1103/PhysRevB.45.6234.

Dresselhaus, M. S., A. Jorio, A. G.
Souza, G. Dresselhaus, and R. Saito. 2002. "Raman spectroscopy on one isolated carbon nanotube." *Physica B-Condensed Matter* 323 (1-4):15-20. doi: 10.1016/s0921-4526(02)00873-6.

Dresselhaus, Mildred S. 2010. "NT10: Recent Advances in Carbon Nanotube Science and Applications." *Acs Nano* 4 (8):4344-4349. doi: 10.1021/nn101845f.

Eggins, B. R. 2002. "Shrouded in mystery." *Chemistry in Britain* 38 (5):18-18.

Espro, Claudia, Nicola Donato, Signorino Galvagno, Davide Aloisio, Salvatore G. Leonardi, and Giovanni Neri. 2014. "CuO Nanowires-based Electrodes for Glucose Sensors." In *10th Esee: European Symposium on Electrochemical Engineering*, edited by S. Palmas, M. Mascia and A. Vacca, 415-420.

Feldman, Dorel. 2016. "Polymer nanocomposites in medicine." *Journal of Macromolecular Science Part a-Pure and Applied Chemistry* 53 (1):55-62. doi: 10.1080/10601325.2016.1110459.

Ferraz, H. C., L. T. Duarte, M. Di Luccio, T. L. M. Alves, A. C. Habert, and C. P. Borges. 2007. "Recent achievements in facilitated transport membranes for separation processes." *Brazilian Journal of Chemical Engineering* 24 (1):101-118. doi: 10.1590/s0104-66322007000100010.

Fiedurek, J., and A. Gromada. 1997. "Screening and mutagenesis of molds for improvement of the simultaneous production of catalase and glucose oxidase." *Enzyme and Microbial Technology* 20 (5):344-347. doi: 10.1016/s0141-0229(96)00148-2.

Finch, C. A. 1973. "Water-based polymers nearly everywhere." *Chemistry & Industry* (16):796-797.

Gao, Yun-Fei, Tian Yang, Xiao-Lu Yang, Yu-Shuai Zhang, Bao-Lin Xiao, Jun Hong, Nader Sheibani, Hedayatollah Ghourchian, Tao Hong, and Ali Akbar Moosavi-Movahedi. 2014. "Direct electrochemistry of glucose oxidase and glucose biosensing on a hydroxyl fullerenes modified glassy carbon electrode."

Biosensors and Bioelectronics 60:30-34. doi: http://dx.doi.org/10.1016/j.bios.2014.04.005.

Golberg, D., P. S. Dorozhkin, Y. Bando, Z. C. Dong, C. C. Tang, Y. Uemura, N. Grobert, M. Reyes-Reyes, H. Terrones, and M. Terrones. 2003. "Structure, transport and field-emission properties of compound nanotubes: CNx vs. BNCx (x < 0.1)." *Applied Physics a-Materials Science & Processing* 76 (4):499-507. doi: 10.1007/s00339-002-2047-7.

Gouka, R. J., P. J. Punt, and Camjj vandenHondel. 1997. "Efficient production of secreted proteins by Aspergillus: Progress, limitations and prospects." *Applied Microbiology and Biotechnology* 47 (1):1-11.

Guo, Ruili, Changlai Hu, Ben Li, and Zhongyi Jiang. 2007. "Pervaporation separation of ethylene glycol/water mixtures through surface crosslinked PVA membranes: Coupling effect and separation performance analysis." *Journal of Membrane Science* 289 (1-2):191-198. doi: 10.1016/j.memsci.2006.11.055.

Hamielec, A. E., R. Gomezvaillard, and F. L. Marten. 1982. "Diffusion-controlled free-radical polymerization effect on polymerization rate and molecular-properties of polyvinyl-chloride." *Journal of Macromolecular Science-Chemistry* A17 (6):1005-1020. doi: 10.1080/00222338208056498.

Han, B., J. Li, C. Chen, C. Xu, and S. R. Wickramasinghe. 2003. "Effects of degree of formaldehyde acetal treatment and maleic acid crosslinking on solubility and diffusivity of water in PVA membranes." *Chemical Engineering Research & Design* 81 (A10):1385-1392. doi: 10.1205/026387603771339609.

Hatzinikolaou, D. G., and B. J. Macris. 1995. "Factors regulating production of glucose-oxidase by aspergillus-niger." *Enzyme and Microbial Technology* 17 (6):530-534. doi: 10.1016/0141-0229(95)91708-7.

Heller, A. 1990. "Electrical wiring of redox enzymes." *Accounts of Chemical Research* 23 (5):128-134. doi: 10.1021/ar00173a002.

Hickey, A. S., and N. A. Peppas. 1995. "Mesh size and diffusive characteristics of semicrystalline poly(vinyl alcohol) membranes prepared by freezing-thawing techniques." *Journal of Membrane Science* 107 (3):229-237. doi: 10.1016/0376-7388(95)00119-0.

Hochella Jr, Michael F. 2002. "Nanoscience and technology: the next revolution in the Earth sciences." *Earth and Planetary Science Letters* 203 (2):593-605. doi: http://dx.doi.org/10.1016/S0012-821X(02)00818-X.

Huang, C. F., and F. C. Chang. 2003. "Comparison of hydrogen bonding interaction between PMMA/PMAA blends and PMMA-co-PMAA copolymers." *Polymer* 44 (10):2965-2974. doi: 10.1016/s0032-2861(03)00188-5.

Huang, Fuying, Yanmei Zhong, Jie Chen, Shunxing Li, Yancai Li, Fei Wang, and Shuqing Feng. 2013. "Nonenzymatic glucose sensor based on three different

CuO nanomaterials." *Analytical Methods* 5 (12):3050-3055. doi: 10.1039/c3ay40342d.

Hui, Jianing, Jiewu Cui, Guangqing Xu, Samuel B. Adeloju, and Yucheng Wu. 2013. "Direct electrochemistry of glucose oxidase based on Nafion-Graphene-GOD modified gold electrode and application to glucose detection." *Materials Letters* 108:88-91. doi: http://dx.doi.org/10.1016/j.matlet.2013.06.097.

Husser, O. E., D. H. Craston, and A. J. Bard. 1989. "Scanning electrochemical microscopy - high-resolution deposition and etching of metals." *Journal of the Electrochemical Society* 136 (11):3222-3229.

Ibupoto, Z. H., K. Khun, J. Lu, and M. Willander. 2013. "The synthesis of CuO nanoleaves, structural characterization, and their glucose sensing application." *Applied Physics Letters* 102 (10). doi: 10.1063/1.4795135.

Jia, Xueen, Guangzhi Hu, Florian Nitze, Hamid Reza Barzegar, Tiva Sharifi, Cheuk-Wai Tai, and Thomas Wagberg. 2013. "Synthesis of Palladium/Helical Carbon Nanofiber Hybrid Nanostructures and Their Application for Hydrogen Peroxide and Glucose Detection." *Acs Applied Materials & Interfaces* 5 (22):12017-12022. doi: 10.1021/am4037383.

Jiang, J., R. Saito, A. Grüneis, G. Dresselhaus, and M. S. Dresselhaus. 2004. "Optical absorption matrix elements in single-wall carbon nanotubes." *Carbon* 42 (15):3169-3176. doi: http://dx.doi.org/10.1016/j.carbon.2004.07.028.

Jorio, A., R. Saito, J. H. Hafner, C. M. Lieber, M. Hunter, T. McClure, G. Dresselhaus, and M. S. Dresselhaus. 2001. "Structural (n, m) determination of isolated single-wall carbon nanotubes by resonant Raman scattering." *Physical Review Letters* 86 (6):1118-1121. doi: 10.1103/PhysRevLett.86.1118.

Kalisz, H. M., J. Hendle, and R. D. Schmid. 1997. "Structural and biochemical properties of glycosylated and deglycosylated glucose oxidase from Penicillium amagasakiense." *Applied Microbiology and Biotechnology* 47 (5):502-507.

Kapat, A., J. K. Jung, and Y. H. Park. 1998. "Improvement of extracellular recombinant glucose oxidase production in fed-batch culture of Saccharomyces cerevisiae: Effect of different feeding strategies." *Biotechnology Letters* 20 (3):319-323. doi: 10.1023/a:1005354608653.

Katz, M. G., and T. Wydeven. 1981. "SELECTIVE PERMEABILITY OF PVA MEMBRANES .1. RADIATION-CROSSLINKED MEMBRANES." *Journal of Applied Polymer Science* 26 (9):2935-2946. doi: 10.1002/app.1981.070260910.

Kurkina, Tetiana, Alexis Vlandas, Ashraf Ahmad, Klaus Kern, and Kannan Balasubramanian. 2011. "Label-Free Detection of Few Copies of DNA with Carbon Nanotube Impedance Biosensors." *Angewandte Chemie-International Edition* 50 (16):3710-3714. doi: 10.1002/anie.201006806.

Kwak, J., and A. J. Bard. 1989. "Scanning electrochemical microscopy - theory of the feedback mode." *Analytical Chemistry* 61 (11):1221-1227. doi: 10.1021/ac00186a009.

Lerner, Mitchell B., Nicholas Kybert, Ryan Mendoza, Romain Villechenon, Manuel A. Bonilla Lopez, and A. T. Charlie Johnson. 2013. "Scalable, non-invasive glucose sensor based on boronic acid functionalized carbon nanotube transistors." *Applied Physics Letters* 102 (18). doi: 10.1063/1.4804438.

Li, D., and Y. N. Xia. 2004. "Electrospinning of nanofibers: Reinventing the wheel?" *Advanced Materials* 16 (14):1151-1170. doi: 10.1002/adma.200400719.

Li, Huihui, Songqin Liu, Zhihui Dai, Jianchun Bao, and Xiaodi Yang. 2009. "Applications of Nanomaterials in Electrochemical Enzyme Biosensors." *Sensors* 9 (11):8547-8561. doi: 10.3390/s91108547.

Li, Jingjing, Ruo Yuan, Yaqin Chai, Xin Che, and Wenjuan Li. 2012. "Construction of an amperometric glucose biosensor based on the immobilization of glucose oxidase onto electrodeposited Pt nanoparticles-chitosan composite film." *Bioprocess and Biosystems Engineering* 35 (7):1089-1095. doi: 10.1007/s00449-012-0693-5.

Li, V. C., T. Horikoshi, A. Ogawa, S. Torigoe, and T. Saito. 2004. "Micromechanics-based durability study of polyvinyl alcohol-engineered cementitious composite." *Aci Materials Journal* 101 (3):242-248.

Liang, D., B. S. Hsiao, and B. Chu. 2007. "Functional electrospun nanofibrous scaffolds for biomedical applications." *Advanced Drug Delivery Reviews* 59 (14):1392-1412. doi: 10.1016/j.addr.2007.04.021.

Lisdat, Fred, Roman Dronov, Helmuth Moehwald, Frieder W. Scheller, and Dirk G. Kurth. 2009. "Self-assembly of electro-active protein architectures on electrodes for the construction of biomimetic signal chains." *Chemical Communications* (3):274-283. doi: 10.1039/b813559b.

Liu, G. D., and Y. H. Lin. 2005. "Electrochemical sensor for organophosphate pesticides and nerve agents using zirconia nanoparticles as selective sorbents." *Analytical Chemistry* 77 (18):5894-5901. doi: 10.1021/ac0507911.

López-Lorente, Ángela Inmaculada, and Miguel Valcárcel. 2014. "Chapter 1 - Analytical Nanoscience and Nanotechnology." In *Comprehensive Analytical Chemistry*, edited by Valcárcel Miguel and I. López-Lorente Ángela, 3-35. Elsevier.

Luo, Liqiang, Limei Zhu, and Zhenxin Wang. 2012. "Nonenzymatic amperometric determination of glucose by CuO nanocubes–graphene nanocomposite modified electrode." *Bioelectrochemistry* 88:156-163. doi: http://dx.doi.org/10.1016/j.bioelechem.2012.03.006.

Malin, S. F., T. L. Ruchti, T. B. Blank, S. N. Thennadil, and S. L. Monfre. 1999. "Noninvasive prediction of glucose by near-infrared diffuse reflectance spectroscopy." *Clinical Chemistry* 45 (9):1651-1658.

Marozzi, Carlos A., Maria R. Gennero de Chialvo, and Abel C. Chialvo. 2013. "Analysis of the applicability of short time chronoamperometry for the kinetic study of the hydrogen oxidation reaction." *Electrochimica Acta* 112:68-73. doi: http://dx.doi.org/10.1016/j.electacta.2013.08.068.

Mei, H., W. Q. Wu, B. B. Yu, H. M. Wu, S. F. Wang, and Q. H. Xia. 2016. "Nonenzymatic electrochemical sensor based on Fe@Pt core-shell nanoparticles for hydrogen peroxide, glucose and formaldehyde." *Sensors and Actuators B-Chemical* 223:68-75. doi: 10.1016/j.snb.2015.09.044.

Miller, Thomas S., Neil Ebejer, Aleix G. Gueell, Julie V. Macpherson, and Patrick R. Unwin. 2012. "Electrochemistry at carbon nanotube forests: sidewalls and closed ends allow fast electron transfer." *Chemical Communications* 48 (60):7435-7437. doi: 10.1039/c2cc32890a.

Mohareb, Ahmed, Marie France Thevenon, Edmond Wozniak, and Philippe Gerardin. 2011. "Effects of polyvinyl alcohol on leachability and efficacy of boron wood preservatives against fungal decay and termite attack." *Wood Science and Technology* 45 (3):407-417. doi: 10.1007/s00226-010-0344-4.

Moukwa, M., D. Youn, and M. Hassanali. 1993. "Effects of degree of polymerization of water soluble polymers on concrete properties." *Cement and Concrete Research* 23 (1):122-130. doi: http://dx.doi.org/10.1016/0008-8846(93)90142-V.

Niu, Xiangheng, Minbo Lan, Hongli Zhao, and Chen Chen. 2013. "Highly Sensitive and Selective Nonenzymatic Detection of Glucose Using Three-Dimensional Porous Nickel Nanostructures." *Analytical Chemistry* 85 (7):3561-3569. doi: 10.1021/ac3030976.

Odom, T. W., J. L. Huang, P. Kim, and C. M. Lieber. 1998. "Atomic structure and electronic properties of single-walled carbon nanotubes." *Abstracts of Papers of the American Chemical Society* 216:U77-U78.

Ofstead, R. F., and C. I. Poser. 1989. "SEMICRYSTALLINE POLYVINYL-ALCOHOL) HYDROGELS." *Advances in Chemistry Series* (223):61-72.

Osorio, A. G., I. C. L. Silveira, V. L. Bueno, and C. P. Bergmann. 2008. "H2SO4/HNO3/HCl-Functionalization and its effect on dispersion of carbon nanotubes in aqueous media." *Applied Surface Science* 255 (5):2485-2489. doi: 10.1016/j.apsusc.2008.07.144.

Peng, Bo, Jing Lu, Anant S. Balijepalli, Terry C. Major, Bruce E. Cohan, and Mark E. Meyerhoff. 2013. "Evaluation of enzyme-based tear glucose electrochemical sensors over a wide range of blood glucose concentrations." *Biosensors and Bioelectronics* 49:204-209. doi: http://dx.doi.org/10.1016/j.bios.2013.05.014.

Peter, S., N. Hese, and R. Stefan. 1976. "Phenol-selective, highly resistant ro-membranes made from pva for purification of toxic industrial-wastes." *Desalination* 19 (1-3):161-167. doi: 10.1016/s0011-9164(00)88026-1.

Petruccioli, M., F. Federici, C. Bucke, and T. Keshavarz. 1999. "Enhancement of glucose oxidase production by Penicillium variabile P16." *Enzyme and Microbial Technology* 24 (7):397-401. doi: 10.1016/s0141-0229(98)00142-2.

Pluschkell, S., K. Hellmuth, and U. Rinas. 1996. "Kinetics of glucose oxidase excretion by recombinant Aspergillus niger." *Biotechnology and Bioengineering* 51 (2):215-220. doi: 10.1002/(sici)1097-0290(19960720)51:2<215::aid-bit11>3.0.co;2-l.

Pokropivny, V. V., and V. V. Skorokhod. 2008. "New dimensionality classifications of nanostructures." *Physica E-Low-Dimensional Systems & Nanostructures* 40 (7):2521-2525. doi: 10.1016/j.physe.2007.11.023.

Popov, Valentin N. 2004. "Carbon nanotubes: properties and application." *Materials Science and Engineering: R: Reports* 43 (3):61-102. doi: http://dx.doi.org/10.1016/j.mser.2003.10.001.

Putzbach, William, and Niina J. Ronkainen. 2013. "Immobilization Techniques in the Fabrication of Nanomaterial-Based Electrochemical Biosensors: A Review." *Sensors* 13 (4):4811-4840. doi: 10.3390/s130404811.

Qiu, Cuicui, Xia Wang, Xueying Liu, Shifeng Hou, and Houyi Ma. 2012. "Direct electrochemistry of glucose oxidase immobilized on nanostructured gold thin films and its application to bioelectrochemical glucose sensor." *Electrochimica Acta* 67:140-146. doi: http://dx.doi.org/10.1016/j.electacta.2012.02.011.

Rando, D., G. W. Kohring, and F. Giffhorn. 1997. "Production, purification and characterization of glucose oxidase from a newly isolated strain of Penicillium pinophilum." *Applied Microbiology and Biotechnology* 48 (1):34-40.

Rao, A. M., P. C. Eklund, S. Bandow, A. Thess, and R. E. Smalley. 1997. "Evidence for charge transfer in doped carbon nanotube bundles from Raman scattering." *Nature* 388 (6639):257-259.

Reneker, Darrell H., and Alexander L. Yarin. 2008. "Electrospinning jets and polymer nanofibers." *Polymer* 49 (10):2387-2425. doi: 10.1016/j.polymer.2008.02.002.

Rosca, I. D., F. Watari, M. Uo, and T. Akaska. 2005. "Oxidation of multiwalled carbon nanotubes by nitric acid." *Carbon* 43 (15):3124-3131. doi: 10.1016/j.carbon.2005.06.019.

Saini, N. L., S. K. Saxena, and A. Bansil. 2010. "The study of matter at extreme conditions conference 2009 (SMEC 2009) Preface." *Journal of Physics and Chemistry of Solids* 71 (8):1031-1031. doi: 10.1016/j.jpcs.2010.06.008.

Song, M. J., S. K. Lee, J. H. Kim, and D. S. Lim. 2013. "Non-Enzymatic Glucose Sensor Based on Cu Electrode Modified with CuO Nanoflowers." *Journal of the Electrochemical Society* 160 (4):B43-B46. doi: 10.1149/2.037304jes.

Soni, Anuradha, and Sandeep Kumar Jha. 2015. "A paper strip based non-invasive glucose biosensor for salivary analysis." *Biosensors and Bioelectronics* 67:763-768. doi: http://dx.doi.org/10.1016/j.bios.2014.09.042.

Suni, Ian I. 2008. "Impedance methods for electrochemical sensors using nanomaterials." *TrAC Trends in Analytical Chemistry* 27 (7):604-611. doi: http://dx.doi.org/10.1016/j.trac.2008.03.012.

Terrones, M. 2003. "Science and technology of the twenty-first century: Synthesis, properties and applications of carbon nanotubes." *Annual Review of Materials Research* 33:419-501. doi: 10.1146/annurev.matsci.33.012802.100255.

Thevenot, D. R., K. Toth, R. A. Durst, and G. S. Wilson. 1999. "Electrochemical biosensors: Recommended definitions and classification - (Technical Report)." *Pure and Applied Chemistry* 71 (12):2333-2348. doi: 10.1351/pac199971122333.

Thong, C. C., D. C. L. Teo, and C. K. Ng. 2016. "Application of polyvinyl alcohol (PVA) in cement-based composite materials: A review of its engineering properties and microstructure behavior." *Construction and Building Materials* 107:172-180. doi: http://dx.doi.org/10.1016/j.conbuildmat.2015.12.188.

Tripathi, S., H. B. Chandalia, P. V. Rao, M. Y. Badgandi, P. K. Subbanna, R. Shetty, and R. Patni. 2010. "Effect of Insulin Detemir on Glycemic Parameters and Weight Gain: Experience from Real Life Practice in India." *Diabetes* 59:A557-A557.

Wan, Ling-Shu, Bei-Bei Ke, and Zhi-Kang Xu. 2008. "Electrospun nanofibrous membranes filled with carbon nanotubes for redox enzyme immobilization." *Enzyme and Microbial Technology* 42 (4):332-339. doi: http://dx.doi.org/10.1016/j.enzmictec.2007.10.014.

Wang, Yan, Ruo Yuan, Yaqin Chaia, Wenjuan Li, Ying Zhuo, Yali Yuan, and Jingjing Li. 2011. "Direct electron transfer: Electrochemical glucose biosensor based on hollow Pt nanosphere functionalized multiwall carbon nanotubes." *Journal of Molecular Catalysis B: Enzymatic* 71 (3–4):146-151. doi: http://dx.doi.org/10.1016/j.molcatb.2011.04.011.

Wild, S., G. Roglic, A. Green, R. Sicree, and H. King. 2004. "Global prevalence of diabetes - Estimates for the year 2000 and projections for 2030." *Diabetes Care* 27 (5):1047-1053. doi: 10.2337/diacare.27.5.1047.

Witt, S., M. Singh, and H. M. Kalisz. 1998. "Structural and kinetic properties of nonglycosylated recombinant Penicillium amagasakiense glucose oxidase expressed in Escherichia coli." *Applied and Environmental Microbiology* 64 (4):1405-1411.

Witt, S., G. Wohlfahrt, D. Schomburg, H. J. Hecht, and H. M. Kalisz. 2000. "Conserved arginine-516 of Penicillium amagasakiense glucose oxidase is essential for the efficient binding of beta-D-glucose." *Biochemical Journal* 347:553-559. doi: 10.1042/0264-6021:3470553.

Wohlfahrt, G., S. Witt, J. Hendle, D. Schomburg, H. M. Kalisz, and H. J. Hecht. 1999. "1.8 and 1.9 angstrom resolution structures of the Penicillium amagasakiense and Aspergillus niger glucose oxidases as a basis for modelling substrate complexes." *Acta Crystallographica Section D-Biological Crystallography* 55:969-977. doi: 10.1107/s0907444999003431.

Wu, Hui-Xia, Wei-Man Cao, Yan Li, Gang Liu, Ying Wen, Hai-Feng Yang, and Shi-Ping Yang. 2010. "In situ growth of copper nanoparticles on multiwalled carbon nanotubes and their application as non-enzymatic glucose sensor materials." *Electrochimica Acta* 55 (11):3734-3740. doi: http://dx.doi.org/10.1016/j.electacta.2010.02.017.

Yadav, Jyoti, Asha Rani, Vijander Singh, and Bhaskar Mohan Murari. 2015. "Prospects and limitations of non-invasive blood glucose monitoring using near-infrared spectroscopy." *Biomedical Signal Processing and Control* 18:214-227. doi: http://dx.doi.org/10.1016/j.bspc.2015.01.005.

Yang, Jiang, Liao-Chuan Jiang, Wei-De Zhang, and Sundaram Gunasekaran. 2010. "A highly sensitive non-enzymatic glucose sensor based on a simple two-step electrodeposition of cupric oxide (CuO) nanoparticles onto multi-walled carbon nanotube arrays." *Talanta* 82 (1):25-33. doi: http://dx.doi.org/10.1016/j.talanta.2010.03.047.

Yang, Ning, Xianping Chen, Tianling Ren, Ping Zhang, and Daoguo Yang. 2015. "Carbon nanotube based biosensors." *Sensors and Actuators B: Chemical* 207, Part A:690-715. doi: http://dx.doi.org/10.1016/j.snb.2014.10.040.

Yeom, C. K., and K. H. Lee. 1996a. "Pervaporation separation of water-acetic acid mixtures through poly(vinyl alcohol) membranes crosslinked with glutaraldehyde." *Journal of Membrane Science* 109 (2):257-265. doi: 10.1016/0376-7388(95)00196-4.

Yeom, Choong-Kyun, and Kew-Ho Lee. 1996b. "Pervaporation separation of water-acetic acid mixtures through poly(vinyl alcohol) membranes crosslinked with glutaraldehyde." *Journal of Membrane Science* 109 (2):257-265. doi: http://dx.doi.org/10.1016/0376-7388(95)00196-4.

Yu Ri, Kang, Hwang Kyung Hoon, Kim Ju Hwan, Nam Chang Hoon, and Kim Soo Won. 2010. "Disposable amperometric biosensor based on nanostructured bacteriophages for glucose detection." *Measurement Science and Technology* 21 (10):105804.

Yu, Yanyan, Zuanguang Chen, Sijing He, Beibei Zhang, Xinchun Li, and Meicun Yao. 2014. "Direct electron transfer of glucose oxidase and biosensing for glucose

based on PDDA-capped gold nanoparticle modified graphene/multi-walled carbon nanotubes electrode." *Biosensors and Bioelectronics* 52:147-152. doi: http://dx.doi.org/10.1016/j.bios.2013.08.043.

Zaidi, Shabi Abbas, and Jae Ho Shin. 2016. "Recent developments in nanostructure based electrochemical glucose sensors." *Talanta* 149:30-42. doi: http://dx.doi.org/10.1016/j.talanta.2015.11.033.

Zhai, Dongyuan, Borui Liu, Yi Shi, Lijia Pan, Yaqun Wang, Wenbo Li, Rong Zhang, and Guihua Yu. 2013. "Highly Sensitive Glucose Sensor Based on Pt Nanoparticle/Polyaniline Hydrogel Heterostructures." *Acs Nano* 7 (4):3540-3546. doi: 10.1021/nn4004132d.

Zhao, Q., Z. H. Gan, and Q. K. Zhuang. 2002. "Electrochemical sensors based on carbon nanotubes." *Electroanalysis* 14 (23):1609-1613. doi: 10.1002/elan.200290000.